EFFICIENT TECHNIQUES FOR CLASSIFICATION OF MEDICAL IMAGES

A Thesis Submitted

In Fulfillment of the Requirements

for the Degree of

Doctor of Philosophy

by

KAMAKSHI RAUTELA

(2K19/PHDEC/06)

Under the supervision of

Prof. DINESH KUMAR
Professor, DTU, New Delhi

and

Dr. VIJAY KUMAR
Associate Professor, Dr B R Ambedkar NIT Jalandhar

Department of Electronics & Communication Engineering

Delhi Technological University

Shahbad Daulatpur, Bawana Road, Delhi-110042

August 2024

DECLARATION

I declare that I have carried out the research work presented in this thesis entitled **"Efficient Techniques for Classification of Medical Images"** for the award of Doctor of Philosophy from Delhi Technological University, New Delhi. I also declare that the thesis embodies the results of original work and studies carried out by myself, and the contents of the thesis do not form the basis for the award of any other degree to me or anybody else from this or any other university or institution.

<div align="right">

Kamakshi Rautela

(2K19/PHDEC/06)

</div>

Date:

CERTIFICATE

It is certified that Ms. Kamakshi Rautela (2K19/PHDEC/06) has carried out the research work presented in this thesis entitled **"Efficient Techniques for Classification of Medical Images"** for the award of Doctor of Philosophy from Delhi Technological University, New Delhi. This thesis embodies the results of original work and studies carried out by the candidate herself, and the contents of the thesis do not form the basis for the award of any other degree to me or anybody else from this or any other university or institution.

Prof. Dinesh Kumar

Department of Electronics and Communication Engineering

Delhi Technological University

Delhi-110042, India

Dr. Vijay Kumar

Department of Information Technology

Dr B R Ambedkar NIT

Jalandhar-144011, India

Date:

ACKNOWLEDGEMENT

thank the members of the technical and administrative staff of the department for their help during the course of my study.

"Outstanding achievement is not possible in vacuums. It needs a lot of help and assistance besides a healthy environment, luckily, I have."

Kamakshi Rautela

ABSTRACT

Breast cancer is a major global health concern due to the potential for early detection to dramatically improve patient prognosis. Recent advances in screening methods and technologies have boosted the precision and efficacy of detecting and characterizing breast cancer. This study provides a thorough examination of reliable screening methods such as ultrasound, mammography, MRI, and thermography for the detection and classification of breast cancer.

Numerous artificial intelligence (AI) and computational techniques are investigated to improve the efficiency of screening procedures. Convolutional neural networks (CNNs), a type of deep learning algorithm, have shown remarkable promise for automatically classifying and detecting breast cancer in medical images. Combining AI with screening methods can decrease human error, increase diagnostic precision, and speed up the detection of malignant cases.

The development of new strategies for detecting and classifying breast cancer is highlighted in this work, along with the significance of ongoing research and collaboration between the medical and technical communities to enhance existing screening methods. It also highlights the importance of stringent validation and regulatory compliance to ensure the safe and efficient implementation of these technologies into clinical practice. This emphasizes how important it is to create an efficient preprocessing and enhancement strategy. Here, synthetic images are generated using a multimodal medical dataset-based method.

To better detect cancer, researchers are exploring multimodal image fusion. It offers a wide range of visual qualities for precise medical diagnosis. However, this method necessitates precise registration of all image modalities involved. To solve this problem, a new method is proposed for building synthetic mammograms. The image quality is improved using an

image enhancement technique. The thermal image segment is converted into a mammogram using a mapping function based on dual-modality structural features (DMSF). This study also proposes a modified Differentiable ARchiTecture Search (DARTS) called (U-DARTS) to further aid in the detection and classification of breast lesions. U-DARTS makes use of a stochastic gradient descent optimizer. The proposed method is evaluated using both DMR and INbreast datasets. Based on the obtained data, the proposed model outperforms the currently used methods by a wide margin. Accuracy levels of 98% in validation and 91% in testing are attained. The proposed approach is unrivaled for creating mammograms and subsequently detecting lesions.

The concept of fusing two different modality datasets is inspired by the results of synthetic mammograms created using a mammography-thermography multi-modal dataset. By combining the images, more specific information about the tumor's location can be gleaned. However, the output image may have spectral variations, making it challenging to use in the medical field when fusing two images from different modalities.

Multimodal image fusion is a crucial topic of research since it has been demonstrated to be effective in producing high-quality results for healthcare diagnostics and treatment. In medicine, however, fusing images from different modalities has always been difficult due to the resulting image's distorted spectral information. In this work, Super-Pixel Segmentation (SPS-AWT) is proposed using an advanced wavelet transformation method to combine breast cancer images taken in different settings and at different times. Discrete wavelet transformation (DWT) is used to combine spectral and spatial information from both mammographic and thermal images in order to make the evaluation. The obtained coefficients are divided into spherical patches using super-pixel segmentation to generate pixels with similar visual characteristics. The effectiveness of the proposed fusion method

is measured using a standard data set. Images fused using the proposed method are of high quality.

However, image enhancement using the ultrasonic modality is a challenging task. Ultrasound images contain noise that is visible in the form of dots, and shadows are noticeable as tissue-related textures. This makes it hard to understand. To make the breast ultrasound image more informative, a method is proposed to combine Active Contour and Texture Feature Vectors for finding the discriminative patterns. A comprehensive set of discriminative features for cancer detection in ultrasound images is created by combining the two learning models. Breast Ultrasound Images dataset is used to evaluate the suggested method and compare it to the recently developed algorithms. Experimental results reveal that the proposed approach outperforms the existing algorithms in terms of accuracy, recall, precision, Jaccard index, and F1 score.

Next, a deep-learning model with a modified transformer is proposed for breast lesions detection in order to classify the pre-processed and enhanced medical images efficiently. A deep learning model with a tweaked transformer is proposed to identify breast lesions based on the benefits of residual convolutional networks and the multiple-layer perceptron (MLP)-based transformer. The support residual deep learning network generates the deep features, and the transformer classifies breast cancer using self- and cross-attention mechanisms. The proposed model is effective at detecting breast cancer across both the basic (3-stage) and multi-classification (5-stage) settings. Data collection, preprocessing, patch creation, and the creating stage for identifying breast lesions all adhere to the same framework. Positive evaluation results are obtained using the INbreast mammograms, with the basic and multi-class approaches achieving accuracies of 98.17% and 96.74%, respectively. The experimental results demonstrate the proposed model can differentiate between cancerous,

noncancerous, and benign breast tissues. In addition, the modified transformer showed promising results in evaluating multiple classes of cancer.

In the next step, deep neural networks and thermographic images are used to create a real-time solution for diagnosing breast cancer. For this, two different experiments are performed. Firstly, thermal imaging is used as a method of breast cancer detection in this study. The model first applies a memory-efficient network to the entire image to determine where the most relevant information is likely to be found. The dataset of thermal images is then passed through a relatively deep CNN to extract relevant information. The model achieved an accuracy of 92.52%.

When it comes to modeling dependencies, particularly long-range ones like those required for accurately determining or recognizing corresponding breast lesion features, CNNs typically perform poorly due to the inherent locality of the convolution operation. Due to this, the Vision Transformer block is used in conjunction with VGG19. In addition, this work introduces a powerful model that integrates global and local features. Finally, the model is trained separately using the Database for Mastology Research and INbreast. The model is then trained with 80% training data and 20% test data from both datasets using transfer learning. To train the network, a learning rate of 0.01, a batch size of 50, and 100 epochs are used. Test accuracy of 98% and 89.9% are achieved for the INbreast and DMR datasets, respectively.

TABLE OF CONTENTS

LIST OF ABBREVIATIONS AND SYMBOLS

The list of abbreviations and symbols used in this thesis is given below. Some other abbreviations / symbols, which are not mentioned here are described locally.

ABUS	Automated Breast Ultrasound System
Acc	Accuracy
ACFV	Active Contour Feature Vector
ACS	American Chemical Society
ANN	Artificial Neural Network
AUC	Area Under the Curve
BRCA	Breast Cancer Gene
BN	Batch Normalization
BSE	Breast Self-Examination
BUS	Breast Ultrasonography
CAD	Computer-Aided Diagnosis
CBE	Clinical Breast Examination
CDCNN	Convolutional And De-Convolutional Neural Networks
C_K	Cohen's Kappa Coefficient
CLAHE	Contrast Limited Adaptive Histogram Equalization
CNN	Convolutional Neural Networks
CT	Computed Tomography
DARTS	Differentiable Architecture Search
DAS	Delay And Sum Algorithm

DCE-MRI	Dynamic Contrast-Enhanced Magnetic Resonance Imaging
DES	Diethylstilbestrol
DCIS	Ductal Carcinoma In Situ
DMR	Database For Mastology Research
DMSF	Dual-Modality Structural Feature
DSM	Dual Scan Mammoscope
DWT	Discrete Wavelet Transformation
EEMD	Ensemble Empirical Mode Decomposition
EIS-HB	Electrical Impedance Spectroscopy Hand Breast
FC	Fully Connected
FEM	Finite Element Method
FN	False Negative
FP	False Positives
GAHT	Gender Affirming Hormonal Treatment
GELU	Gaussian Error Linear Units
GLCM	Gray Level Co-Occurrence Matrix
GMM	Gaussian Mixture Model
H	Hausdorff Distance
IDC	Invasive Ductal Carcinoma
ILC	Invasive Lobular Carcinomas
IRI	Infrared Imaging
JI	Jaccard Index
KNN	K-Nearest Neighbors
LBP	Local Binary Pattern
LOO	Leave-One-Out

LBP	Local Binary Pattern
LCIS	Lobular Carcinoma In Situ
LN	Layer Normalization
MAE	Mean Absolute Error
M_{CC}	Matthews Correlation Coefficient
MI	Multi-Instance
ML	Machine Learning
MLP	Multilayer Layer Perceptron
MS	Multispectral
MSA	Multi-Head Self-Attention
MSE	Mean Square Error
MRI	Magnetic Resonance Imaging
NBCC	National Breast Cancer Coalition
NCDIR	National Centre for Disease Informatics and Research
NPV	Negative Predictive Value
OMT	Otsu Multilevel Thresholding
PAN	Panchromatic
P	Precision
PEM	Positron Emission Mammography
PIG	Poisson Inverse Gradient
PNN	Probability Neural Networks
PPV	Positive Predictive Value
PSNR	Peak Signal-To-Noise Ratio
RAR	Robust And Artifact Resistant
RBFN	Radial Basis Function Networks

RC	Recall
REIS	Resonance-Frequency-Based Electrical Impedance Spectroscopy
RMSE	Root Mean Square Error
ROC	Receiver Operating Characteristic
SF	Spatial Frequency
SMA	Slime-Mold-Algorithm
SMCM	Synthetic Mammogram Construction Model
SNR	Signal To Noise Ratio
SPS-AWT	Super-Pixel Segmentation-Based Advanced Wavelet Transformation
SR	Systematic Review
SSIM	Structural Similarity Measure
SVM	Support Vector Machine
TFV	Texture Feature Vector
WFM	Wavelet Fusion Module
WHO	World Health Organization
TN	True Negative
TP	True Positive
A_c	Accuracy
C_K	Cohen's Kappa Coefficient
FP_r	False Positive Rate
I_{TH}	Thermal Image
I_{MM}	Mammogram
M_{CC}	Matthew's Correlation Coefficient

μ   Mean

σ Standard Deviation

S_n Sensitivity

S_p Specificity

TP_r True Positive Rate

LIST OF FIGURES

LIST OF TABLES

LIST OF PUBLICATIONS

Published articles (International SCI/SCIE Journals):

1. **Rautela, Kamakshi**, Dinesh Kumar, and Vijay Kumar. "A systematic review on breast cancer detection using deep learning techniques." Archives of Computational Methods in Engineering 29, no. 7 (2022): 4599-4629.

2. **Rautela, Kamakshi**, Dinesh Kumar, and Vijay Kumar. "Dual-modality synthetic mammogram construction for breast lesion detection using U-DARTS." Biocybernetics and Biomedical Engineering 42, no. 3 (2022): 1041-1050.

3. **Rautela, Kamakshi**, Dinesh Kumar, and Vijay Kumar. "Active contour and texture features hybrid model for breast cancer detection from ultrasonic images." International Journal of Imaging Systems and Technology 33, no. 6 (2023): 2061-2072.

4. **Rautela, Kamakshi**, Dinesh Kumar, and Vijay Kumar. "A comprehensive review on computational techniques for breast cancer: past, present, and future." Multimedia Tools and Applications (2024): 1-34.

5. **Rautela, Kamakshi**, Dinesh Kumar, and Vijay Kumar. "Improved GAN for image resolution enhancement using ViT for breast cancer detection." International Journal of Imaging Systems and Technology (2024).

International Conference Proceedings:

1. **Rautela, Kamakshi**, Dinesh Kumar, and Vijay Kumar. "An interpretable network to thermal images for breast cancer detection." In 2022 *International Conference*

on Electrical, Computer, Communications and Mechatronics Engineering (ICECCME), pp. 1-5. IEEE, 2022.

2. **Rautela, Kamakshi**, Dinesh Kumar, and Vijay Kumar. "Detection and localization of breast lesion with VGG19 optimized vision transformer." In 2022 *4th International Conference on Artificial Intelligence and Speech Technology (AIST)*, pp. 1-4. IEEE, 2022.

3. **Rautela, Kamakshi**, Dinesh Kumar, and Vijay Kumar, "A Capsule Network-Based Framework for Detecting and Localizing Breast Tumors Using Ultrasonography," *3rd International Conference on Electrical, Computer and Energy Technologies (ICECET2023)*.

Articles (Under Review in International SCI/SCIE Journals):

1. **Rautela, Kamakshi**, Dinesh Kumar, and Vijay Kumar, "Modified Transformer Based Pixel Segmentation for Breast Tumor Detection," *Image and Vision Computing. (Under Review)*

2. **Rautela, Kamakshi**, Dinesh Kumar, and Vijay Kumar, "Bimodal Image Fusion using AWT-SPS for Breast Cancer Detection," *(Under preparation, to be communicated)*.

CHAPTER 1
Introduction and Motivation

Breast cancer is a serious health issue that affects millions of people worldwide. Uncontrolled cell growth and division in the breast tissue are hallmarks of a group of diseases known as breast cancer. Though significant progress has been made in the diagnosis and treatment of breast cancer, it still carries a high mortality rate [1], especially when diagnosed at an advanced stage or when it has spread to other parts of the body. According to the World Health Organization (WHO), breast cancer was first discovered in Egypt in approximately 1600 BC and is one of the most well-known kinds of cancer [2,3]. Breast cancer is responsible for about 15% of all female deaths [4]. It affects both men and women, as well as transgender people. In fact, the breast cancer can strike anyone, but the incidence of cancer is indeed much higher in women than in men or transgender. It is mostly associated with women because of the fact that breast tissue develops more rapidly in women due to hormonal factors. The presence of estrogen and progesterone in women's bodies may lead to the development and spread of cancer. Women also have a higher proportion of glandular tissue in their breasts, which is more susceptible to cancerous changes.

There have been cases of transgender men and women acquiring breast cancer [5,6]. According to the studies, transgender women receiving long-term estrogen therapy may be slightly more likely to develop breast cancer than cisgender men. However, compared to cisgender women, this risk seemed to be lower. Transgender men seemed to have a similar risk of developing breast cancer. According to the WHO, the number of instances of breast cancer would rise to 2.7 million by 2040 [7].

Most breast cancers develop in the mammary glands or the networks that link the glands to the nipple [4]. This is an extremely sensitive area, and detection is only feasible if someone is vigilant. However, once diagnosed, breast cancer needs significant medical treatment and regular check-ups.

The current medical environment in many developing countries is still recuperating from the effects of the epidemic. This is causing emerging economies to be concerned [5]. According to statistics from the "National Centre for Disease Informatics and Research" (NCDIR), breast cancer is one of the top five most often discovered malignancies in India. In the year 2020, India had a total female population of 662,903,415, and it was estimated that there would be 178,361 new cases of breast cancer, constituting approximately 26% of all cancer cases.

Breast cancer detection must be quick and precise to combat its fast development. This will increase the likelihood of survival. However, the task of early identification may not be so easy. Hence efforts are underway to develop methods that detect cancer as early as possible. Another challenge is predicting the progression of breast cancer and then designing a treatment plan as per the suitability and comfort of the patient.

A breast cancer patient is often subjected to a battery of tests, including Mammography, Magnetic Resonance Imaging (MRI), Computed Tomography (CT), and B-ultrasonography [8]. Mammography is the most commonly used approach for detection of breast cancer [9]. It is well known for its potential to reduce breast cancer mortality by detecting tumors when these are small and easier to treat [10–12]. It has a sensitivity range of 77% to 95% and a specificity range of 92% to 95% [13]. However, because of the thick tissue in the breast, mammography findings may be unsatisfactory [14].

Today's technology enables researchers to gain a deeper comprehension of a patient's tumor type and to modify treatment strategies accordingly. According to a viewpoint [14],

this strategy has "made excellent progress in perception" with the aid of machine learning (ML). In addition to mammography and other sophisticated imaging modalities, researchers have investigated machine learning (ML) tactics to increase illness diagnosis accuracy.

Breast cancer is a common health issue that affects women, with a one-in-eight mortality rate. Unfortunately, many women, because of safety concerns, disregard the significance of breast cancer screening which involves radiation exposure. Existing screening techniques have limitations such as invasiveness, unsafe radiation, and difficulty in accurately diagnosing breast tumors. Deep learning techniques are becoming increasingly popular in medical imaging. This chapter covers a comprehensive survey of breast cancer screening techniques, including their benefits and drawbacks. This chapter talks about the use of deep learning techniques in the detection of breast cancer. The performance metrics and datasets used in breast cancer research are also investigated. The primary goal is to provide an in-depth investigation in this field.

Breast cancer is categorized among the most frequently reported cancers in the World. It has been reported in both males and females. However, its frequency in females is far beyond the comparison. In 2018, as many as 6,27,000 women died due to breast cancer, which was approximately 15% of all cancer deaths among women [15,16]. The early detection of breast cancer may help the patient to recover in time. However, it is advisable not to go for frequent breast cancer screening due to the lack of convenience and discomfort with traditional examinations such as mammograms.

The frequency of breast cancer in transgender individuals, as well as the impact of gender-affirming hormonal treatment (GAHT) on the risk of breast cancer, remains largely unexplored. It is less clear, however, what risk breast cancer poses to the transgender individual and how, if at all, physicians should screen these patients. Reports of transgender

men's breast cancer have been mentioned in the medical literature [17]. The number of incidences of breast cancer in trans women receiving GAHT remains vague. As of 2018, two population-based studies assessed the breast cancer risk attributable to GAHT. Both studies were limited by a small number of breast cancer cases and a lack of genetic risk stratification [18,19]. Considering trans-male case, ductal carcinoma in situ (DCIS) was diagnosed during chest reconstruction surgery. To maintain masculinization, low-dose transdermal application of testosterone may be used as these doses may minimize the amount of circulating testosterone and thus avoid unnecessary aromatization to estradiol [20]. In [19], authors suggested the risk of breast cancer in transgender people is lower than in cisgender women, however, it is comparable to the risk in cisgender men. They also concluded that the overall risk of breast cancer in transgender people remains low. Therefore, it seems sufficient for transgender people using hormone treatment to follow screening guidelines as for cisgender people. Table 2.1 shows the cancer data statistics for 2020 for India. This data is obtained from the National Centre for Disease Informatics and Research (NCDIR). According to the data, Breast Cancer is among the top 5 most frequent cancers in India.

Normally, patients with breast tumors undergo multiple different examinations including B-ultrasonography, Mammography, Computed Tomography (CT), and Nuclear Magnetic Resonance Imaging (MRI) [21]. Mammography is most common method used for screening breast cancer [8,10,22]. It does not prevent cancer. However, the early detection of cancer can be possible through mammography [11]. The sensitivity of mammography is estimated between the range of 77% and 95%. The specificity estimated through mammography lies in the range of 92% to 97% [23]. However, mammography is suboptimal in breasts with dense tissue [9]. Due to this, approximately 38% of tumors are missed or misdiagnosed [13]. Another drawback of mammography is patients' discomfort

and radiation exposure. The interpretation of mammograms is a time-consuming and error-prone task [14].

Table 1.1 Statistics of Cancer Data in India during 2020 Statistics of Cancer Data in India during 2020.

	Male	Female	Total
Population	717100976	662903415	1380004378
Number of Cancer Cases	646030	678383	1324413
Number of Cancer Deaths	438297	413381	851678
Age-standardized incidence rate (World)	95.7	99.3	97.1
Age-standardized mortality rate (World)	65.4	61	63.1
5-year prevalent cases	1208835	1511416	2720251
Top 5 most frequent cancers excluding non-melanoma skin cancer (ranked by cases)	Lip, oral cavity Lung Stomach, Colorectum, Oesophagus	Breast Cervix uteri Ovary Lip, oral cavity Colorectum	Breast Lip, oral cavity Cervix uteri Lung Colorectum

1.1. Motivation

Despite tremendous improvements, cancer prevalence appears to be increasing, as per the literature. Breast cancer is the most common cancer among women across the world. It affects one out of every eight women today [24,1]. As a co-morbidity of breast cancer, aging-related transcriptome changes can promote breast cancer growth [25,26]. More so, the average age for diagnosing a female with cancer is decreasing, from more than 50 to less than 40 years [27].

According to the WHO, early detection of breast cancer improves prognosis [28]. As the literature reports, mammography is the most often used method for detecting breast cancer.

As breast thickness increases, mammography's sensitivity decreases [40,98,107]. Understanding breast cancer detection methods is essential for improving the accuracy of diagnosis. The following considerations prompted me to perform this study:

- In order to propose some better breast cancer detection approach/system, it becomes imperative to examine the distinctive characteristics of various breast cancer screening techniques. Understanding the strengths and limitations of each screening method is essential for choosing the most suitable and efficient method. Researchers and healthcare professionals can tailor the screening process based on patient characteristics like age, breast density, and risk factors by understanding the benefits and drawbacks of each method. This individualized screening strategy may enable early diagnosis and better patient outcomes by improving breast cancer detection. Additionally, ongoing studies and evaluations of these methods are necessary to stay at the forefront of breast cancer detection because ongoing research and technological developments are continuously evolving breast cancer screening methods.

- The application of machine and deep learning methods is a key component of breast cancer screening. The use of machine and deep learning in medical research, including breast cancer detection systems, has increased significantly. Due to the potential for developing cutting-edge optimization methods and techniques, researchers are motivated to study and analyze these systems. Medical experts can develop more advanced and precise screening models by utilizing machine and deep learning algorithms. To find patterns and risk factors related to breast cancer, these algorithms can analyze a large amount of patient data, including medical histories, imaging results, and genetic data. By customizing the screening process to the needs

and characteristics of each patient, personalized screening approaches can be developed.

- Using various evaluation parameters, which can produce a range of results, is necessary for the validation of breast cancer detection techniques. Each evaluation metric evaluates a particular aspect of the screening method, so a new technique may perform exceptionally well in some areas while falling short in others. The variability in performance traits raises doubts about the overall efficacy of breast cancer screening methods and technology. Researchers and medical professionals must consider a variety of evaluation criteria when comparing various screening methods, including sensitivity, specificity, accuracy, positive predictive value (PPV), negative predictive value (NPV), and area under the curve (AUC) of the receiver operating characteristic (ROC) curve.

The ability of the screening method to accurately identify positive cases (true positives) is measured by sensitivity, and the ability to accurately identify negative cases (true negatives) is measured by specificity. On the other hand, accuracy reflects how accurate the screening results were overall. In the end, this ongoing research and evaluation process helps to improve the effectiveness of breast cancer detection techniques, ensuring that patients get the best care possible.

1.2. Organization of Thesis

The whole thesis is organized into eight chapters. Chapter 1 discusses the basic concepts of breast cancer and the motivation to work on this topic. Chapter 2 implicitly deals with obtaining the necessary insights and the required background on breast cancer detection. Chapter 3 is the literature survey of previous research done on breast cancer detection. Multimodal image fusion is a new area of study for the diagnosis of cancer. Proper registration of all image modalities is essential for this procedure to yield useful results.

Chapter 4 proposes a novel model for the construction of synthetic mammograms, which can help with the aforementioned problem. The goal of this Chapter is to provide a multimodal approach to breast cancer detection, which may improve the screening technique's efficacy. Chapter 5 proposes an Advanced Wavelet Transformation (AWT) method called Super-Pixel Segmentation to combine breast cancer images taken in different settings and at different times.

Ultrasound of the breast is commonly used for screening for breast cancer. Current geodesic-based methods rely on manually applied filters. Most ultrasound images have noise and acoustic shadowing, which reduces the precision of tumor detection. To locate comprehensive and distinguishable patterns, Chapter 6 suggests combining Active Contour and Texture Feature (ACTF) Vectors. By fusing (a) the Active Contour Feature Vector (ACFV) model and (b) the Texture Feature Vector (TFV) model, a rich set of discriminative features is generated for cancer detection in ultrasound images.

Chapter 7 uses residual convolutional networks, and the multiple-layer perceptron (MLP) based transformer to advocate for a deep learning model that employs a tweaked version of the transformer in the detection of breast lesions. The proposed model is capable of detecting breast cancer at both the Basic and Multi-classification (Stage 3) levels.

CNN has been widely used in a variety of medical imaging tasks. However, CNNs perform poorly when modeling dependencies, especially long-range dependencies, which are necessary for accurately determining or recognizing corresponding breast lesion features. To overcome the above-mentioned problem, Chapter 8 shows the use of VGG19 and the Vision Transformer block to integrate both global and local factors for efficient breast cancer detection.

Chapter 9 talks about the most important parts, the contributions that were made, the main findings, and future directions about where this field of study might go in the future.

1.3. Research Objectives

- To investigate existing enhancement and classification techniques for medical images.

- To develop a pre-processing technique for medical images.

- To develop a novel image enhancement technique for multimodal medical datasets.

- To efficiently classify the pre-processed and enhanced medical images.

Fig 1.1 shows the relationship between the chapters and contribution to the overall aim of the research.
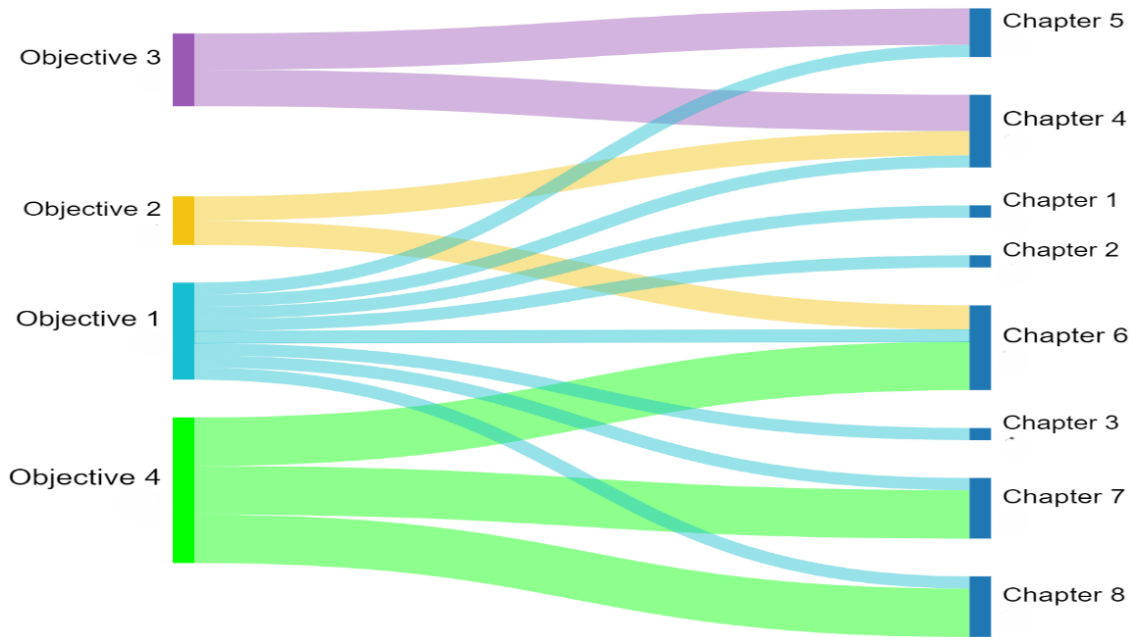
Fig. 1.1 Relationship between chapters and objectives of the research.

1.4. Contribution

This work focuses on the study of breast cancer screening techniques with their pros and cons. This study discusses mainly:

- Theoretical aspects of breast cancer for females, males, and transgenders including deep learning implementations for its detection.

- The different breast cancer screening approaches/techniques, risk factors, target connection, and common datasets.

- The mathematical representations of performance evaluation measures.

- Multimodal image fusion for the diagnosis of cancer.

- The comparative analysis of deep learning-based breast cancer prediction techniques in terms of performance measures.

- The possible future research directions for breast cancer detection.

CHAPTER 2
Background

2.1. Types of Breast Cancer

Breast cancer is categorized as Non-invasive (benign) and Invasive (malignant). Benign tumors develop slowly and do not invade neighboring tissues or migrate to other parts of the body [1]. Malignant tumors are potentially fatal. Fig. 2.1 depicts the different types of breast cancers for simplicity of comprehension. Non-invasive cancer does not spread beyond the lobules where they initially developed. Therefore, they do not endanger the patient's life [13].
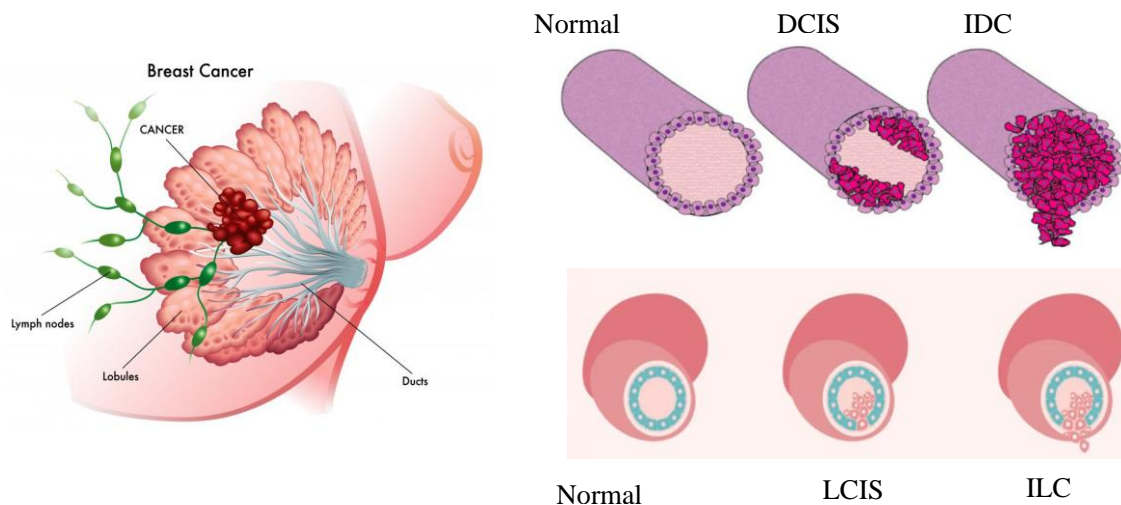
Fig. 2.1 Types of Breast Cancer

Mucinous, Paget, and mixed tumors, on the other hand, are malignant. Mucinous breast cancer, also known as colloid breast cancer, is a rare kind of invasive ductal breast cancer that affects fewer than 2% of all women. A mixed tumor has both ductal and lobular cells, both of which are cancerous in nature. A rare form of breast cancer known as Paget cancer gathers tumor cells in or near the nipple [32].

2.1.1. Non-Invasive Breast Cancer
(a) Ductal carcinoma in situ (DCIS)

DCIS is a non-invasive type of breast cancer in which cancer cells are contained within the milk ducts of the breast and are not spread to the surrounding healthy breast tissues. DCIS has a high cure rate and is considered highly treatable with a very high chance of success.

(b) Lobular carcinoma in situ (LCIS)

LCIS is the presence of cell changes in the lining of the milk-producing glands (lobules) in the breast. These changes have been linked to an increased risk of developing breast cancer in the future. While lobular neoplasia does not always progress to breast cancer, it does necessitate regular check-ups and monitoring.

2.1.2. Invasive Breast Cancer
(a) Invasive ductal carcinoma (IDC)

IDC are breast cancer cells that spread from the ducts and invade the surrounding breast tissue. IDC accounts for roughly 80% of all breast cancer cases, making it the most common type of breast cancer [33].

(b) Invasive lobular carcinomas (ILC)

ILC is characterized by breast cancer cells that spread beyond the lobules and invade the surrounding breast tissue. ILC accounts for approximately 10%-15% of all breast cancer cases [34].

2.2. Risks Involved in Breast Cancer

Breast cancer is a disease that affects women of all ages. Only 5-10% of all the women suffering from breast cancer have a mutant gene in recognized breast cancer (e.g., BRCA1 (BReast CAncer gene) and BRCA2). These hereditary mutations are not commonly reported in breast cancer patients.
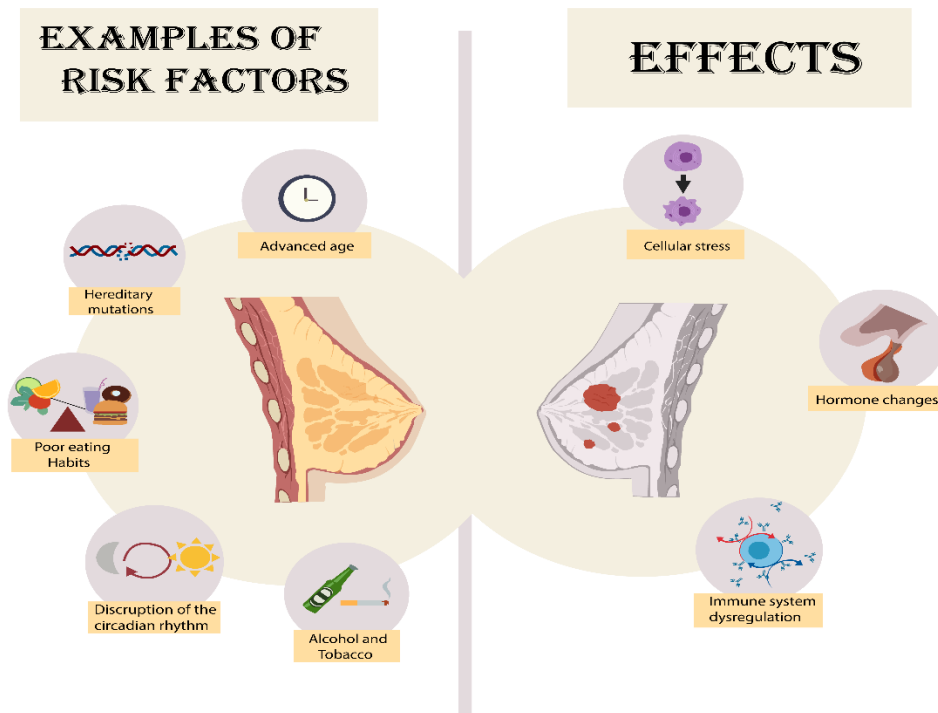
Fig. 2.2 Risk factors associated with breast cancer.

Fig. 2.2 depicts the different risk factors that may be responsible for breast cancer. Personal risk variables include age, family history, reproductive characteristics, previous treatments, and lifestyle [35]. Gender also has an impact on the likelihood of developing breast cancer. Being a woman is one of the most important risk factors for breast cancer development. As a woman gets older, her chances of developing breast cancer rise. Women who start menstruation late or early in menopause are at a slightly increased risk of developing breast cancer. A sedentary lifestyle, which is associated with alcohol intake and poor dietary habits can also cause breast cancer growth. This causes cellular stress, hormonal changes, and immune system dysregulation.

2.2.1. Risk Factors Associated with Breast Cancer
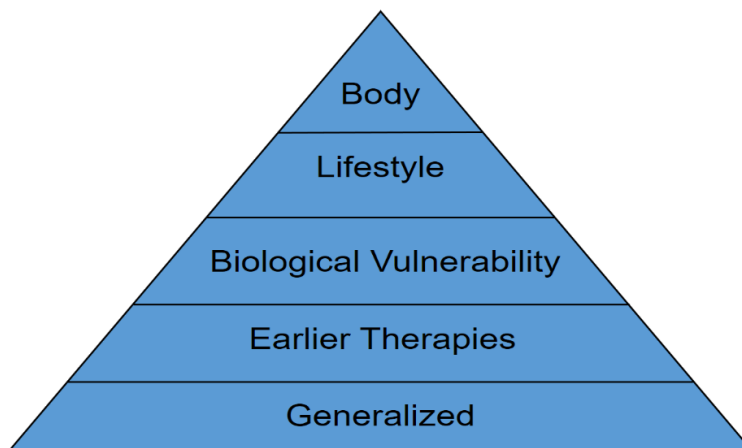
Fig. 2.3 Risk factors associated with breast cancer.

According to the American Cancer Society, many factors are responsible for enhancing the likelihood of breast cancer [19]. Fig. 2.3 depicts the risk factor associated with breast cancer. The well-known risk factors are age, family history, reproductive factors, earlier therapies, and lifestyle. A detailed description of these factors is mentioned in Table 2.3.

Table 2.1 Description of risk factors related to breast cancer.

Risk Factor	Factor	Explanation
Generalized	Gender	Being a female is perhaps the most critical risk factor for breast cancer growth.
	Age	The risk of breast cancer rises as the woman grows older.
	Race	Pretty much across the globe, white women tend to get breast cancer marginally more often than African American women.
Body	Menstrual history	The risk of breast cancer is marginally higher among women who start menstruation early (before age 12) and/or menopause early (after age 55). This rise in risk may have been caused by the progesterone and estrogen hormones being released longer in life.

	High breast density	Dense breast tissue means more tissue and less tissue is contained in the gland. The risk of breast cancer is higher for women with denser breast tissue.
	Not having offspring	Females who do not have babies or who were later pregnant might be more likely to develop breast cancer. Breastfeeding may contribute to reducing your risk of breast cancer.
	Weight	Fat tissue can increase estrogen after menopause, and high estrogen levels can increase the risk of breast cancer. Adult weight gain and excess corporeal fat may also be significant around the waist.
Lifestyle	Inactive Lifestyle	Breast cancer risk reduction is helped by physical activity.
	Alcohol	An increased risk of breast cancer is associated with consumption of alcohol. With alcohol consumed, the risk increases.
Earlier therapies	Therapy with DES	The risk of breast cancer is marginally higher for women who have been given DES (diethylstilbestrol) in the course of pregnancy.
	Hormone treatment after menopause	The risk of breast cancer is raised by the use of estrogen and progesterone during menopause.
Biological Vulnerabilit y	Family Background	A mother, sister, or daughter who experiences breast cancer may increase the risk.
	Ancestral Factor	Hereditary modifications (genetic changes) may increase risk in certain genes, such as the BReast CAncer gene (BRCA) 1 and 2.

2.3.   Challenges of Breast Cancer Detection Techniques

Breast cancer is a group of diseases in which the cells of the breast tissue change and break uncontrollably, resulting in a tumor or lump. Breast cancer screening techniques help with its detection. Breast cancer screening techniques aim to identify the position, size, and characteristics of the affected area and have proved to be excellent tools for extracting valuable information from vast amounts of data. Due to the discomfort involved, many women put off getting a diagnosis done for breast cancer. Most of the screening methods are invasive. Breast cancer screening without piercing the skin requires an alternative technique. The following are some of the significant issues that arise when applying breast cancer screening techniques:

- Uncomfortable screening methods

Direct body exposure to radioactive or ionizing radiation raises serious safety concerns. Many screening techniques use harmful waves that may cause allergic reactions or contraindications in some patients. So, it becomes important to develop systems that can use non-ionizing radiation and still provide accurate results.

- Need for a multimodal approach

Different imaging modalities have their strengths and weaknesses in detecting various types of tumors. By combining multiple imaging modalities, the overall sensitivity and specificity of the screening process can be significantly improved. This reduces the likelihood of false negatives and false positives, leading to more accurate diagnoses.

- Continuous change in model

In recent years, significant progress has been made in the detection of breast cancer using machine and deep learning techniques. However, the performance of these models can vary from applications to applications like preprocessing, segmentation, feature extraction and

classification. To address this, developing a generalized model for breast cancer detection is an important goal.

2.4. Breast Cancer Datasets

A variety of datasets is required to develop computational methods for breast cancer detection. Some datasets have a small number of features and tuples. Whereas others have many features and tuples. Researchers use a variety of breast cancer databases for the development and evaluation of computational methods. Some datasets are open to the public and some are limited to specific categories. Table 2.1 shows the detailed description of breast cancer datasets. Table 2.2 depicts the dataset used by researchers in recent years.

Table 2.2 Detail description of breast cancer datasets

Datasets	Ref.	Description	Resource	Comment
Mammographic Image Analysis Society (MIAS)	[36]	The database is available on 2.3GB 8mm (Exabyte) tape andcontains 322 digitized films. The database has been padded/ clipped and reduced to a 200-micron pixel edge, resulting in images that are all1024x1024.	Available at the Pilot European Image Processing Archive (PEIPA) at the University of Essex	Improves logistical practice, allows forthe use of computer-aided detection programs, and has a cancer detection rate comparable to that of the screen- lm mammography. It's unclear how this will affect recall rates.
Digital Database for Screening Mammography (DDSM)	[37]	The database is now fully functional, with 2620 cases. This is a mix of benign withouta callback, benign,normal, and cancervolumes that were specially selectedand digitized for DDSM.	The research community has made extensive use of the DDSM. It is kept at the Universityof South Florida so that it can be accessed via the Internet.	
IN breast	[38]	The images were taken at the Breast Centre in CHSJ, Porto,	IN Breast dataset can be requested online at	

		between 2008 and 2010, with approval fromboth the Hospital'sEthics Committeeand the NationalCommittee for Data Protection.	http://medicalresearch.ine scporto.pt/breastresearch/ index.php/GetINbreast Database.	
US1	[39]	The data came from an expert didactic media le for-breast screening specialists in 2001. The dataset contains 306 images with a mean image size of 377x396 pixels from various cases.	To acquire this dataset, the user must purchase it from Prapavesis et al.	
US2	[40]	This data was gathered in 2012 from the Parc Taul Corporation's UDIATDiagnostic Centrein Sabadell (Spain). The database contains 163 images from variouswomen, with an average image size of 760x570 pixels.	The breast lesions dataset is available on the internet (goo. gl/SJmoti) forresearch purposes.	Requires a skilled operator, the examination technique is not standardized, the interpretation criteria are variable, and microcalcificationsare not detected.
Breast Ultrasound Dataset	[41]	Breast ultrasound images from womenaged 25 to 75 years old were collectedat the start ofthe study. This information was gathered at Baheya Hospital in 2018. The total number of female patientsis 600. There are 780 images in the database, with an ordinary image size of 500x500 pixels.	https://cholar.cu.edu.eg/? q=afahmy/pages/dataset [42]	

Reference Image Databaseto EvaluateTherapy Response (RIDER)	[43]	Data was gathered to reach an initial agreement onhow to harmonize thecollection of data and analyze quantitative imaging techniques for assessingdrug or radiation therapy response.	https://wiki.cancerimagei ngarchive.net/display/Pu blic/RIDER+Breast+ MRI	In women at increased risk, it ismore sensitive andmarginally less specific than mammography. No radiation necessitates intravenouscontrast, which is time-consuming and inconvenientfor some women, such as those who have a pacemaker, aneurysm clips, or claustrophobia.
QIN Breast DCE-MRI	[44]	The breast DCE- MRI data set used for the study was collected provisionallyunder a HIPAA (Health Insurance Portability andAccountability Actof 1996)-compliant,Approval From theinstitutional Boardwith the exemption of consent.	https://wiki.canceri magingarchive.net/displa y/Public/QIN+ Breast+DCE-MRI	
DBT-TU-JU	[45]	There are 1100 breast thermogramsof 100 subjects in the DBT-TU-JU database. This research reflectsthe generation of ground truth images of the hotspot areas, whose presence in breast thermograms indicates the presence ofbreast abnormality, due to the necessity of evaluating any breast abnormalitydetection system.	Only patients andtheir physicians have access to private databases that are only accessible for internal purposes.	
DMR: Database For Mastology	[46]	Thermal and mammography imagesobtained by ourresearch groupare among the images available in this database. For a	DMR-IR is accessible on the website http://visual.ic.u .br/dmi	Not harmful, non-invasive, time-consuming,

Research		sample of 64 breasts, the accuracy was 100% (composed of 32 healthy and 32 unhealthy).		Requires more workto be done, still inpractice

Table 2.3 Breast cancer datasets used by researchers

Ref	Year	Dataset									
		MIAS	DDSM	INbreast	US1	US2	BUSI	ABUS	DCE-MRI	DBT-TU-JU	DMR
[47]	2015	✗	✗	✗	✗	✗	✗	✗	✓	✗	✗
[48]	2016	✓	✗	✗	✗	✗	✗	✗	✗	✗	✗
[46]	2017	✗	✗	✗	✗	✗	✓	✗	✗	✗	✗
[49]	2018	✗	✗	✗	✗	✗	✗	✗	✗	✗	✓
[40]	2018	✗	✗	✗	✓	✓	✗	✗	✗	✗	✗
[50]	2019	✗	✗	✗	✗	✗	✗	✗	✗	✗	✓
[51]	2019	✗	✗	✗	✗	✗	✗	✗	✗	✓	✗
[52]	2020	✗	✓	✓	✗	✗	✗	✗	✗	✗	✗
[53]	2020	✗	✗	✗	✗	✗	✗	✓	✗	✗	✗
[54]	2020	✗	✓	✓	✗	✗	✗	✗	✗	✗	✗

2.5. Breast Cancer Screening Techniques

Breast cancer awareness provides help to the affected people so that they can take better decisions about their health. Hormonal changes, genetics, breast density, and lifestyle have greatly affected the appearance of breasts. Understanding the morphology and physiology of usual breast tissue is essential for predicting any development of breast cancer and may

aid in the early diagnosis of abnormal lesions. Fig. 2.4 shows breast cancer detection in asymptomatic females.
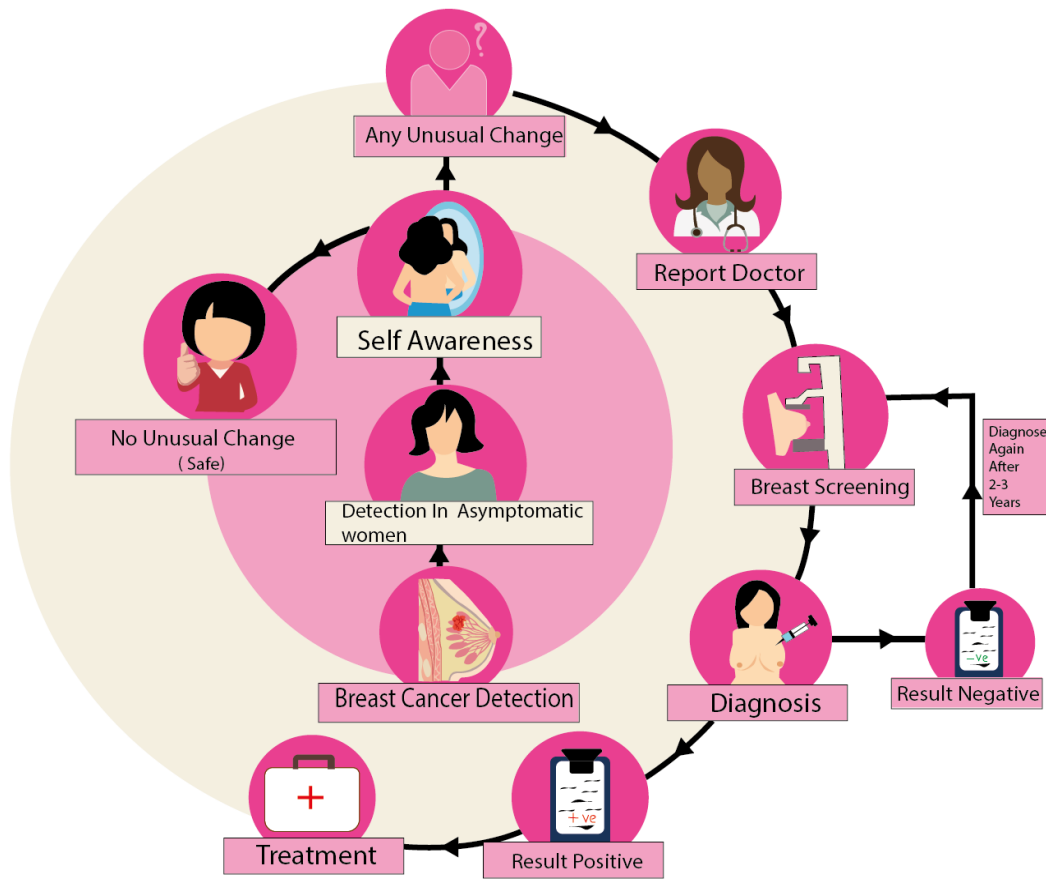
Fig. 2.4 Breast Cancer detection for asymptomatic women.

Breast cancer diagnosis entails a variety of screening techniques to improve the accuracy of diagnosis. The well-known breast cancer screening techniques are X-ray mammography, breast ultrasound, Magnetic Resonance Imaging (MRI), and Positron Emission Mammography (PEM) [20]. X-ray mammography is the most effective technique. Breast Ultrasound uses sound waves to create a picture of tissues inside the breast. However, this technique suffers from low specificity, high cost, and a lack of availability [30]. The accuracy of breast ultrasound is approximately 67.8%. MRI is another technique for breast cancer detection. It creates detailed images of organs by combining a large magnet, radio waves, and a computer. This technique has a higher sensitivity, however, high cost and low

specificity that can lead to overdiagnosis [30,55,56]. The accuracy obtained from MRI may lie in the range of 70% to 72%. PEM is an alternate method for breast cancer screening [55]. It has high specificity as compared to the other techniques. However, it suffers from low sensitivity and high radiation exposure. Breast cancer screening techniques are broadly categorized into three main groups such as physical, electrical, and mechanical (see Fig. 2.5).
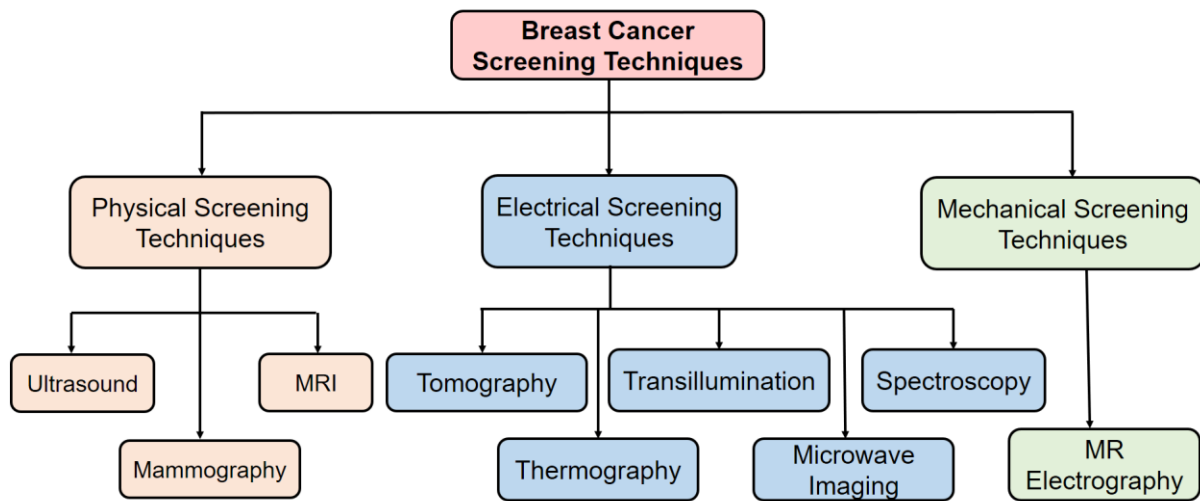
Fig. 2.5 Breast cancer screening techniques

2.5.1. Physical Screening Techniques

The well-known physical screening techniques are mammography, ultrasound, and MRI. A detailed description of these techniques is given in the succeeding subsections.

Mammography

Breast self-examination (BSE), Clinical breast examination (CBE), and mammography are commonly used screening techniques for breast cancer detection [57,58]. Nowadays, digital mammograms are widely used for breast cancer detection. In digital mammograms, X-rays are replaced with solid-state detectors that translate X-rays into electrical signals. It is also known as full-field digital mammography (FFDM). The detectors in digital cameras

are identical. Electrical impulses are used to create breast images and displayed on a computer screen [59]. Computer-aided detection (CAD) solutions are created to read mammographs. CAD systems usually interpret a mammogram and identify questionable places, which are investigated by the radiologist [60].

Ribli et al. [49] proposed a CAD program focused on Faster R-CNN. This program was able to classify malignant or benign tumors in a mammogram without user intervention. Wang et al. [52] proposed an end-to-end method for mammographic diagnosis. This approach eliminated manual preprocessing. The treatment of mammograms was introduced in one situation with a different approach focused on the Multiscale (MS) system and Multi-Instance (MI) system. MS module selects the basic features of mammograms, and the MI module took the general situation into account in one event. The output of these modules is combined to get better results. Heidari et al. [61] introduced a new computer-aided diagnosis (CADx) scheme based on the analysis of global mammographic image features. This research demonstrates the possibility to build a modern CADx mammogram high-performance global picture processing scheme. This technique is more effective and reliable than the previous techniques. Ekici et al. [50] utilized a convolution neural network (CNN) for thermographic breast cancer screening. They used five different processes namely, data acquisition, image processing, segmentation, extraction, and classification. CNN provides better results than the other techniques in terms of prediction results.

Ultrasound

Breast ultrasound is a common way to test for breast cancer as it allows the screening sensitivity can be increased in thick breasts [62–64]. Various deep-learning models have been used in the last two decades. Muñoz-Meza and Gómez [65] used ultrasound pictures to classify breast tumors using 3 M- dimensional sets of characteristics and principal component analysis with shared information. They addressed the segmentation process in

breast ultrasound images using a watershed transformation mechanism. The feature extraction method was used for the classification of breast cancer.

Qin et al. [66] proposed a computer-aided diagnosis method to detect cancer tumors and segmented the tumor region from ultrasound images automatically. But this method excludes normal images before segmentation. The probability of a case where a benign tumor may be considered a normal case cannot be ruled out and can be excluded. Tanaka et al. [67] developed a diagnostic system for detecting lesions in ultrasound pictures using deep learning approaches. They used a hybrid strategy for data preprocessing and achieved an accuracy of 75%. Wang et al. [68] suggested a breast cancer classification system based on CNNs. The system used InceptionV3 pre-trained model to facilitate feature extraction in ABUS imaging. The model demonstrated a method for obtaining multi-view features. The approach produced a 0.9468 area under the curve (AUC).

Lotfollahi et al. [69], present an effective and semi-automated segmentation approach for BUS images. This method has been applied to 36 breast ultrasound images. It generates true-positive and false-positive results, and similarity of 95%, 6%, and 90%, respectively. Liang et al. [70], propose an image augmentation method named super-pixel elastic deformation and employ a semantic segmentation convolutional neural network called mask region-based convolutional neural network (Mask R-CNN) to automatically segment breast lesions from ultrasound images and make the classification simultaneously. However, their performance may degrade due to a vanishing gradient. The limitation of this research work leaves the scope for further improvement.

Nyayapathi et al. [71] introduced a new photoacoustic tomography device that displays angiographic features with mammogram-like images of the breast. The mechanism portrays a highly compact breast of two flat, 2.25 MHz transceiver clusters of 128 components, and line optical fiber bundles from top to bottom. The soft compression is

done using silicone prints, which allows the woman more relaxed than the hard metal plate used with conventional mammograms. Dual Scan Mammoscope (DSM), is the technology that utilizes the properties of both ultrasound and photoacoustic tomography for breast cancer detection.

Magnetic Resonance Imaging

Magnetic resonance imaging (MRI) plays a significant role in the medical field. The scan in this method is used to produce detailed images of the inner body utilizing intense magnetic fields and radio waves [72]. MRI scans are being used to investigate nearly any area of the body including the brain, bones, breasts, heart, and even internal organs. MRI is widely used in breast cancer imaging. Sun et al. [73] identified glioma classification methods for the prediction of radio mics features. MRI extracted quantitative features from tumor areas. The modality of extraction by radio mics was greater than the other combinations of the tumor area. Whereas, Li et al. [74] used ultra-wideband microwave imaging for early breast cancer detection. They also used an ensemble empirical mode decomposition (EEMD) for direct extraction of tumors. Only isolated signals from as-detected waveforms are required for the reconstruction of the picture for tumor detection. They used MRI to create more precise models for electromagnetic analysis. Here, a tumor of 4 mm in diameter within the glandular or at the interface between fat and the gland has been shown by the proposed procedure. In case the glandular tissue has a bigger dielectric constant of 35, tumor reaction may also be identified. Their research showed that the solution presented could serve as an important alternative to direct tumor response extraction. Mahrooghy et al. [75] suggested the spatiotemporal dynamic properties of wavelets from dynamic contrast-enhanced magnetic resonance imaging (DCE-MRI) to quantify breast cancer intra-tumor heterogeneity.

Table 2.4 Classification of breast cancer detection using physical screening methods.

Ref.	Input	Classification model	Performance measures	Challenges	Advantages
[49]	mammography	Pre-processing+ Faster R-CNN+ Regional proposal network	AUC= 0.85 lesion detection sensitivity = 90%	The detection performance could only be evaluated on the small INbreast dataset	The model reaches high sensitivity with very few false positive marks
[52]	mammography	Pre-processing and image cropping+ CNN for feature selection+ multi-instance module+ final diagnosis of the whole case	AUC= 0.865	In the future author could assist other advanced applications, such as size measurement, lesion characterization	Their method learned the unique features of lesions via the multiscale module.
. [76]	mammography	Pre-processing + CS-LBP features from each 2 × 2 blocks in Wavelet Domain + SVM-RFE based feature selection + Random Forest classification	Acc: 97.25%, P: 97.3%, Rc: 97.2%, F1: 97.2% MCC: 94.1% ROC Area: 97.61%	The author can further classify the type of tumor	Fast feature extraction, small feature dimension, fast modeling, and prediction
[54]	mammography	Image enhancement and segmentation + DenseNet169 for feature extraction + Region-based Group-max Pooling+ Prediction	(INbreast)RGP: AUC= 0.934 and GGP: AUC= 0.924 (CBIS-DDSM) RGP: AUC= 0.838 and GGP:AUC=0.823	The results of the visualization show that the proposed model can roughly locate suspicious regions.	The ability to learn lesion location information

[77]	mammography	Pre-processing + feature extraction + deep multi-view Classifier	AUC=0.895	AUC could be increased	Their model could improve radiologist sensitivity for breast cancer detection
[53]	Ultrasound	Pre-processing + pre-trained UNet + DDS feature extraction + TM	Sn = 95% with 0.84 false positives per volume.	In the future author could assist other advanced applications, such as size measurement, lesion characterization	High sensitivity and low false positives
[61]	Mammogram	Image segmentation + SSIM feature extraction + DCT feature extraction + FFT feature extraction + SVM classifier	AUC= 0.85-0.91(from one of the three sub categories) AUC= 0.96±0.01(in three sub categories)	Its clinical utility or impact on radiologists' performance in the diagnosis of breast cancer using mammograms has not been tested.	significantly higher performance with AUC
[8]	X-ray + MRI + CT + Ultrasound	HA-BiRNNs	AUC: 0.8854 RC: 0.8771 F1score of prediction:0.9070	The author wishes to develop methods to interpret the representation learned by the Knowledge-powered Deep	The method achieves higher performance

				Breast Tumor Classification model to classify malignant and benign tumor pattern	
[74]	MRI	Pre-processing + canny edge detection technique for boundary selection + Antenna Arrangement and Simulation Process + Extraction of tumor response signals + Result	N/A	Their method offers efficient detection even for a tumor of 4 mm diameter located within the glandular or at the interface between the gland and fat.	They state that their approach can be an effective alternative to direct extraction of the tumor response
[47]	MRI	Pre-processing + DCE-MRI (wavelet transform) + Heatwave feature extraction + classification	(AUC=0.88 HetWave vs. 0.70 standard features). The combination of HetWave and standard features further increase classifier performance (AUCs 0.94)	HetWave could assist other advanced applications such as the feature extraction approach for characterizing tumor heterogeneity, providing valuable prognostic information.	Superior ROC AUC

[78]	MRI	Data Acquisition + Image Preprocessing + Co-Occurrence Analysis Computing Framework + Neural Network Classifier + Hypothesis Testing	TPF= 0.90 FPF= 0.09	The author could help with more advanced applications in the future, such as size measurement and lesion characterization.	It investigates heterogeneous tumors by separately distinguishing the benign and necrotic tissues within a lesion having malignancy
[79]	Mammogram	Pre-Processing + Fuzzy C-means thresholding-based image segmentation + Hybrid Feature Extraction + Feature Selection + Classification	SVM-MLP classifier: 87% Acc, 95% Sn, and 75% Sp SFS-KNN: 87.50% Acc, 95.83% Sn, and 62.50% Sp	Some SVM classifiers are not capable of classifying the negative sample	GA-MI-based feature selection of the SVM classifiers for MLP, linear, and quadratic classifiers are performing better
[30]	Ultrasound	Pre-Processing + Construction of biomechanical model + Image registration + Image fusion + Analysis of USCT images + Result	-	The current limitation of their method is that overall accuracy is not improved with heterogeneous stiffness distribution models.	Smaller training and test error rates.

The receiver operating characteristic (ROC) and area under the curve (AUC) were computed to assess the performance of the classifier using leave-one-out (LOO) cross-validation. The combination of a heatwave and standard features can further enhance the performance of the classifier [80]. Table 2.4 summarizes the physical screening techniques for breast cancer.

2.5.2. Electrical screening techniques

Impedance spectroscopy, thermography, transillumination, microwave imaging, and tomography are well-known electrical screening techniques. A detailed description of these techniques is given in the succeeding subsections.

Impedance Spectroscopy

Researchers are using this technique to improve breast cancer detection techniques. Haeri et al. [81] introduced two experimental breast cancer screening instruments namely, the electrical impedance spectroscopy (EIS)-Probe and the EIS-Hand-Breast (EIS-HB). EIS-Probe and EISHB systems were able to assess the electrical properties of breast tissue. Cancerous tissues were identified by determining the change in parameters of healthy tissues. Huerta-Nuñez et al. [82] utilized bioimpedance spectroscopy to investigate the cancer cells in an aqueous media. Experimental results revealed that impedance spectroscopy has sufficient sensitivity for the identification of extraordinarily low cancer cell composition in an aqueous solution. Lederman et al. [83]. Improving breast cancer risk stratification using resonance-frequency electrical impedance spectroscopy through the fusion of multiple classifiers designed a seven-probe resonance-frequency-based electrical impedance spectroscopy (REIS) system and used the data of 174 females. Artificial neural network (ANN), support vector machine (SVM), and Gaussian mixture model (GMM) were used. The results revealed that ANN attained the maximum values of ROC and AUC as compared to the other classifiers. REIS examinations provide the relevant information to

build a classifier for the stratification of breast cancer risk. Ward et al. [84] evaluated the inter-arm impedance ratio range for evaluating the value of threshold as a standard for detecting lymphedema associated with breast cancer. When an impedance of 1,106 is surpassed by a danger to the neuronal limb and 1,134 when the dominant limb is in danger, relative to those currently in use of 1,066 and 1,139, the existence of lymphedema is recorded. The variation in these values can be considered as a minor significance towards the clinical practice.

Thermography

A special camera is used to measure skin temperature on the surface of the breast and is known as thermography. It is a non-invasive and radiation-free research [85]. Ekici et al. [50] developed an automatic breast cancer detection technique. They used image processing and analytics techniques to analyze the thermal images of the breast. The feature extraction algorithm was proposed to extract the features for the identification of breast images as regular or suspicious. Their technique attained an accuracy of 98.95% for the thermal images of 140 females. Jose-Luis et al. [86] proposed a technique to solve the inverse thermal transfer problem in the Levenberg Marquardt algorithm. This technique was used to identify and locate malignant tumors within the breast using a patient-specific digital breast model and clinical infrared imaging (IRI) images. Digital heat amplification systems were used to tackle the challenges that occurred during the identification of the size and position of malignant tumors within the breast. This technique can be combined with mammography to detect breast cancer, especially in the case of dense breasts. In [87], advancements in thermography-based techniques were investigated for breast cancer detection. It is observed from breast thermograms that breast cancer signs can be detected through the asymmetrical thermal spreads between breasts. Their study showed that the neural network systems enhanced the prediction accuracy of breast cancer thermograms.

Mambou et al. [88] explored infrared digital imaging techniques for breast cancer. The basic assumption in this technique is the increase in thermal activity in the precancerous tissues and the areas surrounding developing breast cancer. They concluded that infrared image processing techniques require a CAD system for detection. Roslida et al. [54] studied the three convolutional neural network (CNN) models namely, ResNet101, DenseNet201, MobileNetV2, and ShuffleNetV2 for breast cancer detection. Database for Mastology Research (DMR) was used to evaluate the performance of the above-mentioned models. DenseNet201 was capable of classifying both static and dynamic images.

Transillumination

Transillumination is a procedure used in an organ or part of the body to detect anomalies. The examination is conducted in a dark room with a light-reflecting on a particular body segment to look under the skin [89]. It is an invasive method and is not being used much nowadays.

Microwave imaging

Microwave imaging is a promising method for detecting early-stage breast cancer [90]. Li et al. [91] proposed a direct tumor response extraction technique based on the ensemble empirical mode decomposition for early breast cancer detection. The extracted signals were used to reconstruct the image for tumor detection. M. diFlorio [92] designed some enhancements in both hardware and software for microwave breast imaging. The hardware monitors the signals down to sub-centimeter screen resolution compatible with a test time of less than 2 minutes. The software resolves the huge time workload and produces accurate images in less than 20 minutes. They were able to produce the first microwave tomographic images. Klemm et al. [90] studied the imaging of inhomogeneous breast phantoms for microwave breast cancer. They introduced an image enhancement algorithm,

which utilizes the concepts of the delay and sum algorithm (DAS) and coherence factor. Their proposed approach was able to reduce clutter and provide better images as compared to the previous techniques. Tuncay et al. [93] presented an effective way to design 3D microwave models. Yin et al. [94] suggested ultrawideband radar imaging for breast cancer detection. A robust and Artifact Resistant (RAR) algorithm was developed to overcome the negative effects of both artifact and glandular tissues. RAR enhanced the identification capacity, robust artifact resistance, and high detection range.

Tomography

Tomography is a technique that creates images of single planes of tissue. Kao et al. [95] studied Electrical Impedance Spectroscopy (EIS) to locate and differentiate cancer from normal tissues and benign tumors. The tumors are different from the normal tissue in terms of their conductivity and permittivity. The high contrast tissue, which occurs between several kHz and several MHz, can be able to distinguish malignant from benign. In a silicone phantom breast, the system can detect a 10 mm tumor. Baran et al. [96] investigated the potential clinical usability of phase-contrast micro-computed tomography (micro-CT) with high spatial Resolutions. SYRMEP beamline of the Elettra Synchrotron was scanned with 10 breast tissue specimens of 2 mm in diameter using the phase-contrast micro-tomography propagation method. The high-resolution images were able to provide detailed tissue design assessment at a close-to-histological level. Table 2.5 summarizes the electrical screening techniques in terms of performance measures and datasets.

Table 2.5 Classification of breast cancer detection using electrical screening techniques

Ref.	Technique Used	Classification model	Performance measures	Challenges	Advantages
[97]	Tomography	Image-Based 3-D Surface Reconstruction + Model-Based Segmentation of Breast + Data Collection and accuracy evaluation + Result	The system can detect a 10 mm tumor in a silicone phantom breast	A limitation of these dense optical flow techniques is their sensitivity to the lighting variation	Their system can reconstruct the breast surface with average errors of less than 1 mm
[81]	Tomography	Two innovative instruments setups for the early detection of breast cancer were used	Method exposes promising validity in comparison to other breast cancer detection tools	The LSM error function has not been used due to its higher sensitivity	Promising validity
[50]	Thermography	Data acquisition + preprocessing + segmentation + feature extraction + CNN classifier	98.95 % Testing Accuracy	The author can further classify the type and size of the tumor	Obtained good accuracy rate was obtained for the thermal images
[86]	Thermography	Breast imaging + Patient-specific digital breast model + extract temperature of a region of interest + levenverg-marquardt algorithm	The screening technique is found to be more accurate and harmful radiation-free	Requires more computation time	The technique has the potential to be an accurate adjunct to mammography

[92]	Microwave imaging	combination of hardware and software to create 3-D microwave tomographic images of the breast	The hardware used in this work has the capability of gathering data up to 3 GHz	The results can be improved by operating at higher frequencies and/or using a multi-frequency approach over an ultra-wideband.	Its advantage is its specificity driven by the wide range of dielectric properties
[93]	Microwave imaging	Preprocessing of MRI data + Bias Field Correction + Segmentation of Two Main Tissues + Electromagnetic Properties Mapping +Building the 3-D Structure	The test conducted was successful	Work could be done to improve the correlation between mammographic density and the MRI density	More consistent to classify ARN-MBPs with BTI score rather than ACR classification.
[83]	Impedance Spectroscopy	Breast REIS + mirror matched feature extraction + ANN/SVM/GMM + fusion	ANN classifier was found to be the best single classifier among the three tested classifiers, with an AUC of 0.81 and sensitivity of 75% at 80% specificity.	The main limitation of their work is a smaller sample size.	The REIS-based classification decisions are consistent with biopsy recommendations

2.5.3. Mechanical Screening Techniques

MR elastrography is a well-known mechanical screening technique. A detailed description of this technique is mentioned in the succeeding subsection.

MR Elastrography

In [98], electromechanical operators vibrate the breast in MR electrography and produce acoustic sound waves. An algorithm was used to produce quantitative images from these waves. This technique was evaluated on six healthy people and six patients. then described by MRI. Goddi et al. [99] presented a review on breast elastography. They discussed future techniques, which are not yet in clinical practice. Table 2.6 depicts the classification of breast cancer detection using MS Elastography.

Table 2.6 Classification of breast cancer detection using MS Elastography

Ref.	Screening Technique	Classification model	Performance measures	Challenges	Advantages
[98]	MR Elastography	Acoustic shear waves generating device + elasticity imaging + an algorithm for processing the wave images to generate quantitative images depicting tissue stiffness + prototypic breast MR elastography technique + results	The results confirm the hypothesis that the prototypic breast MR elastographic technique can quantitatively depict the elastic properties of breast tissues in vivo and reveal high shear elasticity in known breast tumors	Considerable scope exists for technical improvement to determine the possible performance of an optimized MR elastographic technique in terms of resolution and quantitative accuracy	Their work shows that it is feasible to use a technique combining MR imaging and acoustic technologies

2.6. Performance Evaluation Measures

Different performance measures are used to evaluate the performance of breast cancer prediction models. The performance measures are generally classified into two main categories namely, prediction and classification measures [100]. Fig. 2.6 shows the classification of performance measures.
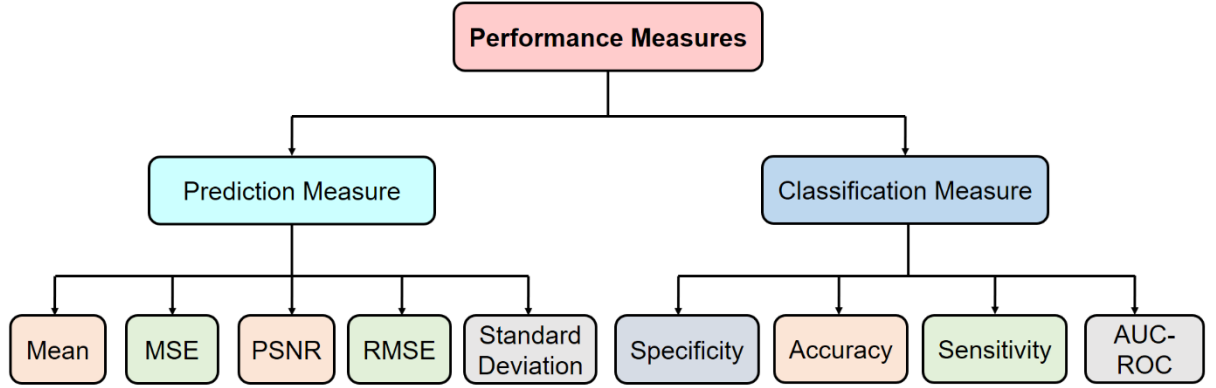
Fig. 2.6 Classification of performance measures.

2.6.1. Prediction Measures

Mean, standard deviation, mean square error (MSE), root mean square error (RMSE), and peak signal-to-noise ratio (PSNR) are well-known prediction measures. The mathematical formulation of these measures is given in succeeding subsections.

Mean (μ)

Mean represents the average brightness of an image. If the average intensity of a breast cancer image is much high, then the density of tissue is also high. The mathematical formulation of the mean (μ) is defined as [101]:

$$\mu = \frac{1}{mn} \sum_{a=1}^{m} \sum_{b=1}^{n} pA(a, b) \tag{2.1}$$

Where m and n signify the number of rows and columns in an image. pA is the coefficient of approximation. The value of the mean should be high for better results [101].

Standard Deviation (σ)

Standard deviation (σ) can be described as a measure of how much the contrast intensity increases when the texture irregularity increases [102]. It is defined as:

$$\sigma = \sqrt{\frac{1}{mn} \sum_{a=1}^{m} \sum_{b=1}^{n} (pA(a,b) - \mu)^2} \qquad (2.2)$$

Mean Square Error

The differential between observed and predicted values is measured using the mean square error (*MSE*) [103]. The mathematical formulation of *MSE* is given below:

$$MSE = \frac{1}{mn} \sum_{a=1}^{m} \sum_{b=1}^{n} \left(I_o - I_p\right)^2 \qquad (2.3)$$

Where I_o and I_p denote the observed and predicted values, respectively.

Root Mean Square Error

The square root of the second moment of difference between the observed and predicted values is known as root mean square error (*RMSE*) [104]. It can be defined as the standard deviation of prediction errors.

$$RMSE = \sqrt{\frac{1}{mn} \sum_{a=1}^{m} \sum_{b=1}^{n} \left(I_o - I_p\right)^2} \qquad (2.4)$$

RMSE is a reliable indicator of the accuracy obtained from the prediction model. *RMSE* has a non-negative value at all times. It is proportional to the scale. It is sensitive toward the outliers.

Peak Signal-to-Noise Ratio

Peak signal-to-noise ratio (PSNR) is the ratio of an image's maximum achievable power to the power of degrading noise that influences its representation quality [105].

$$PSNR = 10\log_{10} \frac{(l-1)^2}{MSE} \qquad (2.5)$$

Here, l is the number of highest allowable intensity levels in an image.

2.6.2. Classification Measures

The performance of the breast cancer prediction model is evaluated by using classification measures. These measures are positive predictive value, sensitivity, accuracy, specificity, and area under receiver operating characteristics. The mathematical formulation of these measures is mentioned in the succeeding subsections.

Positive Predictive Value (PPV)

Positive predictive value (PPV) is the fraction of suitable instances among the recovered instances [106]. It is also known as Precision and is defined as:

$$PPV = \frac{TP}{TP+FP} \tag{2.6}$$

Here, TP is the number of true positives and FP is the number of false positives, respectively. The true positives are the positive tuples that the prediction model accurately predicts. The false positives are the negative tuples that the model predicts incorrectly. The value of PPV lies in the range of [0, 1].

Sensitivity

Sensitivity (S_n) is a metric for assessing the efficacy of breast cancer detection prediction models. S_n is also known as the rate of recognition [106]. It specifies the percentage of positive tuples that the prediction model successfully predicts.

$$S_n = \frac{TP}{TP+FN} \tag{2.7}$$

Here, FN shows the number of false negatives. The false negatives are the positive tuples that the prediction model predicts incorrectly.

Accuracy

The percentage difference of projected synergy scores from observed results within the allowable error range is called accuracy [106]. It is defined as:

$$A_{cc} = \frac{(TP+TN)}{(TP+TN+FN+FP)} \times 100 \qquad (2.8)$$

Here, *TN* represents the number of true negatives. The term "true negative" refers to negative tuples that the prediction model accurately predicts.

Specificity

The true negative rate is used to describe the specificity. It refers to the percentage of negative tuples properly predicted by the prediction model [107].

$$S_p = \frac{TN}{TN+FP} \qquad (2.9)$$

Area Under Receiver Operating Characteristics Curve

Receiver Operating Characteristic (ROC) represents the tradeoff between the true positive rate (TP_r) and the false positive rate (FP_r) [107]. The false positive rate and true positive rate are represented by the x-axis and y-axis of the ROC curve, respectively. The area under the ROC curve (AUC-ROC) is a metric for computing the model accuracy. The value of AUC-ROC lies in the ranges of [0.5, 1].

$$TP_r = \frac{TP}{TP+FN} \qquad (2.10)$$

$$FP_r = \frac{FP}{FP+TN} \qquad (2.11)$$

2.7. Summary

This chapter considers the general perspectives and background of one of the world's most significant threats – breast cancer, focusing on the challenges of offering early diagnosis and qualified treatment. From here it is quite clear that breast cancer is a disease that affects women, but men and transgenders are also at high risk; this makes breast cancer a disease

with social, economic, political, cultural and even religious impacts. This chapter deliberates on how the accuracy rate of the diagnosis could be boosted. These technologies because of the capacity to handle large volumes of data can detect such patterns and anomalies which may not be apparent if the conventional method of analysis is used, thus making the identification of mammary carcinoma less intrusive. The chapter also underlines the need for improving many current screening methods and also for one topic advocating the need to tailor treatment according to tumor characteristics.

CHAPTER 3
Literature Review

3.1. Survey Methodology

This section presents the survey papers related to breast cancer detection techniques.

3.1.1. Existing Surveys

In the recent past, several research papers were published to summarize breast cancer detection techniques. The relevant survey papers are discussed below:

Yassin et al. [108] presented the findings of a systematic review (SR) aimed at determining the current state-of-the-art computer-aided diagnosis and detection (CAD) systems for breast cancer. They provided a broad assessment of CAD systems for image modalities and machine learning-based classifiers. Prospective research studies to develop more objective and efficient CAD systems have been discussed. A brief review of various reported methods and systems for early breast cancer detection was presented by Gupta et al. [109]. A variety of microwave imaging approaches such as microwave tomography and radar-based imaging were investigated. Lu et al. [110] presented some diagnostic imaging methods for breast cancer diagnosis. Breast cancer detection using computer vision and machine learning techniques was investigated. The performance of various methods was analyzed on mammographic images. Huppe et al. [111] presented a comprehensive review of molecular breast imaging. Their research covered the current literature, indications, clinical application, screening techniques, integration into medical practice. Oyelade et al. [112] analyzed various deep-learning methods for the detection of architectural distortion from digital mammography. The focus of their study was the detection of abnormalities such as masses and micro-calcification, which are indicators of the disease's advanced

stage. Husaini et al. [113] studied the use of thermography and artificial intelligence techniques for breast cancer detection. Various deep learning models such as Radial Basis Function Networks (RBFN), K-Nearest Neighbors (KNN), Probability Neural Networks (PNN), Support Vector Machine (SVM), ResNet50, SeResNet50, V Net, Bayes Net, Convolutional Neural Networks (CNN), Convolutional and De-Convolutional Neural Networks (C-DCNN), VGG-16, Hybrid (ResNet-50 and V-Net), ResNet101, DenseNet, and InceptionV3 were analyzed to process thermographic images of breast cancer. Some research works discussed breast cancer in transgender patients [17–20,114]. The qualitative analysis was performed on patient demographics, breast cancer characteristics, breast cancer presentation, and management. According to their study, breast cancer present in transgender men mainly depends upon the top surgery.

Due to advancements in deep learning techniques for medical imaging, a need was felt to prepare a survey of research articles summarizing the applications of deep learning techniques for breast cancer detection. Our survey presents computational studies on breast cancer detection over the last decade, i.e., from the year 2000 to 2023.

3.1.2. Survey Methodology

This study on breast cancer detection is conducted through PRISMA [109–111,115–117]. The reason behind the use of PRISMA is that it covers a list of recommendations designed to increase the quality of publications of systematic review and meta-analysis. It involves a structured four-phase process: identification, screening process, and criterion respectively for the selection and inclusion. At this phase, the focus is directed to search for as many articles as possible that are related to the field of study in the various databases and sources. The first step in this procedure is to wave off the replicate studies, and the other studies that do not meet the defined parameters made for consideration based on title and abstracts. During the eligibility phase, certain subsequent articles are assessed and if not in

compliance with the goals of the review they are excluded. The process of finally choosing the studies is called the inclusion phase in which the researcher picks up all the studies that meet all the specifications for the general analysis. Like most other guidelines, PRISMA also has a checklist where the process of including the studies is described by a flowchart. This approach makes it possible to have a standard way of tackling systematic reviews and hence increases the reliability and the reproducibility of the research hence improving the results attained.

Four different databases namely Google Scholar, Scopus, PubMed, and Preprint platforms have been used for this study. Four preprint platforms namely ArXiv, TechRxiv, MedRxiv, and ChemRxiv have been used to search for appropriate papers. The search string consisted of "breast cancer" or "cancer" or "((deep learning) AND (breast cancer))" or "((machine learning) AND (breast cancer))" or "((Artificial Intelligence) AND (breast cancer) AND (detection techniques))" or "breast cancer detection techniques". Fig. 3.1 shows the search string used for searching. A manual search was also conducted to find out the relevant research papers. In the identification phase, a total of 1600 research publications were chosen.
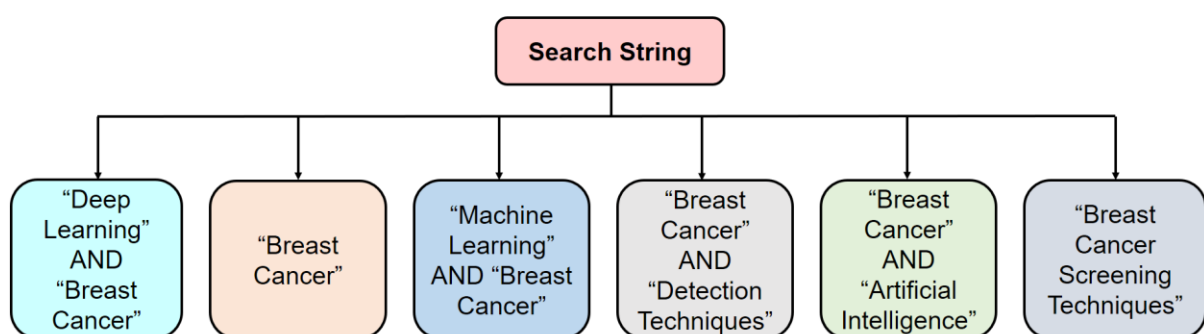
Fig. 3.1 Search string for searching the research articles.

In the screening phase, 900 research articles were selected after the removal of unsuitable, duplicate, and irrelevant research articles. 750 research articles were excluded after reading the title, abstract, and introduction. The remaining 150 research articles were analyzed

through removal criteria and 90 research articles were excluded. Thereafter, 60 research articles were moved to the next phase. In the eligibility phase, 30 research articles were eliminated after the evaluation of all the papers. Ultra-wideband radar imaging [118], ensemble empirical mode decomposition by the ultra-wideband [74], flexible 16 antenna array for microwave [15], and Ion-Sensitive Field-Effect Transistor based CMOS integrated Lab-on-Chip system [119] are a few related schemes other than deep learning, used for detection of breast cancer. The research articles on these techniques were also eliminated. 30 research articles were designated for review of breast cancer detection techniques. The selection and removal criteria for research articles are mentioned in Table 3.1. Fig. 3.2 depicts the different phases of PRISMA for this review.
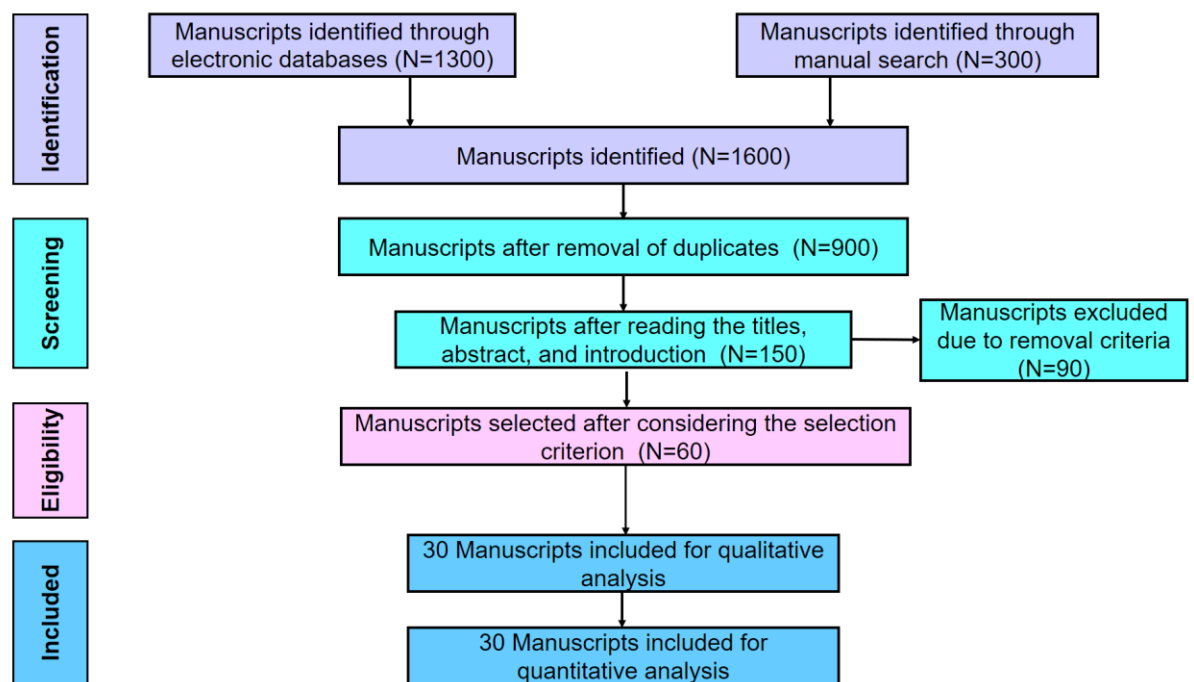
Fig. 3.2 PRISMA flow diagram on breast cancer review strategy.

Table 3.1 Selection and removal criteria for Selection of research articles.

S. No.	Parameter	Selection Criteria	Removal Criteria
1	Time duration	Research articles published from 2010-2021	Research articles published before 2010
2	Analysis	Research articles including breast cancer detection	Research articles including different cancer detection
3	Comparison	The research article focuses on deep-learning techniques used for breast cancer detection	The research article focuses on other techniques used for breast cancer detection
4	Study	Research involving mathematical foundation and experimental results	Research involving case studies and articles in different languages other than English

3.1.3. Research Question Asked by Researchers

The work in this chapter addresses several breast cancer detection-related questionnaires, some of which are listed in Table 3.2.

Table 3.2 Research questions related to breast cancer detection.

Questions	Research Questions
Q1	What is breast cancer?
Q2	Explain breast cancer in females, males, trans males, and trans females, along with detection techniques.
Q3	What are the risk factors associated with breast cancer?
Q4	What are the different types of screening methods involved in breast cancer detection?
Q5	What are the different types of deep learning techniques in breast cancer detection?

Q6	What are the performance evaluation measures for validating deep learning-based breast cancer detection techniques?
Q7	What are the challenges of breast cancer detection using deep learning?
Q8	What are the future research directions for breast cancer detection using deep learning?
Q9	What is the role of deep learning in breast cancer detection?
Q10	How breast cancer detection using deep learning is different from the other approaches?

Table 3.3 summarizes the comparison between the existing surveys and the proposed one in terms of research questions. In this table, ✓ denotes that the survey has answered the respective research question, while ✗ indicates otherwise.

Table 3.3 Comparative analysis of survey papers on breast cancer detection in terms of research questions.

Survey	Review Year	Research Questions									
		Q1	Q2	Q3	Q4	Q5	Q6	Q7	Q8	Q9	Q10
Yassin et al. [108]	2018	✓	✗	✗	✓	✓	✗	✗	✓	✗	✗
Gupta et al. [109]	2020	✓	✗	✗	✓	✗	✗	✗	✓	✗	✗
Lu et al. [110]	2018	✓	✗	✗	✓	✓	✓	✗	✗	✗	✗
Huppe et al. [111]	2017	✓	✗	✗	✓	✗	✗	✗	✗	✗	✗
Oyelade et al. [112]	2020	✓	✗	✗	✗	✓	✓	✓	✓	✗	✗
Husaini et al. [113]	2020	✓	✗	✗	✓	✓	✗	✓	✓		✓
Hartley et al. [114]	2018	✓	✓	✗	✗	✗	✗	✗	✗	✗	✗
Stone et al. [17]	2018	✓	✓	✗	✗	✗	✗	✗	✗	✗	✗
Proposed study	2021	✓	✓	✓	✓	✓	✓	✓	✓	✓	✓

3.2. Deep Learning Techniques for Breast Cancer

This section presents the importance of deep learning in the field of breast cancer followed by the classification of deep learning-based breast cancer detection techniques.

3.2.1. Importance of deep learning in breast cancer

The literature reports that machine learning is a widely used technique for breast cancer research. K-Nearest Neighbor (KNN), support vector machines (SVM), and naive Bayes classifier perform better in their respective fields. However, the tracking and detection processes in machine learning are done manually. For efficient cancer detection, the system needs to process 200 to 300 cells per frame, which is not possible through manual tracking. Hence, there is a need to develop efficient methods for breast cancer detection. Whereas deep learning can identify complex patterns in raw data. Nowadays, deep learning is widely used to identify breast cancer. According to a study published in Nature Medicine, deep learning models are capable of detecting breast cancer one to two years earlier than those with the standard clinical methods [120] would have. Deep learning models can learn the most relevant features to solve the problem optimally. Due to this, deep learning models can serve as the best hierarchical feature extractors [121]. The above-mentioned facts motivate the researchers to use learn and hence apply deep learning techniques for breast cancer detection.

3.2.2. Deep learning-based breast cancer detection techniques

Deep learning architectures are successfully used in the detection of breast cancer. Fig. 3.3 shows the general framework for breast cancer detection using deep learning techniques.
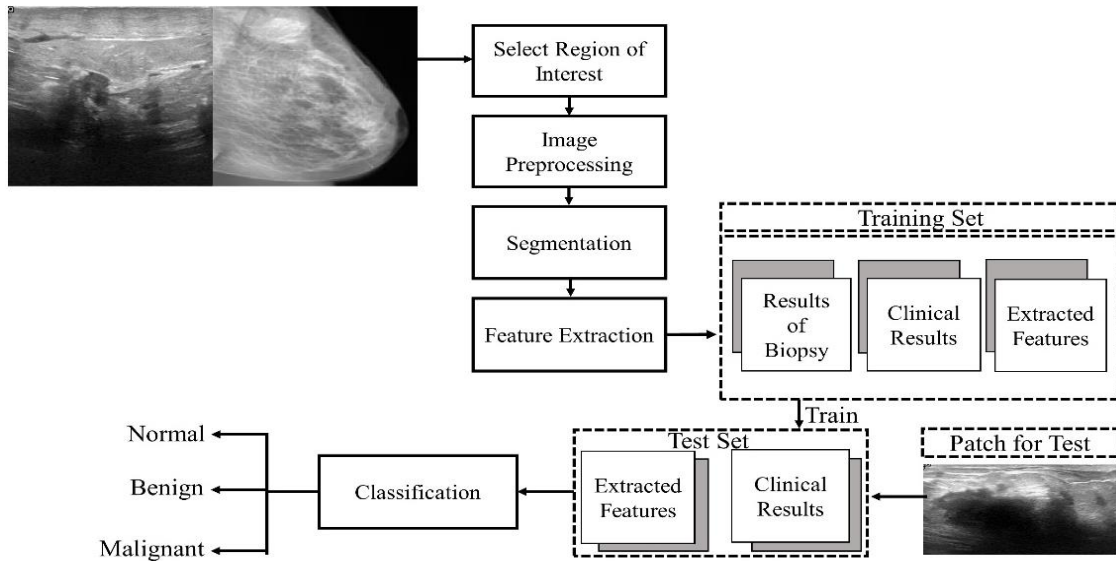
Fig. 3.3 General framework for breast cancer detection using deep learning.

Breast cancer detection techniques are broadly categorized into four classes such as image enhancement, lesion segmentation, feature extraction, and classification techniques (see Fig. 3.4). Deep learning techniques are used in the fourth category, i.e., classification.
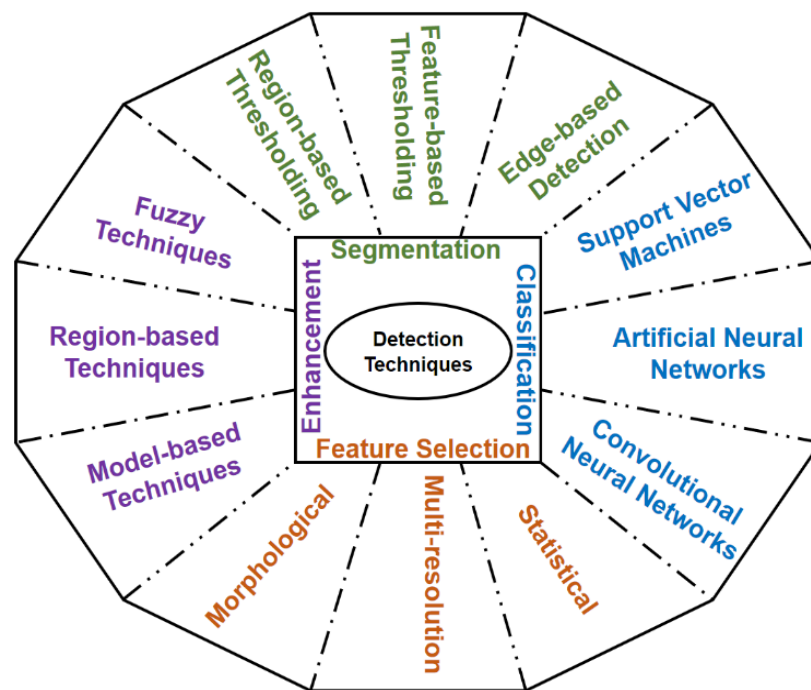
Fig. 3.4 Classification of Breast Cancer Detection Techniques.

Fig. 3.5 shows the connection of authors with the deep learning techniques that have been used for breast cancer detection for the last 5 years.
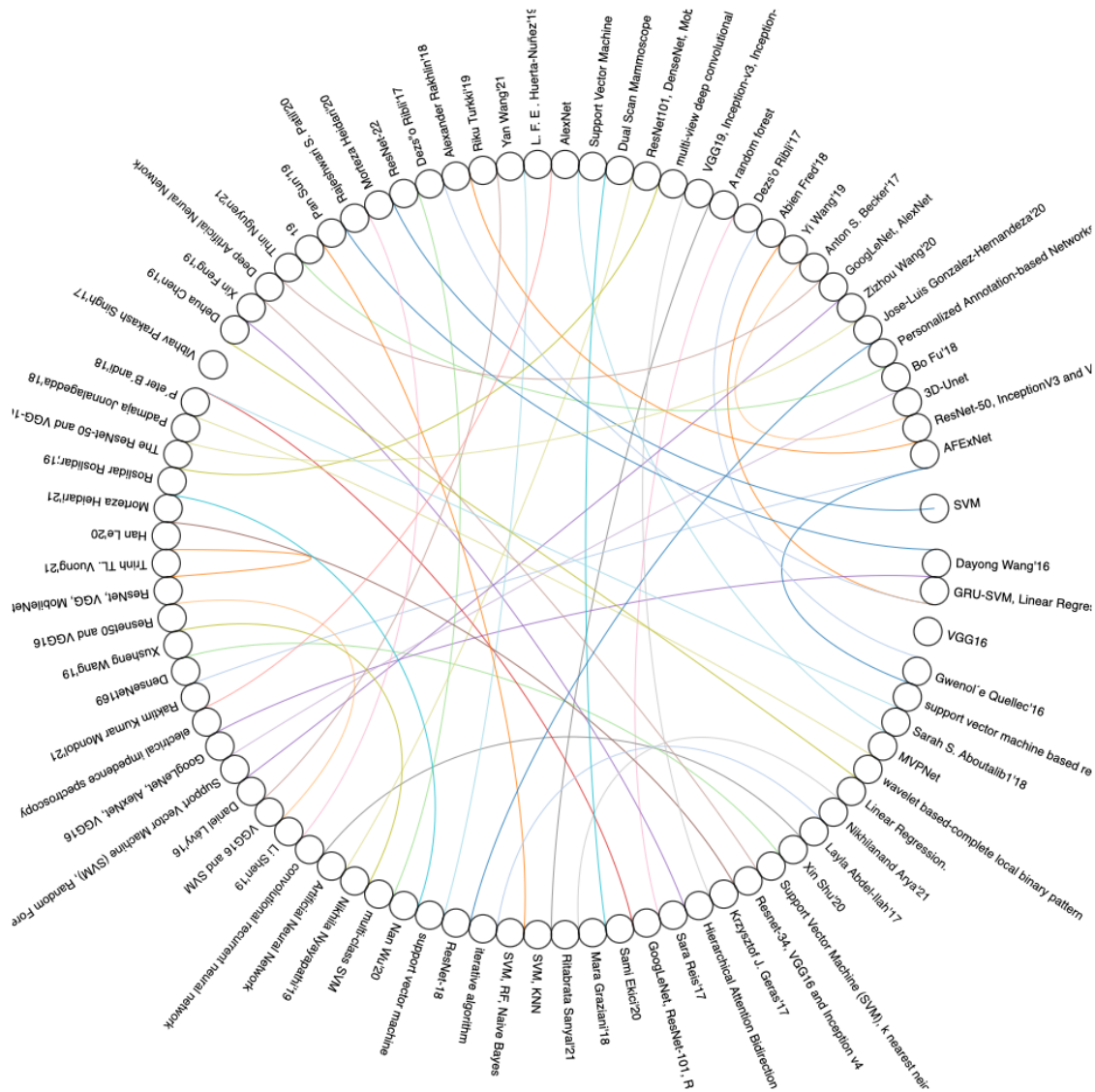
Fig. 3.5 Chord chart showing the connection of the author with deep learning and machine learning techniques from the last 5 years.

Wang et al. [52] used ResNet-50 to detect breast lesion regions. They used a self-created dataset with the help of West China Hospital. Wang et al. [53] created a dataset using the Invenia ABUS system at Sun Yat-Sen University Cancer Center. They used Unet and DDS pooling to enhance the detection sensitivity for breast cancer. The sensitivity obtained from their model was 0.95. Shu et al. [54] used the INbreast dataset and CBIS dataset for breast cancer detection. Pre-trained CNNs and deep machine learning models were used for the classification of breast lesion regions. Heidari et al. [122] used an SVM classifier for breast images. Fu et al. [123] proposed a model to predict Invasive Disease-Free Survival (iDFS)

for the early-stage breast cancer patients. They used XGBoosting and attained an AUC of 0.845. The dataset was self-created with the help of CRCB in West China Hospital of Sichuan University. Nyayapathi et al.[71] shown the fusion of ultrasound images with photoacoustic images for the early detection of breast cancer. Experimental results revealed an improvement in probability, speed, and also the patient's comfort zone. Ekici et al. [50] used CNN classifier on the DMR dataset and obtained an accuracy of 98.95%.

Yin et al. [118] proposed a new scheme for early detection using the UWCEM database. They created 3-D anatomically accurate FDTD-based breast models, which resulted in improved identification capability, robust artifact resistance, and high detectability of tumors. Srivastava et al. [79] used different SVM classifiers (i.e., MLP, Quadratic, linear, and RBF) to achieve good accuracy. SVM-RBF performed better than the others. SVM-RBF attained an accuracy of 87.5%. Dheeba et al. [124] worked on the detection of tumors from breast tissue structure using a mammogram. MIAS dataset and ANN classifier were used. The recognition score obtained from this method was 97.8%. Wang et al. [52] used the SoftMax classifier on the DDSM dataset to detect the size of breast lesions. The value of AUC obtained from this method was 0.865. However, there is a need to develop more advanced automatic breast cancer detection techniques to improve the diagnosis of breast cancer. Table 3.4 shows the advancement in breast cancer detection techniques.

Table 3.4 Advancement in breast cancer detection techniques.

Ref.	Proposed Approach	Targeted Problem	Models	Classifier	Measures	Challenges	Advantages
[52]	Create dataset + Multiscale module (screening of unique features) + multi-instance module	Detection of the breast lesion regions	CNN (ResNet-50)	-	AUC: ResNet-50 MSMI = 0.901	In the future author could assist other advanced applications, such as size measurement, lesion characterization	Their method learned the unique features of lesions via the multiscale module.
[53]	Pre-processing + pre-trained UNet + DDS feature extraction + TM	Enhance the detection sensitivity for breast cancer	3D CNN (U-net + DDS Pool)	-	Sn = 95% with 0.84 FP per/volume	The author could help with more advanced applications in the future, such as size measurement and lesion characterization.	High sensitivity and low false positives
[54]	Edge detection and segmentation + feature extraction + RGP/GGP	Classification based on breast lesion region	CNN (DenseNet169 + max pooling)	Pretrained CNNs and deep MIL models	Acc: INbreast dataset= 0.934 ± 0.0003(RGP)	The results of visualization show that the proposed model can roughly locate suspicious regions	The ability to learn lesion location information

					0.922 ± 0.0002(GGP) CBIS dataset= 0.838 ± 0.0001(RGP) 0.767 ± 0.0002(GGP)		
[61]	Data Preprocessing + Image feature extraction + Classification	Classification based on image feature extraction	CNN (SVM)	SVM (FFDM image, DCT maps, FFT maps, fusion of features)	FFT: 66-77% DCT: 64-83% SSIM: 63-71% Fusion: 67-89%	Its clinical utility or impact on radiologists' performance in the diagnosis of breast cancer using mammograms has not been tested.	significantly higher performance with AUC
[123]	Statistical Feature Selection + Ensemble Feature Selection +	Predict the relapse or metastasis of breast cancer	ANN (XGBoost)	PREDICT and Adjuvant Online	AUC: 0.8451	In future works, additional clinical data can be collected for improving the accuracy	XGBoost algorithm performance improved by 3%

	XGBoost algorithm + PREDICT and Adjuvant Online					of the 5-year iDFS prediction algorithm	
[71]	System Design + Breast Coupling + Imaging Procedure + Reconstruction and Alignment	Early detection of tumor	-	Fusion of ultrasound images with photoacoustic images	benefits of portability, speedy scanning, and patient comfort	Patients with different tumor characteristics and breast sizes should be imaged to identify the photoacoustic features of different tumor grades and types	Their system possesses the benefits of portability, speedy scanning, and patient comfort
[50]	Data acquisition + Pre-processing + Segmentation + Feature Extraction + Classification	Classification based on image feature extraction	CNN	CNN (Bayes algorithm)	Acc: 98.95%	The author can further classify the type and size of the tumor	Obtained good accuracy rate was obtained for the thermal images
[86]	Digital breast model + Parameter	Detect and localize the tumor		iCAD	-	Requires more computation time	The technique has the potential to be an accurate adjunct to mammography

	estimation for thermal images					
[125]	Data acquisition + designed deep model + cross-domain SVM	learning deep features from large-scale X-ray images	CNN	CNN (multi-class SVM)		The author could help with other advanced applications in the future, such as size measurement and lesion characterization.	Good effectiveness and efficiency of the proposed recognition system
[97]	Create dataset + Model-Based Segmentation + Compute optical flow	Accurately measuring 3-D surface motion.	-	DIET machine	The system can detect a 10 mm tumor in a silicone phantom breast	A limitation of these dense optical flow techniques is their sensitivity to the lighting variation	Their system can reconstruct the breast surface with average errors of less than 1 mm
[47]	Heterogeneity Wavelet Kinetic Features + Classification	Quantify intra-tumor heterogeneity in breast cancer	-	dynamic contrast-enhanced magnetic	AUCs: 0.94	HetWave could assist other advanced applications such as feature extraction approach for characterizing tumor heterogeneity,	Superior ROC AUC

					resonance imaging		providing valuable prognostic information	
[94]	3-D anatomically accurate FDTD-based breast models + Preprocessing for Artifact Removal + RAR algorithm	Early-stage detection	Robust and Artifact Resistant	DAS, DMAS, MWDAS, and FDAS	Improved identification capability, robust artifact resistance, and high detectability	The investigation of RAR's performance for further enhancement of tumor detection in severely dense breasts is missing	Their results show the high potential of RAR for early-stage cancer detection in low to medium-density breasts.
[126]	Breast-Body Segmentation	Automatically compute breast density in breast MRI	-			Complex analysis	Their proposed method is good at investigating the correlation between breast density measurements obtained from MRI and mammograms.
[16]	Input raw pixels of training patches +	The appearance of breast cancer nuclei	SSAE	Softmax Classifier	SSAE + SMC: P= 88.84%	Stacked Sparse Autoencoder could be integrated with	Their framework can provide accurate seed points or

	Feature representation (SSAE) + SoftMax classifier	in histopathological images			F1= 84.49% AveP= 78.83%	feature extraction methods to characterize cancer better	vertices for developing cell-by-cell graph features that can enable the characterization of cellular topology features on tumor histology
[79]	Data Acquisition + Segmentation + Feature extraction and selection + Classifier	Feature extraction	ANN (GA-MI)	SVM (MLP, Quadratic, linear, RBF)	SVM-MLP: Acc 84.3750% SVM-linear: Acc 81.25% SVM-quadratic: Acc 84.3750% SVM-RBF: Acc 87.5%	Some SVM classifiers are not capable of classifying the negative sample	GA-MI-based feature selection of the SVM classifiers for MLP, linear, and quadratic classifiers are performing better

[124]	Data acquisition + ROI Selection + Feature extraction + classification	Detection of tumors from breast tissue structure using a mammogram	ANN	ANN (Modified Genetic Algorithm)	Recognition score of 97.8%	The results are not comparatively good on other mammogram datasets.	The classifier is good at recognition
[127]	Data acquisition + slide level preprocessing + ResNet Classifier	cancer metastases in lymph nodes	CNN	ResNet	The best results were obtained with pre-trained architectures such as ResNet.	At the slide level, the best-ranked team misclassified 67 of the 500 slides in the test set.	The submitted algorithms were not only able to detect the presence of metastases but also measure their extent to derive the metastasis category, including ITC, and to determine the pN-stage that is used in clinical practice

3.3. Comparative analysis

The effectiveness of deep learning-based breast cancer detection techniques is assessed using the performance measures mentioned in Section 1.7. Table 3.5 shows the comparative analysis of deep learning and machine learning techniques in terms of performance measures. In this table, ✓ denotes that the approach has used the associated performance measures, while ✗ indicates otherwise. The quantitative analysis of different deep learning and machine learning techniques is illustrated in Table 3.6.

Table 3.5 Comparative analysis of breast cancer detection techniques in terms of performance measures.

Ref.	Technique	Prediction Measure					Classification Measure				
		μ	σ	MSE	RMSE	PSNR	PPV	S_n	A_{cc}	S_p	AUC-ROC
[128]	Resnet-34, VGG16	✗	✗	✗	✗	✗	✗	✗	✓	✗	✓
[129]	Resnet50, VGG16	✗	✗	✗	✗	✗	✗	✓	✗	✓	✓
[49]	VGG16	✗	✗	✗	✗	✗	✗	✓	✗	✓	✓
[130]	Linear Regression	✗	✗	✗	✗	✗	✗	✓	✓	✗	✗
[53]	3D-Unet	✗	✗	✗	✗	✗	✓	✓	✗	✗	✗
[54]	DenseNet169	✗	✗	✗	✗	✗	✗	✗	✓	✗	✓
[131]	MVPNet	✗	✗	✗	✗	✗	✗	✓	✓	✓	✓
[132]	EfficientNet	✗	✗	✗	✗	✗	✓	✓	✓	✓	✓

[133]	AFExNet	✓	✓	✗	✓	✗	✓	✓	✓	✓	✓
[134]	GoogLeNet, AlexNet	✓	✗	✗	✗	✗	✗	✓	✓	✗	✓
[135]	Random forest	✗	✗	✗	✗	✗	✗	✗	✓	✗	✓
[136]	DTree, RF, XGBoost	✗	✗	✗	✗	✗	✗	✓	✓	✓	✗

Table 3.6 Quantitative assessment of breast cancer prediction technique on classification measures.

Ref	Technique	Classification Measures				
		PPV	S_n	A_{cc}	S_p	AUC-ROC
[128]	Resnet-34, VGG16	-	-	89.0%	-	0.950
[129]	Resnet50, VGG16	-	86.7%	-	96.1%	0.98
[49]	VGG16	-	0.9	-	-	085
[130]	Linear Regression	-	-	92.43 ± 0.657	-	-
[53]	3D-Unet	0.84	95%	-	-	-
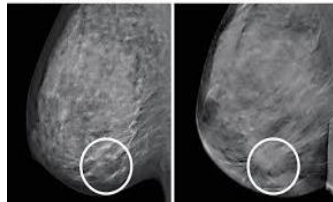
Ref	Model					
[54]	DenseNet169	-		0.923 ± 0.0003 0.762 ± 0.0002		0.762 ± 0.0002 0.838 ± 0.0001
[131]	MVPNet	-	94.2 ± 2.2%	92.2%	92.3 ± 2.4%	0.91=/-0.05
[132]	EfficientNet	0.819	0.74	90.2%	95%	0.93
[133]	AlexNet	98.57	98.58	98.57	98.57	-
[134]	GoogLeNet, AlexNet	0.7051	-	-	-	0.925
[135]	Random forest	-	-	84%	-	0.84-0.86
[136]	DTree, RF, XGBoost	-	0.8429	86.96%	0.8964	-
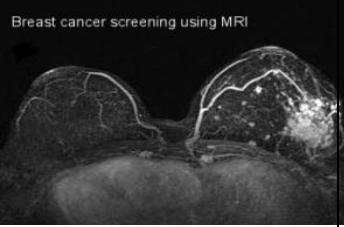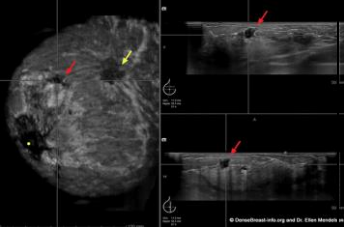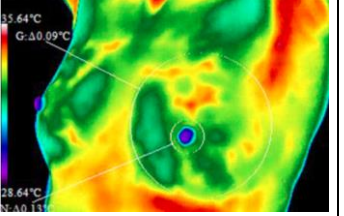
3.4. Discussion

To assist in cancer treatment, diagnostic imaging modalities are important for tumor classification. Over the last few years, imaging has been considered an important tool for the diagnosis of tumors. Various screening techniques are used to detect and characterize tumors. Screening techniques do not prevent cancer; however, they make early detection possible to

make the patient alert for their treatment. Every screening technique has its advantages and disadvantages. The most common screening method for breast cancer detection is an X-ray mammogram. Breast Ultrasound creates an image of tissues inside the breast using sound waves. The advantages involve non-invasive, quick visualization of breast tissue, the area closest to the chest wall, which is difficult to study with a mammogram, can be seen with ultrasound. Breast ultrasound has a low specificity and is more expensive. MRIs use a large magnet and radio waves to produce excellent tissue differentiation and sensitivity for breast cancer detection. CT scan images are made up of X-rays taken from various angles. Patients look for non-invasive and non-contact screening techniques as all the above-mentioned techniques involve contact. Thermography is one such technique. It uses infrared sensors to detect heat and increased vascularity as the result of biochemical reactions. Table 3.7 depicts the comparison of different breast tumor screening techniques in terms of pros and cons.

Table 3.7 Comparison of different breast tumor screening techniques for the diagnosis of tumor.

Screening Technique	Spatial Resolution	Advantages	Disadvantages	Image
Mammogram	Lower Spatial resolution	Time efficient requires a lower average radiation dosage.	Lower spatial resolution uses X-rays, costly.	
CT scan	High Spatial resolution	Precise, High spatial resolution,	Uses X-rays, which can cause an allergic reaction	

MRI	High Spatial resolution	No-ionizing radiation, high sensitivity, good tissue differentiation	A costly, invasive procedure, low specificity	
Ultrasound	Moderate spatial resolution	Less expensive, uses soundwaves	Low specificity, not able to detect all types of tumors.	
Thermography	Low spatial resolution	Non-invasive does not involve exposure to radiation	It can only alert a person to changes that may need further investigation	

The performance of a system can be judged by its accuracy, sensitivity, and specificity. The value of these measures should be high to achieve good results. When the likelihood of malignancy is established using a system, lively observation or biopsy can be recommended to evade inadequate and further invasive treatment. The focus of this study is to provide a multi-modal approach to improve the performance of breast cancer diagnosis.

3.5. Research Gaps

Breast cancer is an important health issue for everyone, and developing effective screening methods and alternative therapies is critical to improving outcomes. It is important to recognize

gaps or limitations, if any, in the research on deep learning techniques for breast cancer detection. The possible gaps are as follows:

A. Ensure Safe Engagement

Safety is a major issue when radioactive rays or ionizing radiation are directly exposed to one's body. Many screening techniques use harmful waves that may cause allergic reactions or contraindicate in some patients. A system should be designed in such a way that it uses non-ionizing radiation and provides accurate results.

B. Multimodal Approaches

 Different imaging modalities reveal different aspects of the anatomy and physiology of the human body. It is possible that a single imaging modality cannot provide sufficient visualization for certain medical conditions.

Multimodality-based approach should be considered for the detection of breast cancer at an early stage. Screening tools for breast cancer need to expand their expertise by providing multimodal methods to enhance precision by improving the outcome of screening techniques.

C. Model Generalization

A variety of deep-learning models are used in breast cancer research. Deep learning models provide different results for different applications. Hence, there is a necessity to develop a generalized model for breast cancer detection.

D. Clinical Implementation

Deep learning-based breast cancer detection models proved their significance in medical research. However, the practical implementation of these models in clinics is still not done. The implementation of these models in clinics will be beneficial for doctors.

The aforementioned gaps provide valuable insights that motivated the present dissertation to contribute towards the development of more effective strategies for breast cancer detection and treatment.

3.6.   Summary

Chapter 3 surveys existing literature on breast cancer detection techniques, with major focus on survey approaches to detection and recent developments in deep learning algorithms. It includes systematic reviews of the imaging procedures, deep learning, and machine learning solutions and explains the most relevant articles focusing on the main research questions' comparison. The challenges faced in this field are shown as research gaps and are addressed in the chapters ahead. Chapters 4 and 5 responded to the first and second research gaps while chapters 6, 7, and 8 responded to the third research gap. However, the potential of using deep learning-based breast cancer detection models has been proved in many medical studies However, these models are not widely used in clinical practice mainly because there is lack of large number of datasets and cooperation with the clinical settings. These chapters describe these issues and ways to overcome them so that there can be improved translation of research findings to clinical practice.

CHAPTER 4

Dual - Modality Synthetic Mammogram Construction for Breast Lesion Detection using U-DARTS

4.1. Preamble

This chapter introduces a novel model for constructing synthetic mammograms to overcome the challenges of accurate registration of different imaging modalities in multimodal image fusion for cancer detection. The model aims to enhance the visual quality of medical images, enabling more precise and efficient cancer diagnosis. A dual-modality structural feature (DMSF) based mapping function is developed to transform mammograms obtained from thermal image segments.

Additionally, the chapter presents a modified version of Differentiable Architecture Search (DARTS), called U-DARTS, which incorporates a stochastic gradient descent optimizer for improved breast lesion detection and classification.

To ensure accurate construction, the resultant synthetic mammograms are compared to the INbreast dataset to unbiasedly evaluate proposed approach's success. This comparison aims to evaluate the effectiveness of the DMSF-based mapping function in producing synthetic mammograms that closely resemble real mammograms, thus validating the accuracy and reliability of the proposed method. The flow of the proposed method is illustrated in Fig. 4.1.

4.2.   Proposed Methodology

In pre-processing, the histogram is decomposed into subparts. A logarithmic transform between sub-histograms is used, which is shown in Fig. 4.2.
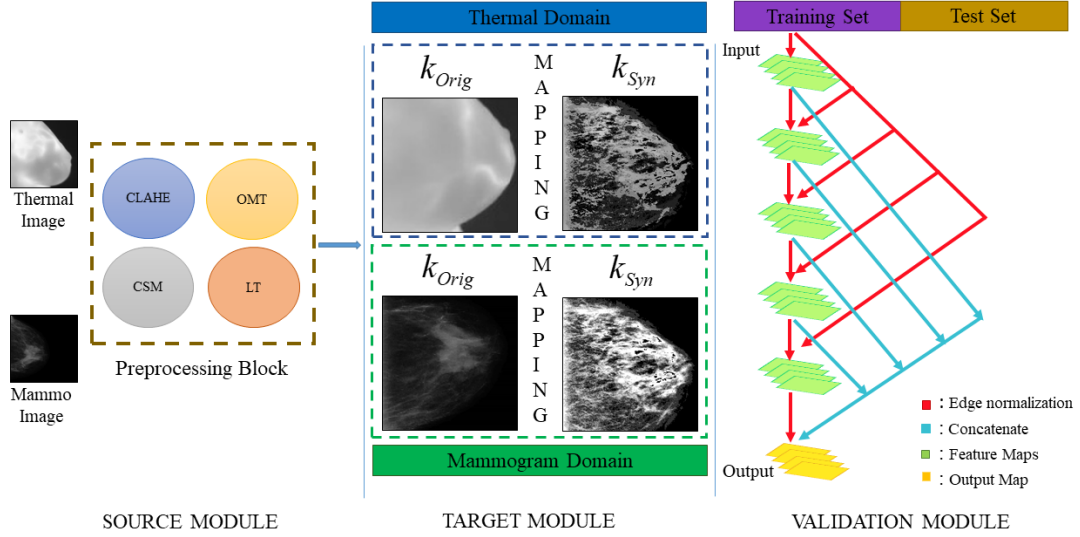
Fig. 4.1 Proposed synthetic mammogram construction model.

There are four sub-steps in the pre-processing phase.

- Apply CLAHE to both the input images.

- Applying logarithmic transform (LT) to CLAHE output of mammogram and thermal images.

- Contrast stretching method (CSM) followed by Otsu multilevel thresholding (OST) for the histogram splitting process.

- Output is obtained as an equalized histogram.
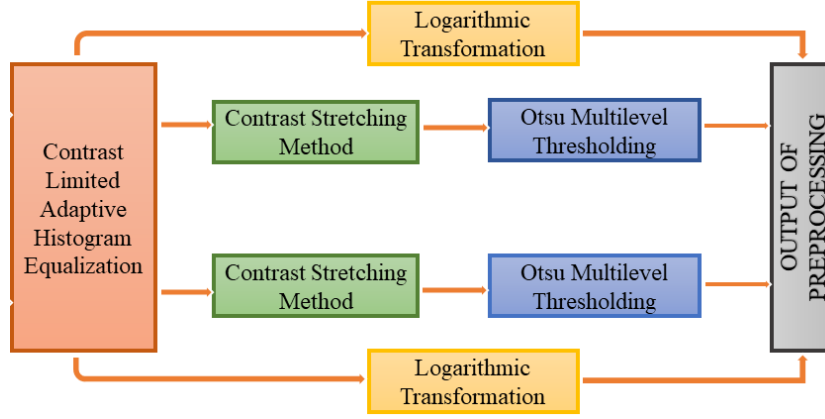
Fig. 4.2 Block diagram of the proposed preprocessing method.

CLAHE has proved to be beneficial in medical images. Adaptive Histogram Equalization (AHE) determines the mapping for a given pixel by computing the histogram of a local window centered at that pixel. This results in the enhancement of local contrast [137]. For CLAHE, the given image is decomposed into multiple non-overlapping areas of nearly equal size. Thereafter, the histogram of each area is computed. The clipping histogram computes the clip limit using the favored contrast expansion limit.

$$k_{CL\_out} = [ki_{CL\_in_{CL\_min}}CL\_min_{CL\_max} \tag{4.1}$$

Here k_{CL_max} and k_{CL_min} are the maximum and minimum permissible intensity levels and it also sets the threshold to an optimal value. $E_i(k_{CL\_in})$ shows the function for cumulative distribution where k_{CL_in} is the input and k_{CL_out} is the contextual output. The CLAHE output sends for logarithmic transformation and contrasts the stretching method as well.

In contrast stretching, the intensity value of the pixel I can be obtained as follows:

$$I_o = (I_i - r)(\frac{q-p}{s-r}) + p \tag{4.2}$$

68

Here s and r are the minimum and maximum pixel intensity values. The top pixel intensity value limit q and bottom pixel intensity value limit p over which the image will be normalized.

The output of CSM is further processed using OMT because different images require different stages of smoothing and detaining, the Otsu multilevel thresholding is designed to provide image intensity exposure. As an outcome, the threshold (u) is calculated as follows:

$$u = \frac{1}{M} \frac{\sum_{m=1}^{M-1} k(m)m}{\sum_{m=1}^{M-1} k(m)} \qquad (4.3)$$

Where, the input intensity level of the input image (k) is denoted by (m), and the range is 0 to $M - 1$.

Further, logarithmic transformation can be performed using Eq. (3.4).

$$k^{"} = c \, log(1 + j) \qquad (4.4)$$

Here, $k^{"}$ is the output modified histogram obtained through logarithmic transformation, j stands for the intensity value in the image's original histogram, and c is the constant set to 0.5. The output generated from OSM and LT are then merged to obtain a single modified histogram.

4.3. Feature Extraction and Mapping

To ensure that the tissues or structures in the input and synthetic images have the same anatomy, they are mapped into a shared architectural feature space using Dual-Modality Structural Features (DMSF). Further, U-Net is used to test the consistency of the shared architecture. DMSF is obtained by using a patch (not neighbor) based self-similarity method that relies on the structure of input images rather than intensity levels. Yang et al. [138] proposed MIND, a similarity metric to classify MR/CT images.
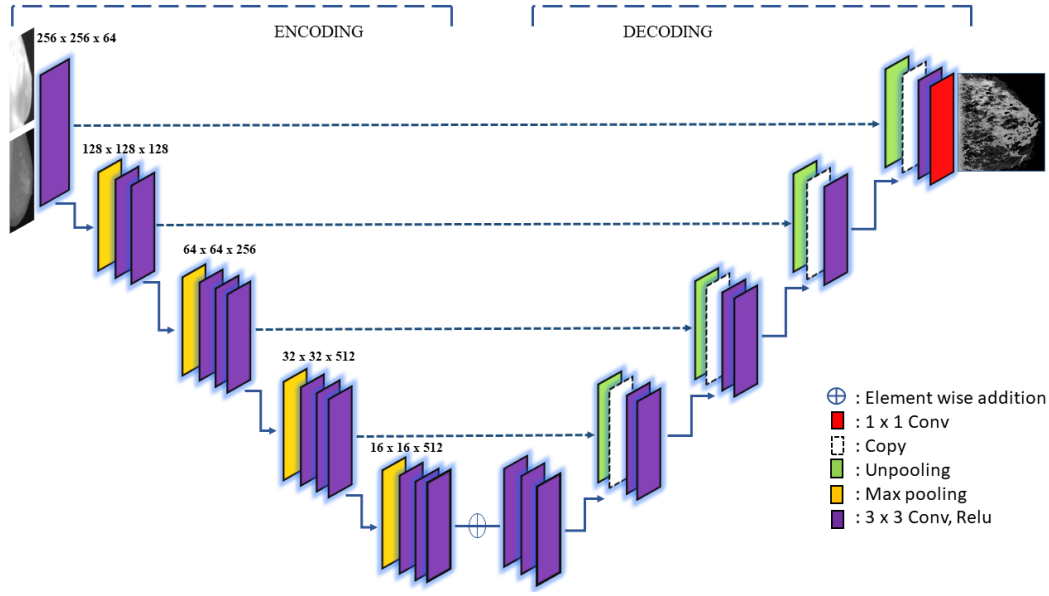
Fig. 4.3 Overall architecture of the proposed DMSF model.

To create a mapping function that translates a thermal image segment into its corresponding mammogram image, a deep CNN model with U-Net is employed. By gathering all thermal patches and corresponding mammogram patches for each patient, the model is trained using the thermal/mammogram pairings. The final mammogram is then generated by combining the data. The proposed mapping model's architecture, which is separated into two sections—an encoding section and a decoding section—is shown in Figure 4.3.

The encoding section functions similarly to a conventional CNN, learning to extract a hierarchy of increasingly complex features from a thermal image input. This involves several layers of convolutional operations that capture different levels of abstraction, starting from simple edges and textures to more intricate patterns and structures present in the thermal image.

In the decoding section, these extracted features are then transformed and used to reconstruct the synthetic mammogram projection. This reconstruction process progresses from low to high resolution, gradually refining the image details through successive layers. The final output

from the network is designed to match the dimensions of the original thermal image, ensuring that the synthetic mammogram retains the same spatial resolution and anatomical context.

A key aspect of this model is the use of high-resolution features from the encoder as supplementary inputs for the convolutional layers in the decoder. These high-resolution characteristics help in preserving fine details and enhancing the quality of the reconstructed mammogram.

Ultimately, the network's performance is evaluated based on Mean Absolute Error (MAE) against validation data. The model iterates over the data, continuously adjusting and improving its outputs. The best image, which is the one with the lowest MAE, is retained as the final synthetic mammogram. This method ensures that the generated mammogram is as accurate and detailed as possible, providing a reliable representation for further analysis or clinical use.

Mean Absolute Error (MAE) is used as a loss function.

$$MAE = \frac{1}{N}\sum_{n=1}^{N}||A_n - G(B_n; \varphi)|| \tag{4.5}$$

ϕ is the network parameter, which can be achieved by minimizing the loss between the synthetic image $G(B_n; \phi)$ and the original mammogram image (A_n). N is the number of images used. When MAE is used as the loss function, the learning becomes more resistant to outliers, such as many artifacts as well as improper alignment between thermal and mammogram images.

It is worth noting that the two different modality images used for mapping are of the same patient, to ensure that the comparison is unbiased. Due to the inadequate training data in this study, it was not possible to train the model directly. Consequently, the data was trained and tested using zero-shot learning. The model was tested on the INbreast dataset. Zero-shot

learning makes it easier to transfer knowledge from the training domain to the testing domain for effective learning because the information in the training and testing instances is different.
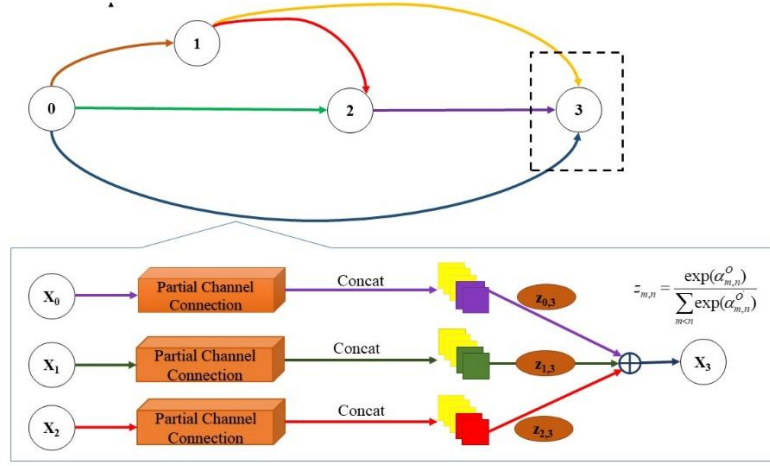
Fig. 4.4 DARTS classifier for the proposed technique.

DARTS is utilized in this section since it blends the searching and evaluating steps into one. During the search step, the proposed network is optimized using a stochastic gradient descent optimizer, whereupon the best features are retained and trained again [139]. The architecture of the proposed DARTS is shown in Fig. 4.4.

The search space is specified to find the network model. The directed acyclic graph is a search space with E nodes $\{e_0, e_1, ..., e_E\}$, as shown in Fig. 4.4. Each component, of the pre-defined space of operations denoted by C is a defined operation performed at a layer of the network. Within a cell, the goal is to choose one operation from C to connect each pair of nodes (m, n). There are m directed input edges $(x_{m,0}, x_{m,1}, ..., x_{m,m})$ for each node x_m, with each edge $x_{m,n}$ transforming T_m with certain operation $z_{(m,n)}$. The attribute of each node is the sum of its preceding nodes' operations, as expressed below.

$$T_m = \sum_{n<m} z_{m,n}(T_m) \tag{4.6}$$

were,

$$z_{m,n}(T_m) = \sum_{O \in C} \frac{exp(\alpha_{m,n}^O)}{\sum_{O' \in C} exp(\alpha_{m,n}^{O'})} O (T_m) \hspace{3cm} (4.7)$$

In this work, two different datasets for training and testing were used. U-DART is a modified classifier that is trained on a digital mammogram dataset i.e., INbreast. Edge normalization preserves the boundary condition of the lesion in the breast and concatenation helps in producing a result of the model. Finally, the synthetic mammogram results are tested for DARTS processed dataset.

Algorithm 1: Preprocessing for Synthetic Mammogram Construction Model

---

1: Input: T_{ORI} (mxn); Original thermal image with m = no. of rows and n = no. of column

   M_{ORI} (mxn); Original mammo image with m = no. of rows and n = no. of column

2: Preprocessing: Initialize the image T_{ORI} and M_{ORI} for preprocessing

3: Apply CLAHE of T_{ORI} and M_{ORI} to get kCL_out

   Fed kCL_out as input to logarithmic and CSM block and get k" as output.

   k" ← kCL_out

   LT block

      u ← Io ← kCL_out

4: return: output = u + k"

Algorithm 2: Feature extraction for Synthetic Mammogram Construction Model

---

1: Input: u + k"

2: Output: M_{SYN}; Synthetic Mammogram

3: Feature Descriptor- Apply DMSF to create a mapping function

4: Take M_{ORI} as a reference image to create M_{SYN} from T_{ORI}

5: Set z = 1

6: while (z < $SCM_{iterations}$) {termination condition}do# SCM is the synthetic construction

model

7: for each patch do

8: Calculate Dual-modality structural features

 Get the best model for M_{SYN} with the help of MAE

9: Update the best model based on the loss function obtained through eq (5)

10: end for

11: end while

12: return M_{SYN}

Create a test set from the output of the Feature Descriptor

Algorithm 3: Classifier for Synthetic Mammogram Construction Model

1: Input: M_{SYN}

2: Create training set M_{TRAIN} with INbreast dataset

        Feature maps   ← M_{TRAIN}

edge normalization

        Output feature map ←   Feature maps

SGD

3: Apply stochastic gradient descent (SGD) optimizer to obtain the best feature map

4: Utilize the obtained image sequences to train/test theproposed U-DART model for

estimation and detection

4.4.   Computational Complexity

This section describes the computational complexity of the proposed synthetic mammogram

construction model (SMCM). The space and time complexities are explained further below.

4.4.1. Time Complexity

- The initialization of SMCM needs $O(T_{ORI}(m \times n)) + O(M_{ORI}(m \times n))$ time where m represents number of rows and n represents number of columns in each image.

- The CLAHE calculation requires $O(T_{ORI}(k_{CL\_out})) + O(M_{ORI}(k_{CL\_out}))$ time.

- The time required for calculating preprocessing block $O\left(T_{ORI}\left(k_{CL\_out} \times I_o \times u \times k''\right)\right) + O\left(M_{ORI}\left(k_{CL\_out} \times I_o \times u \times k''\right)\right)$

Where, k_{CL_out}, I_o, u and k'' are the outputs obtained from CLAHE, CSM, OTM and LT block respectively.

- Mapping DMSF algorithm requires $O(M_{ORI}) = O\left(M_{MAPP}\left(T_{ORI}\left(k_{CL_{out}} \times I_o \times u \times k''\right)\right)\right) + O\left(M_{MAPP}\left(M_{ORI}\left(k_{CL_{out}} \times I_o \times u \times k''\right)\right)\right)$

Where, M_{MAPP} indicates the mapping function to ensure that the tissues or structures in the input and synthetic images have the same anatomy.

- Time taken by training and testing of U-DART model is $O_{TT} = O((M_{TRAIN})(EN + SGD)) + O(M_{TEST})$

Therefore, the overall time complexity of the proposed model is as follows:

$$O\left(M_{MAPP}\left(T_{ORI}\left(k_{CL_{out}} \times I_o \times u \times k''\right)\right)\right) + O\left(M_{MAPP}\left(M_{ORI}\left(k_{CL_{out}} \times I_o \times u \times k''\right)\right)\right) + O_{TT}$$

4.4.2. Space Complexity

The proposed synthetic mammogram construction model space complexity considers its initialization stage, which necessitates space at any given time. As a result, the overall space complexity is:

$$O(T_{\text{ORI}}(m \times n)) + O(M_{\text{ORI}}(m \times n)) + O(M_{\text{TRAIN}}(m \times n))$$

4.5. Results and Discussions

4.5.1. Datasets used

The work is carried out with a FLIR SC-620 IR sensor, having dimensions of 640 x 480 pixels, from the Database for Mastology Research (DMR). DMR includes thermogram as well as mammogram images in jpeg format from frontal images [87]. It has horizontal and vertical resolution of 96 dpi each. It consists of images of 287 patients aged between 29 to 85.

INbreast database is publicly available and can be obtained from [38]. There are 410 FFDM mammograms from 115 patients in this collection. For healthy and unhealthy cases, the INbreast includes both Craniocaudal (CC) and Mediolateral Oblique (MLO) views. Every mammogram has a DICOM file with an XML document, some case-specific information as well as ground truth descriptions of any lesion found in unhealthy mammograms.

To objectively assess the quality of the synthetic mammogram output in comparison to the original image, the values of MAE, Peak Signal Noise Ratio (PSNR), and Structural Similarity measure (SSIM) are computed. These metrics have given quantitative information about how well the synthesis process captures image fidelity, enabling you to make well-informed decisions about algorithmic enhancements and guaranteeing that the quality standards for the output synthetic mammogram have been met.

4.5.2. Performance Evaluation

The outcomes of the suggested methodology are assessed both qualitatively and quantitatively in order to confirm its validity. For this assessment, twenty sets of mammography/thermal images from the same patients in the DMR dataset are used.
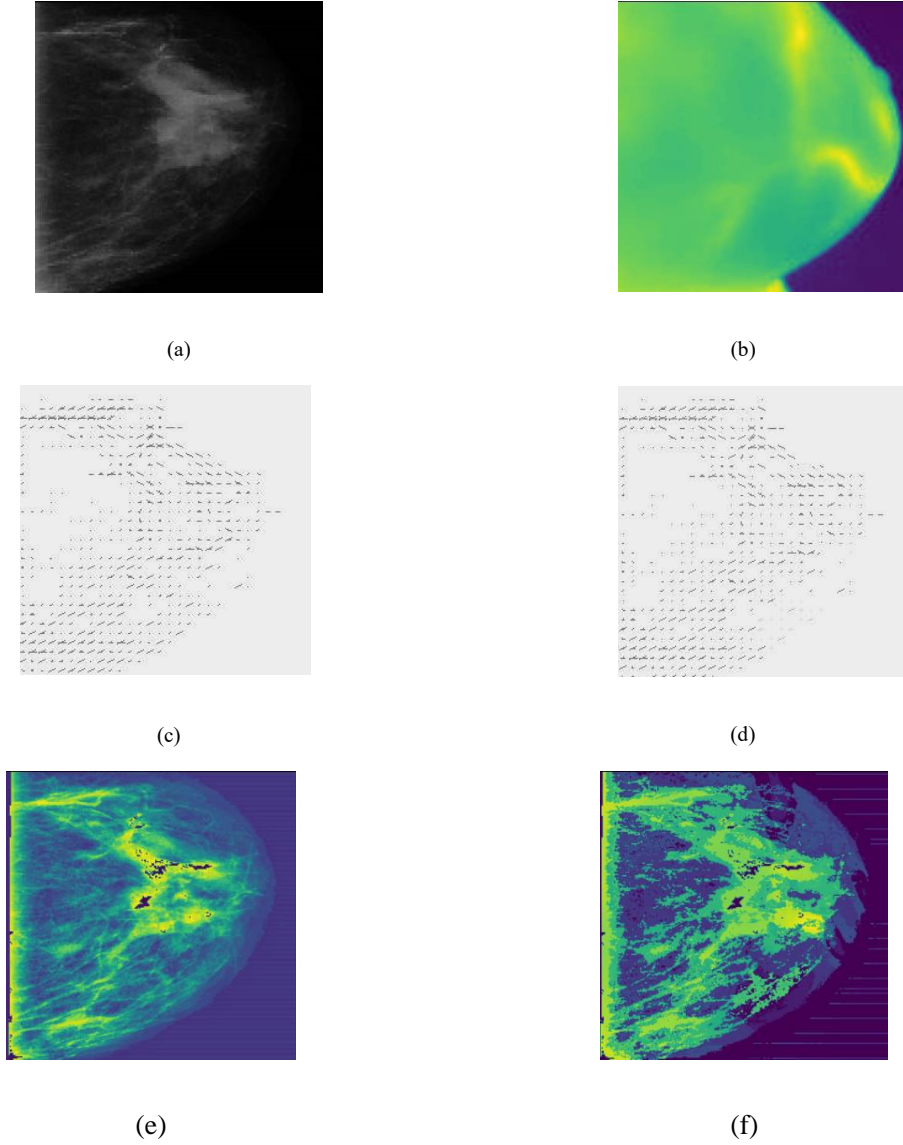
Fig. 4.5 Results obtained from the proposed DMSF method (a) source mammogram, (b) source thermal image, (c) heat map obtained from mammogram image, (d) heat map obtained from thermal image, (e) difference image, and (f) final output synthetic image .

The images are first pre-processed and then mapped into a shared architectural feature space using DMSF to ensure that the tissues or structures in the input and synthetic images have the same anatomy. The visual results obtained can be seen in Fig. 4.5. The proposed model's efficiency and effectiveness are demonstrated using metrics such as Mean Absolute Error (MAE), Peak Signal-to-Noise Ratio (PSNR), and Structural Similarity Index (SSIM) as mentioned above. Additionally, a comparative analysis with various existing multi-modal

approaches is presented in Table 4.1. This table provides a comparison of PSNR, MAE, and SSIM values between the proposed model and several synthetic models used in medical imaging. To ensure impartiality, all values were obtained by testing on the same fused images. Some unsupervised deep learning-based methods [138,140–143] have recently been implemented for MR-to-CT synthesis.

Table 4.1 Comparison of PSNR, MAE, and SSIM values obtained from the proposed Model and various synthetic models.

Model	MAE	PSNR	SSIM
cycleGAN	140.22	23.74	0.751
gc-cycleGAN	139.77	23.79	0.751
sc-cycle GAN	124.8	24.5	0.782
Proposed	**30.92**	**21.99**	**0.88**

Figs. 4.6 and 4.7 show MAE, PSNR, and SSIM values of various synthesized models such as cycleGAN, gc-cycleGAN, sc-cycle GAN, and the proposed one. The proposed method has successfully attained the lowest MAE of 30.92 and PSNR value of 21.99. The value of SSIM is 0.88 which shows the superiority of the proposed method over the existing ones.
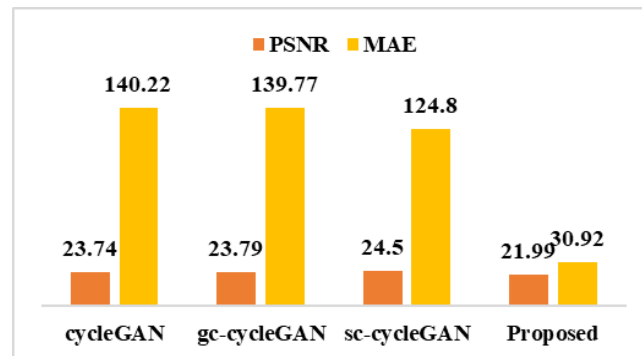
Fig. 4.6 Comparison between PSNR and MAE values for various synthetic models.
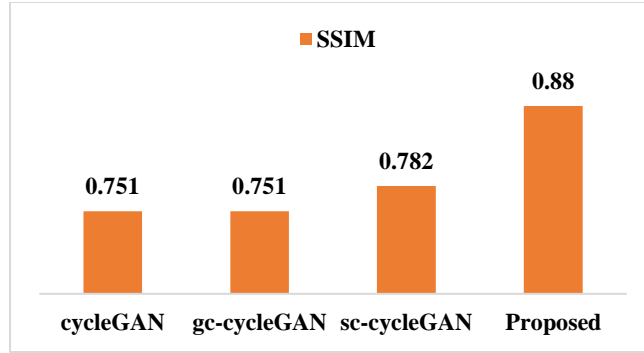
Fig. 4.7 Comparison between SSIM for various synthetic models.

Table 4.2. shows the comparison of the proposed Model to Latest Breast Cancer Detection and Classification Techniques for Mammogram Screening. To ensure accurate construction, the resultant synthetic mammograms are compared to the INbreast (mammogram) dataset to unbiasedly evaluate proposed approach's success.

However, original mammograms inherently contain detailed structural information optimized for breast cancer detection, while thermal images capture different data types, requiring complex transformations that may not fully replicate mammogram details. Despite these challenges, the proposed approach's performance remains commendable.

Table 4.2 Comparison of the proposed Model to Latest Breast Cancer Detection and Classification Techniques for Mammogram Screening.

Ref	Year	Special characteristic	Classification method	Acc
[144]	2018	YOLO-V1 & FrCN	CNN	95.64%
[145]	2021	YOLOV3	Inception V3	89.5%
[146]	2021	2 paths detection based on YOLOV4	InceptionV3	91%
[147]	2021	Multi-fractal dimension	CNN	99%
Proposed	**2022**	**Synthetic mammo construction model**	**U-DARTS**	**98%**

The performance analysis of the proposed synthetic construction model is verified using the INbreast dataset. Figs. 4.8 and 4.9 show the accuracy and loss of the proposed model respectively. The proposed model yielded 98% training accuracy value and the loss obtained is 0.12.
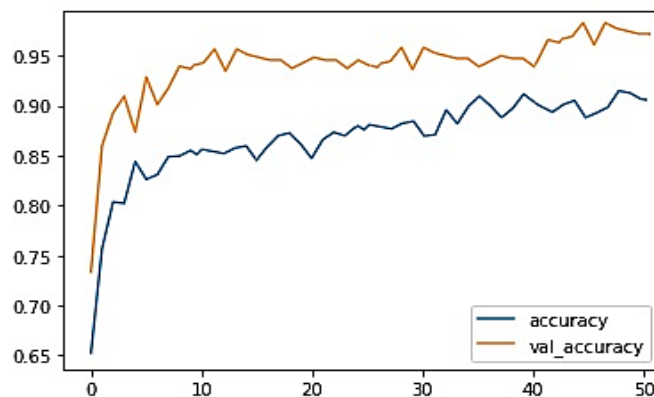
Fig. 4.8 Classification training and validation Accuracy for the proposed model with INbreast dataset.
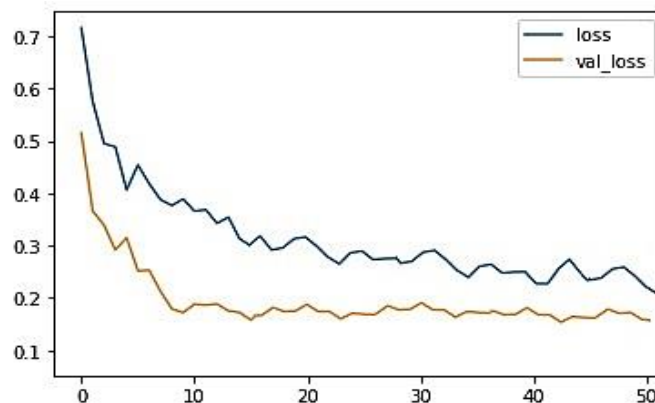
Fig. 4.9 Classification training and validation loss for the proposed model with the INbreast dataset.

4.6. Summary

In this chapter, the U-DARTS method combined with a stochastic gradient descent optimizer is used to detect and classify the breast lesion in synthetic mammogram images created from the proposed model. To verify the efficiency and effectiveness in terms of MAE, PSNR, and

SSIM, extensive experiments are conducted on DMR and INbreast datasets. In addition, on the INbreast dataset, the proposed model achieves a precision of 98%.

When the proposed technique was compared with other methods using the same dataset, INbreast, it was discovered that the proposed technique produced good results both visually and statistically. However, original mammograms inherently contain detailed structural information optimized for breast cancer detection, while thermal images capture different types of data, necessitating complex transformations that may not fully replicate the details of mammograms. Additionally, limited training data and the use of zero-shot learning can affect the model's generalization ability, potentially degrading the fine structural details of the synthetic mammograms. Despite these challenges, the performance of the proposed approach is commendable.

Future work will focus on enhanced data augmentation, advanced mapping techniques, hybrid models, incremental learning, and the development of multi-modal datasets to bridge the accuracy gap and fully harness the potential of safer, radiation-free diagnostic methods.

CHAPTER 5

Bimodal Image Fusion using AWT SPS for Breast Cancer Detection

---

5.1. Preamble

Fusing different modalities of medical images, such as X-ray mammograms and thermal images, presents unique challenges due to variations in imaging environments, angles, and the distinct types of information each modality captures. The proposed Super-Pixel Segmentation-based Advanced Wavelet Transformation (SPS-AWT) technique effectively addresses these challenges, ensuring high-quality image fusion. By utilizing advanced image registration techniques and geometric transformations, the method corrects for environmental and angular differences, while Discrete Wavelet Transformation (DWT) and super-pixel segmentation preserve spectral and spatial information. This fusion process combines structural details from mammograms with functional data from thermal images, enhancing diagnostic capabilities through improved contrast, clarity, and comprehensive visualization.

The effectiveness of the SPS-AWT technique was validated on a well-known dataset, using performance metrics such as structural similarity index (SSIM), peak signal-to-noise ratio (PSNR), and mutual information (MI). These evaluations confirm that the technique maintains critical details and enhances image quality, significantly improving diagnostic accuracy and visualization for breast cancer management. The resulting fused images provide a richer data set, aiding in the detection and monitoring of abnormalities and leading to better diagnostic and therapeutic outcomes.

5.2. Proposed Methodology

Breast cancer has affected both men and women, but the prevalence in women is unimaginably high. Almost one out of eight females are diagnosed with breast cancer and early diagnosis can save their lives. Though single-modal images are in use for the diagnosis of cancer, however, the information so obtained is limited. To help medical practitioners with better clinical diagnosis, we may need more information, which can be achieved by exploring the multimodality-based approach.

5.3. Proposed Technique

The proposed AWT-SPS technique is developed for medical images that have different modalities. When two different sensors are used for diagnosis in medical imaging, an enhanced fusion process is used to preserve spectral information and enhance spatial information. Fig. 5.1 shows the block diagram for the proposed fusion technique. The main steps of the proposed technique are as follows:
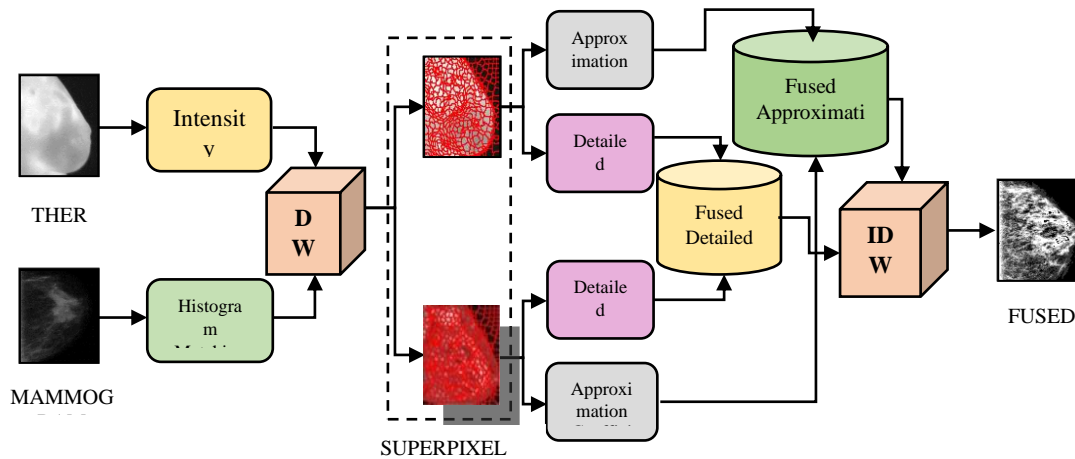
Fig. 5.1 Proposed AWT-SPS image Fusion technique.

Step 1: The study uses two different imaging modalities, infrared and x-ray (mammogram), of the same patient, sourced from the same dataset (DMR). This approach considers the inherent spectral differences between the two types of images. Typically, spectral variations arise when

images are captured at different times and in varying visual environments. By addressing these spectral variations, the method ensures that the fused images maintain critical information from both modalities, thereby enhancing the quality and reliability of the diagnostic data.

To compute the detailed and approximation coefficients, both thermal (I_{TH}) and mammogram (I_{MM}) modalities are applied to DWT separately. The row f_r and column f_c frequencies are calculated as follows:

$$f_r = \sqrt{1 \Big/ mn \sum_{x=0}^{m-1} \sum_{y=0}^{n-1} (f(x,y) - f(x,y-1))^2} \qquad (5.1)$$

$$f_c = \sqrt{1 \Big/ mn \sum_{x=0}^{m-1} \sum_{y=0}^{n-1} (f(x,y) - f(x-1,y))^2} \qquad (5.2)$$

The image (f) with grey scale $f(x,y)$ at pixel coordinates (x,y) is of size $m \times n$.

(a) X1*

(b) X1

(c) X2*

(d) X2

(e) X3*   (f) X3

(g) X4*   (h) X4
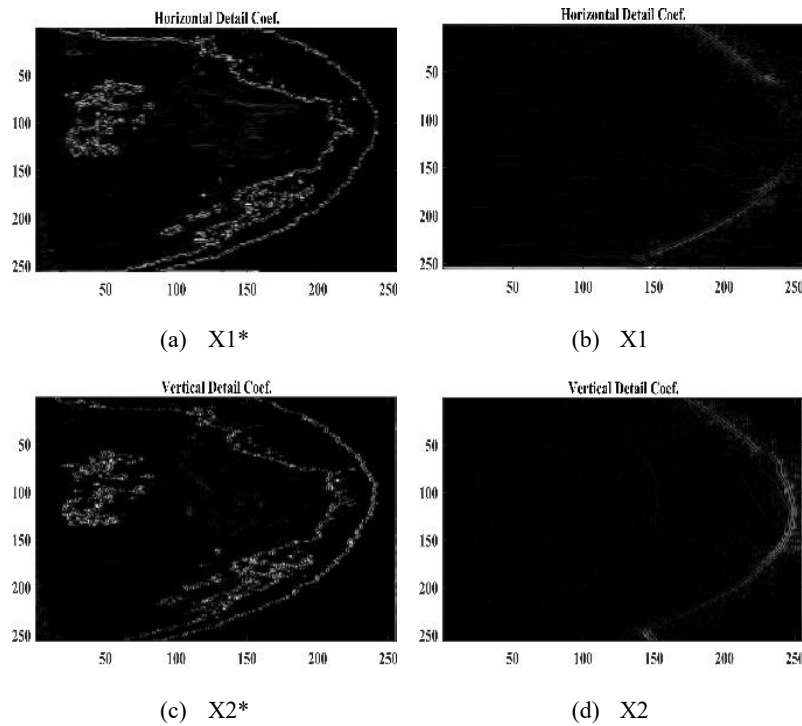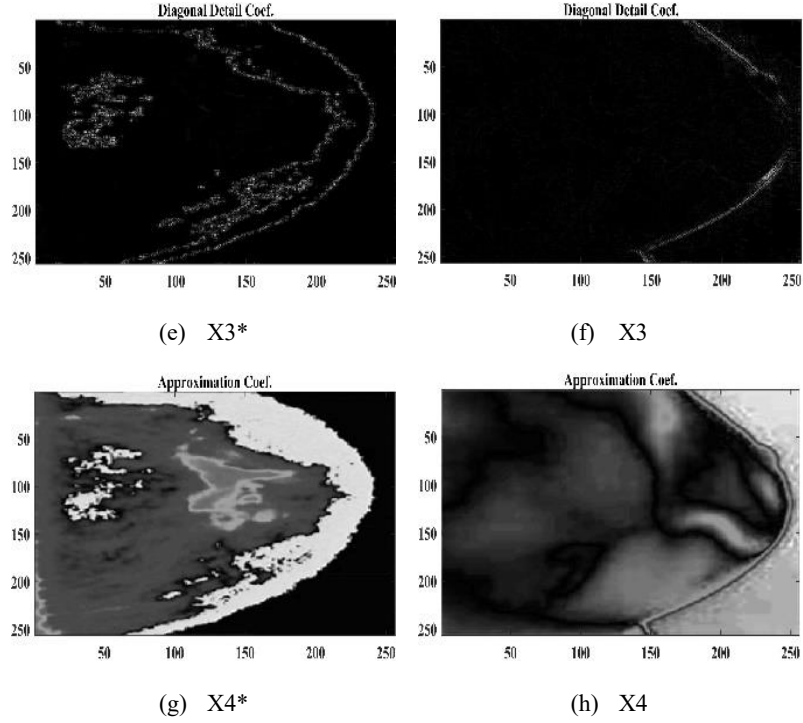
Fig. 5.2 Frequency coefficients obtained for a mammogram and thermal images, where (a) to (f) are the detailed coefficients, (g) and (h) are the approximation coefficients.

Further, the aim is to select an image with the largest contrast among the three detailed coefficient images. Two sets are generated, each with three images (X1, X2, X3 and X1*, X2*, X3*, respectively) corresponding to the three detailed coefficients (H, V, and D), (see Fig. 5.2). Following at the two images with the highest detail coefficient values, are chosen for further processing one from each other. The approximate coefficients for mammogram and thermal imaging are X4* and X4, respectively.

Step 2: Both images (as obtained from Step 1) are partitioned into irregular patches using the super-pixel segmentation (SPS) approach [148]. A reference image (A_r) for SPS is selected using input images from multiple exposures. The reference image for the study is the one with the fewest under or overexposed pixels among all the input images.[149]. A_r reference image is divided into 'z' number of image patches using simple linear iterative clustering, which is denoted as $p_1, p_2, ... p_z$ using super-pixel segmentation process as shown in Fig. 5.3.

$$SPS_{Slic}(A_r) = \{p_1, p_2, \dots\dots\dots p_z\} \tag{5.3}$$

The following is a representation of the segmented image patches:

$$\left(\{A_y(p_z)\}_{y=1\dots,Y,z=1\dots,n}\right) \tag{5.4}$$

Here, $\{A_y(n_z)\}$ represents the zth patch of the yth image.

(a) Reference image (b) Mask (c) Segmented Image
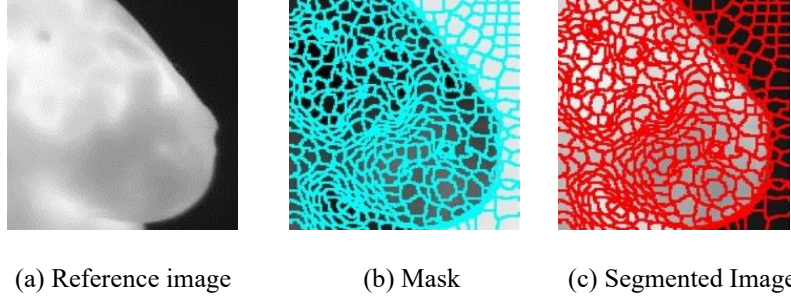
Fig. 5.3 Super-pixel segmentation.

To ensure consistency all other input images are segmented in the same way as the reference image.

Step 3: The patient's segmented thermal and mammogram images are combined using Advanced Wavelet Transformation (AWT). The spatial frequency of the intensity value corresponding to thermal (f_{TH}^N) and mammogram (f_{MM}^N) images is normalized using detail coefficient as given below:

$$f_{TH}^N = \frac{f_{TH}}{(f_{TH} + f_{MM})} \tag{5.5}$$

$$f_{MM}^N = \frac{f_{MM}}{(f_{TH} + f_{MM})} \tag{5.6}$$

where, f_{MM} and f_{TH} represent the spatial frequencies of mammogram and thermal images, respectively.

The fused detail coefficients (f_{fused}) are computed as:

$$f_{fused} = C_{TH} \times f_{TH}^N + C_{MM} \times f_{MM}^N \tag{5.7}$$

where C_{MM} and C_{TH} represent the spatial frequencies of mammogram and thermal images, respectively.

Step 4: The fused image is formed by applying an inverse DWT on the thermal image approximation coefficients.

Fig. 5.4 shows the visual comparison of standard wavelet-based fusion technique and the proposed technique. In the past, feature fusion techniques such as Discrete wavelets transform (DWT), Shape adaptive DWT (SA-DWT), and Spatial frequency DWT (SF-DWT) were used. DWT gives frequency and spatial domain information of the image, simultaneously. Mismatch in image registration is one of the main issues with DWT [104]. SA-DWT and SF-DWT have already been proposed to address this issue. Notably, the difference between SA-DWT and general DWT is the stage-based boundary extension strategy that extends the boundary locally in every lifting stage [150]. SF-DWT, on the other hand, quantifies the amount of frequency content in the image. In other words, it improves the sharpness or clarity of the image [151]. Fig. 5.4 (a) and Fig. 5.4 (b) show thermal and mammography images, respectively. The fusion results obtained using DWT, SA-DWT, SF-DWT, and the proposed method are shown in Fig. 5.4 (c) to (f), respectively. Green arrows illustrate the mismatch between two images created using the traditional fusion techniques. As seen in the figure, the fusion results obtained using the proposed methodology retain the structures of both images.

(a)   (b)
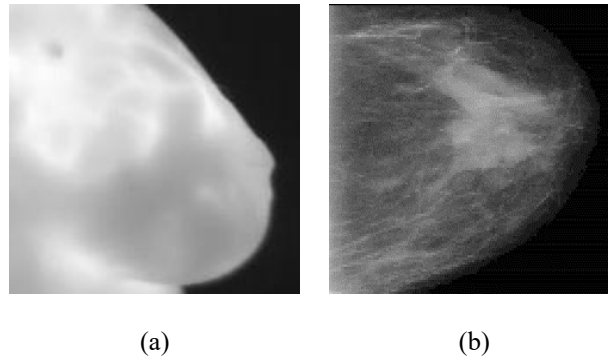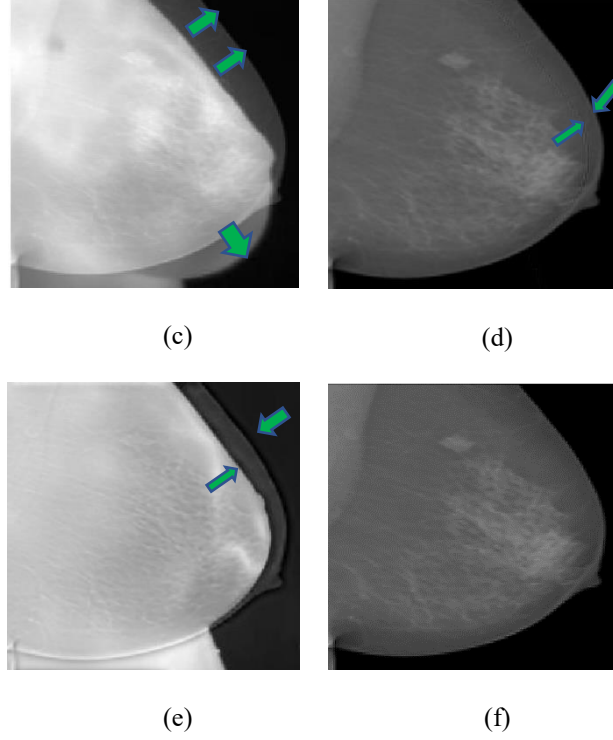
Fig. 5.4 Visual Comparison of the proposed fusion technique to the traditional wavelet transformation fusion techniques. Results of (a) Thermal, (b) Mammogram, (c) DWT, (d) SA-DWT, (e) SF-DWT, and (f) AWT-SPS.

Algorithm: - Proposed Breast cancer detection approach

Input: $I_{TH}(mxn)$; Thermal image with m=no. of rows and n= no. of column

$I_{MM}(mxn)$; Mammogram image with m=no. of rows and n= no. of column

Output: IFUS; Fused image

Procedure SFDWT-SPS

    Initialize the image $I_{TH}(mxn)$ and $I_{MM}(mxn)$

    Apply DWT on ITH and IMM to determine the detailed and accurate representation of coefficients.

$$I_{TH-DWT} \xleftarrow{DWT} I_{TH}$$

$$I_{MM-DWT} \xleftarrow{DWT} I_{MM}$$

    Apply super-pixel segmentation (SPS) on I_{TH} and I_{MM} images simultaneously.

    Find reference image A_r for SPS based on multi-exposure input images.

        while $(x < SPS_{iterations})$ do

        for each patch do

Update the image patches obtained through segmentation using Eq (4.5)

     end for

     end while

Update I_{TH} and I_{MM}

     for $i = 1$ to n (n= no. of the column in the image)

     $S(I_{TH}) = SPS(I_{TH-DWT})$

     $S(I_{MM}) = SPS(I_{MM-DWT})$

Where $S(I_{TH})$ and $S(I_{MM})$ are the superpixel segmented image of the respective thermal image and mammogram image.

     end for

Calculate the detailed coefficients and approximation coefficients for each image.

Calculate fused coefficients.

     for $i = 1$ to n (n= no. of the column in the image)

     $S\_f(I_{fus}) = fusion\_rule(S(I_{TH}), S(I_{MM}))$

where $fusion_{rule}$ is spatial frequency DWT.

     end for

Fused image I_{fus} is reconstructed from pixel segmentation components.

     $I_{fus} = IDWT\{S_{f(I_{fus})}\}$

return archive.

end procedure

5.4.   Complexity

The computational complexity of the recommended algorithm (AWT-SPS) is described in this subsection.

5.4.1. Time Complexity

- The implementation of the AWT-SPS algorithm desires $O(I_{TH}(m \times n)) + O(I_{MM}(m \times n))$ time. Where m and n represent the number of rows and columns in each image, respectively.

- The time required for DWT calculation of each pixel is $O(I_{TH}(DWT \times m \times n)) + O(I_{MM}(DWT \times m \times n))$

- The time required for super pixel calculations is

$$O(I_{TH}(SPS_{iter} \times DWT \times m \times n)) + O(I_{MM}(SPS_{iter} \times DWT \times m \times n))$$

 where SPS_{iter} is the maximum number of iterations to simulate superpixel segmentation.

- The algorithm requires $O(fused) = O(I_{TH}(M)) + O(I_{MM}(M))$ time to calculate the detailed coefficients and approximation coefficients. Here, M indicates the number of fused coefficient values.

- Repeat Steps 2 to 4 until the image is reconstructed.

As a result, the SFDWT-SPS algorithm has the overall time complexity of

$$O(I_{TH}(SPS_{iter} \times DWT \times m \times n \times O(fuse)) + O(I_{MM}(SPS_{iter} \times DWT \times m \times n \times O(fuse)))$$

5.4.2. Space Complexity

AWT-SPS algorithm's space complexity is determined at the initial stage, which at any given time requires space. Due to this, AWT-SPS algorithm's overall space complexity is $O(I_{TH}(m \times n)) + O(I_{MM}(m \times n))$.

5.5.   Results and Discussions

The effectiveness of the proposed scheme is evaluated using both objective and texture features on the DMR dataset of breast thermal images.

5.5.1. Dataset Used

The study utilized the FLIR SC-620 IR sensor, featuring dimensions of 640 x 480 pixels, to capture infrared images from the Database for Mastology Research (DMR) [152]. This comprehensive dataset includes both thermogram and mammogram images in JPEG format, with a resolution of 96 dpi on both vertical and horizontal axes. The DMR dataset comprises images from 287 patients, ranging in age from 29 to 85 years. Table 5.1 provides a detailed description of the DMR dataset, highlighting its diverse patient demographics and the high-quality imaging parameters employed.

Table 5.1 Categorization of patients in the dataset.

Total number of individuals	235
Number of healthy individuals	184
Number of sick individuals	47
Number of unknown individuals	04

5.5.2. Texture Features

Both the image's local spatial intensity variations and its homogeneity are described by the textual features [153]. These are quite useful for selecting features and analyzing textures.

- Mean: The mean is used to calculate the average brightness of a fused image. Its value should be high in order for effective improvement.

$$mean = \frac{1}{mn} \sum_{a=1}^{m} \sum_{b=1}^{n} pA(a,b) \qquad (5.8)$$

Here, m and n signify the number of rows and columns in a fused image. pA is the coefficient

of approximation.

- Standard Deviation: It is used for contrast measurement. A high value of standard deviation indicates that the pixels are scattered and are far from the mean. It can be calculated as [153]:

$$\text{StD} = \sqrt{\sum_{a=1}^{m} \sum_{b=1}^{n} (pA(a,b) - mean)^2} \qquad (5.9)$$

where StD denotes the standard deviation. m and n are the number of rows and columns, respectively.

- Energy (En): The energy is a measure of the image's regional homogeneity. The mathematical formula for energy is given as:

$$En = \sum_{a=0}^{y-1} \left(p(x_i)\right)^2 \qquad (5.10)$$

Here, $p(x_i)$ denotes the probability distribution in each level. y indicates the total number of grey levels.

- Entropy (EnT): It is used to estimate data in the fused image. To get better results, the value of entropy should be high. The entropy is given below [154]:

$$EnT = -\sum_{b=1}^{z-1} m(b) \log m(b) \qquad (5.11)$$

where z represents the total number of grey levels. $m(b)$ denotes the probability density distribution of grey levels.

- Dissimilarity: Dissimilarity is a measure of distance between pairs of objects in the region of interest [104].

$$Diss = |x - y| \qquad (5.12)$$

x and y are the attribute values of two data objects.

Structural similarity measure (SSIM), peak signal-to-noise ratio (PSNR), mean square error (MSE), and signal-to-noise ratio (SNR) are well-known performance measures.

As many as nine parameters serve as the basis for comparing the proposed and the existing techniques. The images used are from the same patient and dataset, guaranteeing an unbiased comparison.

5.6. Performance Evaluation

This section presents the proposed technique's results as well as a comparison with other fusion schemes. The results for fused images are obtained by combining thermal and mammogram images from the same patient who has malignant breast tumor. Texture and objective traits are measured to show the effectiveness of the proposed technique.

(a) Texture Analysis

The proposed SPS-AWT method yielded fused images with excellent geometric content and high radiometric quality. A comprehensive texture analysis was conducted to evaluate the performance of the fusion technique compared to existing approaches. Several key texture features were computed and compared, including mean, standard deviation, energy, entropy, and dissimilarity. Table 5.2 shows the comparative analysis of the proposed approach with the existing techniques in terms of texture features.

The mean value represents the average luminosity of the fused image, with higher values indicating better spectral density. The proposed SPS-AWT method outperformed other techniques, achieving a mean of 1.925 compared to 1.324 for DWT, 0.919 for SA-DWT, and 1.736 for SF-DWT fused images. This significant improvement in mean value demonstrates SPS-AWT's ability to enhance the spectral information content. Standard deviation measures the contrast and dispersion of pixel values from the mean. While SA-DWT yielded the lowest

standard deviation of 54.827, the proposed method's value of 55.351 was comparable, differing by only around 1%. This indicates that SPS-AWT preserves contrast effectively.

Energy quantifies the homogeneity of the image region, where higher values are desirable. The proposed fusion method achieved an energy of 23.876, slightly lower than DWT (24.171) but higher than SA-DWT (23.895) and SF-DWT (23.848), suggesting maintained homogeneity. Entropy estimates the richness of information content in the fused image. SPS-AWT attained the highest entropy of 8.26 among all techniques evaluated, indicating superior information preservation and detail retention. The dissimilarity metric measures the variance between pixel pairs in the region of interest. With a dissimilarity of 0.6279, the proposed approach outperformed DWT (0.4222), SA-DWT (0.598), and SF-DWT (0.6221), signifying its ability to minimize distortions and artifacts.

Overall, the texture analysis validates the effectiveness of the SPS-AWT fusion framework in generating high-quality fused images with enhanced spectral characteristics, preserved contrast and details, reduced artifacts, and high information content compared to conventional wavelet-based fusion methods.

Table 5.2 Comparative analysis of the proposed approach with existing techniques in terms of textural features analysis.

Values / Techniques	Texture Analysis Values				
	Mean	StD	Diss	En	EnT
DWT	1.324	80.572	0.6279	24.171	8.146
SA-DWT	0.919	54.827	0.6221	23.895	8.177
SF-DWT	1.736	104.32	0.598	23.848	8.176
Proposed	1.925	55.351	0.4222	23.873	8.26

(b) Objective Analysis

In addition to texture characteristics, several objective metrics were employed to quantitatively assess the performance of the proposed SPS-AWT fusion technique against existing methods. These include the mean squared error (MSE), peak signal-to-noise ratio (PSNR), signal-to-noise ratio (SNR), and structural similarity index (SSIM). These metrics provide an objective evaluation of the fused image quality and the effectiveness of the fusion process. Table 5.3 depicts the results obtained from the proposed approach and other techniques in terms of the objective feature analysis.

The mean squared error quantifies the average squared difference between the fused and reference images. A lower MSE value indicates a smaller error and better fusion quality. The proposed SPS-AWT method achieved the lowest MSE of 31.367 among all techniques compared, outperforming DWT (108.567), SA-DWT (32.323), and SF-DWT (105.573). This low MSE demonstrates SPS-AWT's ability to effectively minimize distortions and artifacts in the fused output.

The peak signal-to-noise ratio is a measure of the maximum possible signal power relative to the noise power, with higher PSNR values implying better image quality. SPS-AWT attained the highest PSNR of 33.166 dB, surpassing DWT (27.77 dB), SA-DWT (33.04 dB), and SF-DWT (27.89 dB). This significant PSNR improvement indicates that the proposed method can effectively suppress noise and preserve signal integrity during the fusion process. The signal-to-noise ratio quantifies the desired signal level relative to background noise and unwanted distortions. While the proposed technique had a marginally lower SNR of 0.21 compared to DWT (1.643) and SF-DWT (1.553), it outperformed SA-DWT (0.728), suggesting maintained signal fidelity.

The structural similarity index measures the perceived quality of the fused image compared to the reference, considering aspects like luminance, contrast, and structure. With an SSIM of 0.915, SPS-AWT achieved the highest structural similarity among all evaluated methods, indicating superior preservation of structural details and visual quality in the fused output.

Overall, the objective analysis substantiates the effectiveness of the proposed SPS-AWT framework in generating high-quality fused images with minimized distortions, noise suppression, maintained signal integrity, and superior structural similarity compared to conventional wavelet-based fusion techniques.

Table 5.3 Comparative analysis of the proposed approach with existing techniques in terms of objective features analysis.

Values / Techniques	Objective Analysis Values			
	MSE	SNR	PSNR	SSIM
DWT	108.567	1.643	27.77	0.613
SA-DWT	32.323	0.728	33.04	0.914
SF-DWT	105.573	1.553	27.89	0.491
Proposed	31.367	0.21	33.16	0.915

(c) Subjective Analysis

To demonstrate the effectiveness of the suggested fusion method, 30 pairs of mammogram and thermal images with respect to the same patient, designated P-1 to P-30, are chosen. The size of each one is 256×256. The classification outcomes obtained with the suggested model are shown in Figure 5.5. The ResNet-18 model was used in the classification process. Using thermal images from the DMR dataset, the training accuracy—represented by the red line—reached 95%. The green and blue lines show the test accuracy values for thermal images and

fused images from the DMR dataset. The fused images' test accuracy is about the same as the thermal images. The visual comparison revealed that the SPS-AWT fused images successfully preserved both input modalities' structural integrity and complementary information. In contrast, the conventional methods suffered from issues like image mismatch, color asymmetry, and loss of salient details, as indicated by green arrows in the results. The proposed approach effectively addressed these challenges, generating fused images with consistent colors, improved contrast, and clear visualization of diagnostic details from the mammograms and thermal data. This comprehensive representation enhances the ability to detect and localize breast abnormalities accurately.
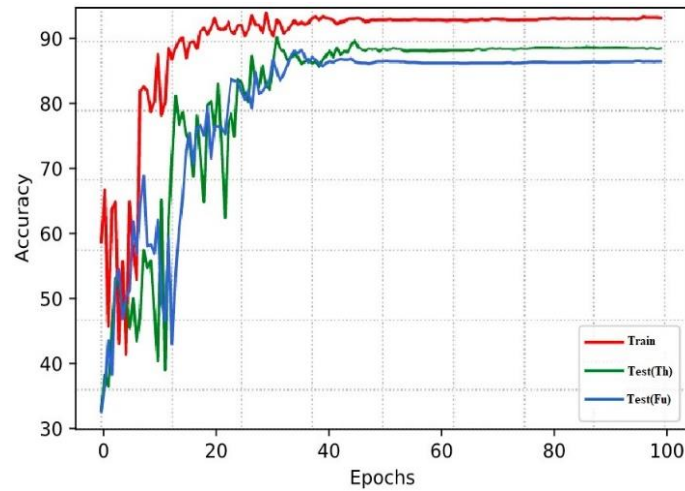
Fig. 5.5 Accuracy comparison of fused images on DMR dataset.

Overall, the subjective evaluation validated the superior performance of SPS-AWT in producing visually interpretable and informationally rich fused images compared to existing techniques, highlighting its potential for reliable multimodal medical image analysis.

(d) Comparative Analysis

Table 5.4 compares the performance of the proposed multimodal breast cancer detection method with several recent works that employ fusion techniques. The comparison is made in

terms of the fusion method used, the classification approach, the dataset employed, and several evaluation metrics like accuracy, Recall, and Precision.

Table 5.4 A comparison of the suggested model with work done on breast cancer detection using fusion technique.

Ref	Year	Fusion	Technique	Purpose	Acc	RC	P
[155]	2021	Multi-scale fusion	CNN	Feature fusion	90.37%	0.9421	0.9345
[156]	2021	Fusion of DenseNet 201- and 24-layer CNN	CNN	Fusion of two models	91.87%	0.9642	0.9533
[157]	2022	Multimodal fusion	CNN	Fusion of gene and image modality	88.07%	0.9388	0.9218
Proposed	-	Bimodal Image Fusion	ResNet-18	Fusion of two different image modalities	91.8%	0.9712	0.9839

The proposed approach utilizes a bimodal image fusion of infrared thermograms and mammograms, followed by classification using a ResNet-18 model. On the INbreast dataset, it achieves competitive performance with a test accuracy of 92.5% for thermal images and 91.8% for the fused images. Li et al. (2021) and Irfan et al. (2021) employ a multi-scale or parallel fusion of deep learning models on the BUSI dataset, attaining accuracies of 90.37% and 91.87%, respectively. Liu et al. (2022) fused gene expression and image data from the TCGA-BRCA dataset using a multimodal CNN, reporting 88.07% accuracy.

Despite using a smaller dataset of 30 fused test images, the proposed method demonstrates promising results, with its Recall of 0.9839 and Precision of 0.9712 being comparable to the state-of-the-art fusion-based approaches. This highlights the efficacy of the novel SPS-AWT fusion framework for multimodal breast cancer detection.

5.7.   Summary

The proposed chapter discusses the fusion of images from different modalities, aiming to leverage the complementary information provided by each imaging technique. Combining thermal images with mammograms enhances the diagnostic process by capturing physiological changes and detailed structural information of breast tissue, respectively. By fusing these modalities, a more comprehensive image can be created, potentially improving the accuracy and reliability of breast cancer detection. Multimodal approaches are crucial in identifying malignancies that might be missed when using a single imaging modality alone. Still, the fusion of images with different modalities has always been challenging in the medical field because of distorted spectral information in the resulting image.

To address this challenge, a novel technique called AWT-SPS was developed for the fusion of breast cancer images. Comparative analysis with standard DWT methods revealed that the proposed technique yielded better results both visually and statistically. The proposed approach aims to efficiently remove redundant information and ambiguities while enhancing image clarity, leading to clear, precise, and comprehensive target predictions.

This advancement holds promise for the accurate early detection of breast cancer without posing any risk to women. By improving the accuracy of breast cancer screening techniques and addressing the issue of multimodal image mismatch, the proposed fusion technique could significantly enhance the effectiveness of breast cancer diagnosis and treatment.

CHAPTER 6
Hybrid Model for Breast Cancer Detection from Ultrasonic Images

6.1. Preamble

Breast ultrasound is commonly used for the early detection of breast cancer. The existing geodesic-based methods use pre-defined filters that necessitate extensive prior knowledge to achieve the region of interest in the input image. Furthermore, the majority of ultrasound images suffer from noise and acoustic shadowing, which reduce the accuracy of tumor detection. To make the breast ultrasound image more informative, the discriminative features can also be extracted to improve detection accuracy. This work proposes a method to combine Active Contour and Texture Feature Vectors to find discriminative patterns. A comprehensive set of discriminative features for cancer detection in ultrasound images is created by combining the two learning models. Breast ultrasound images dataset is used to evaluate the suggested method and compare it to the recently developed algorithms.

In this work, the main concern is the application of the active contour model to medical image segmentation. Here, two types of active contour models namely, the parametric models, such as Snake and PIG, and the geometric models, like geodesic are used.

6.2. Proposed Approach

The proposed model exploits two feature vectors viz., Active Contour Feature Vector (ACFV) and Texture Feature Vector (TFV) (see Fig. 6.1). ACFV is used to separate the pixel values of interest from the image to further analyze and process these values. On the other hand, TFV is

used for pattern recognition of cancerous images. This may be attributed to the fact that the majority of elements on the surface of cancerous organs are irregular.
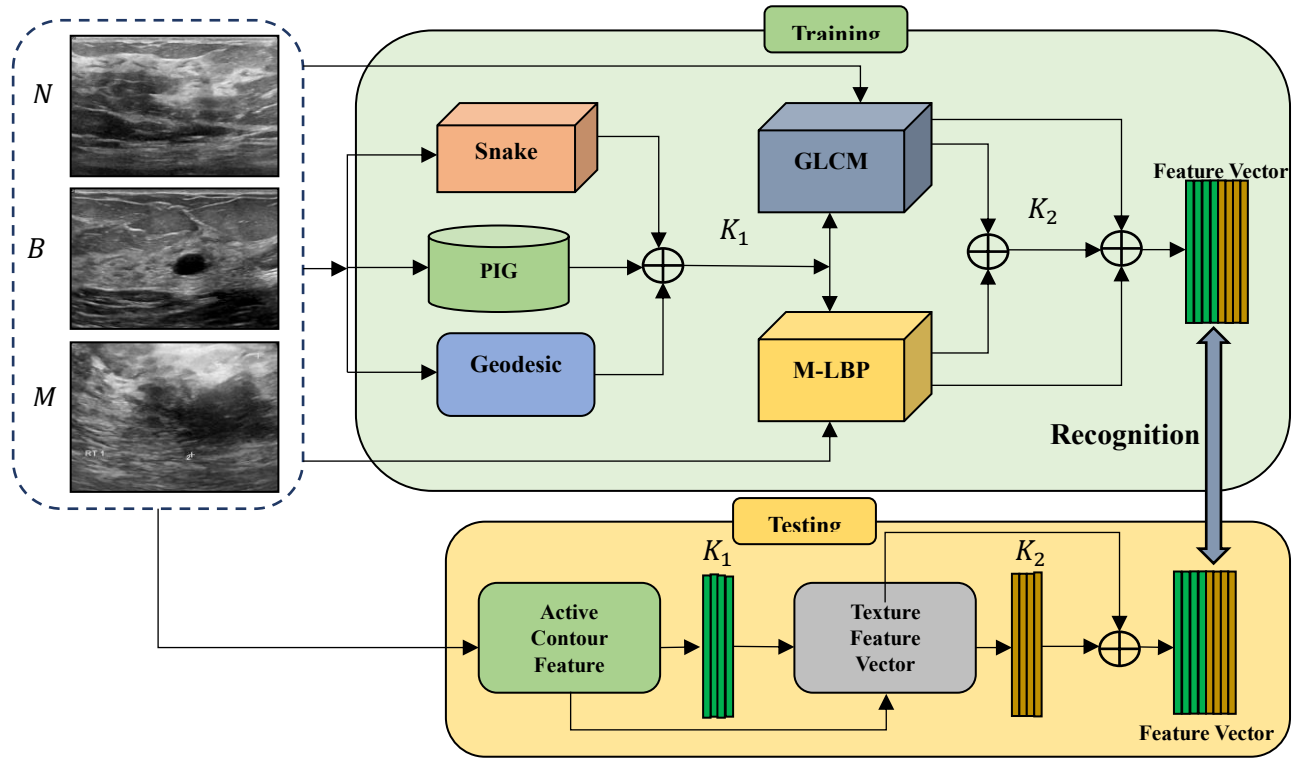
Fig. 6.1 Training and testing model for our proposed model.

6.3. Active Contour Feature Vector

Active Contour Feature Vector (ACFV), is defined in terms of the length and area of the input image, based on the idea of active contour model construction. Kass et al. [158] were the first to propose an active contour model, which transforms problems of image segmentation into energy minimization problems where the active contour energy is optimized towards the boundaries of the object. In respect of cancerous tumors, different active contours may be used to segment tumor images with precise boundary lines, as these lines are critical for the diagnosis and detection of any abnormalities. Three types of active contours are used in this work, i.e., snake, geodesic, and Poisson inverse gradient (PIG). The snake contour identifies

and outlines the target object [159]. To define the contour flow, geodesic contour uses a gradient vector flow field as an energy constraint [160]. Whereas PIG estimates the energy field from the force field.

6.3.1. Texture Feature Vector

Distinguishing cancerous tissues from non-cancerous ones can be challenging, even though each tissue type has distinct characteristics. Textures can be characterized by the spatial distribution of intensity levels in the neighborhood. In this work, Local Binary Pattern (LBP) and Gray Level Co-Occurrence Matrix (GLCM) are used for the detection of structural and statistical textures features, by analyzing grey-level spatial correlation and defining the allocation of pixels within the image space [161], respectively. LBP is used to extract the position and structure of local features [160]. However, GLCM describes the texture.

6.3.2. Proposed Model

This work proposes a technique comprising two models for the identification of breast cancer lesions. Fig. 6.1 depicts the framework for the proposed model. The Active Contour Feature Vector (ACFV) and Texture Feature Vector (TFV) are extracted from the input image, followed by the fusion of these two vectors to yield a single feature vector. This information helps us discriminate the cancerous from non-cancerous images. The single feature vector thus obtained, provides us with a discriminative feature (K) about shape, size, and texture for breast cancer detection, it is computed as:

$$K = K_1 + K_2 \tag{6.1}$$

where $+$ denotes the addition of two vectors. K_1 and K_2 represent the features that are output from the proposed models. Finally, K is fed to ResNet-18 for classification.

6.3.3. Optimization

Model I (ACFV model)

Active Contour Feature Vector (ACFV) model (see Fig. 6.2.) is used to extract features related to the shape and size of the cancerous area(s) involving every pixel in the input image of the breast. Based upon the idea proposed in [162], the active contour features are extracted.
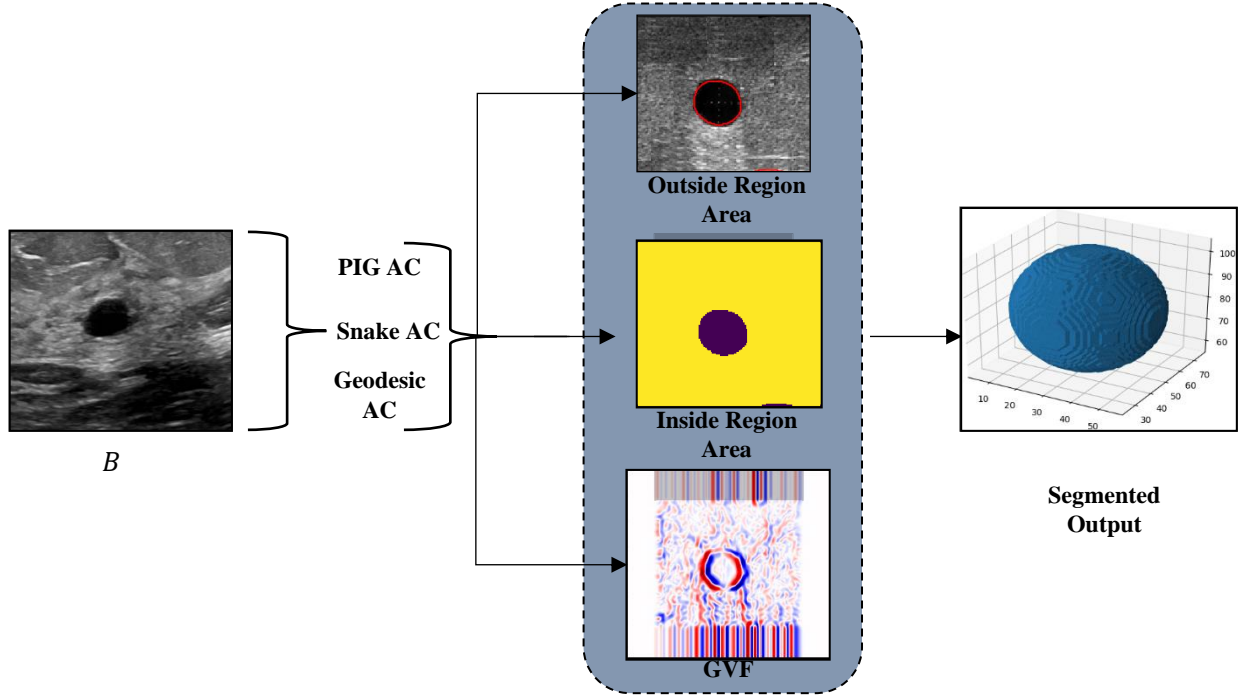
Fig. 6.2 Proposed Active Contour Feature Vector model.

For accurate interpretation of cancer detection, the foreground and background are separated using the active contour technique. The segmented region of interest is subjected to further image analysis. The output vector of active contour features (K_1) is the fused output has features of length, area, and energy related to the input image. Hence, it is expressed as:

$$K_1 = \text{Length} + \text{C*(Area)} + E_{\text{AC}} \qquad (6.2)$$

103

Here, C is constant for balancing regularization and the area curve. C is usually set to 1. *Area* represents "region in + region out" of the input image (white portion of Figs. 6.3. (b) and 6.3 (c). E_{AC} is the energy for contour formation. The length is defined as:

$$\text{Length} = \int_{\text{CUR}} |\nabla z| ds \tag{6.3}$$

where CUR denotes the length of the curve. z is the characteristic function valued between 0 and 1.

Let CUR_1 and CUR_2 represent the energy of the curve value of the foreground and background regions, respectively.

The mathematical formulation of Area is given below:

$$\text{Area} = \int \Psi((CUR_1 - y)^2 - (CUR_2 - y)^2) z dx \tag{6.4}$$

Where Ψ represents the domain of an image with pixel positions indicated by x and y

E_{AC} can be defined as:

$$E_{AC} = E_{IN} + E_{EX} + E_{IM} \tag{6.5}$$

Where E_{IN} represents the internal energy that imposes piecewise smoothness limitations in the contour. The internal energy (E_{IN}) can be mathematically formulated as:

$$E_{IN} = \gamma \left|\frac{\partial m}{\partial w}\right|^2 + \eta \left|\frac{\partial^2 m}{\partial w^2}\right| \tag{6.6}$$

γ defines how far the snake may be stretched and how much flexibility it has. Snake's stiffness level is denoted by η. m is a spline parameter with a range of [0,1]. w is a linear parameter with a value of 0 or 1.
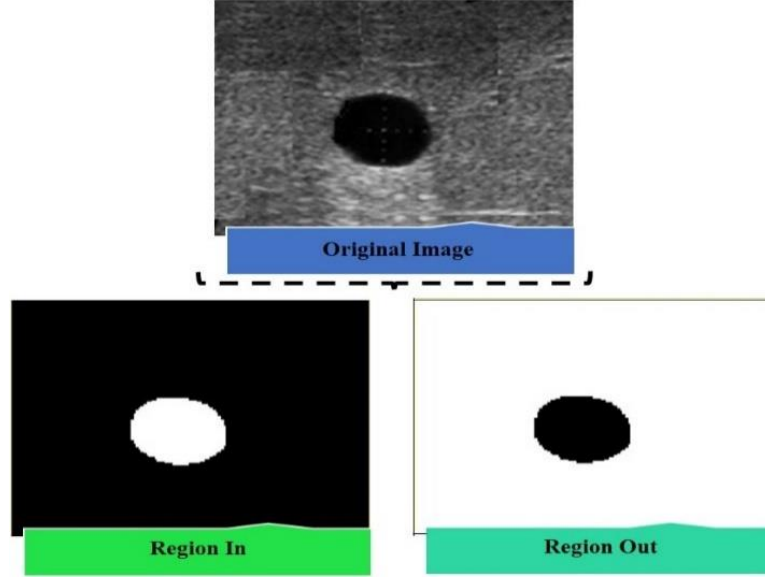
Fig. 6.3 Active contour region constraints for image segmentation.

E_{EX} denotes the external force that propels a snake toward the image's focal point. E_{EX} can be defined by high-level perception and interaction.

$$E_{EX} = \int f(\partial m)\partial w \tag{6.7}$$

The contour of the object (E_{IM}) is defined as:

$$E_{IM} = \alpha_1 i(x,y) + \alpha_2 |\nabla i(x,y)|^2 \tag{6.8}$$

Here, α_1 and α_2 are the line and edge coefficients, respectively. In case of positive values, the snake will align itself to darker pixel regions, whereas in case of negative values, it will progress towards bright pixels. The Active Contour Feature Vector (ACFV) can approximate the entire geodesic features of a breast ultrasound image.

Model II (TFV model)

The texture feature vector is then calculated by concatenating both GLCM and M-LBP features (see Fig. 6.4). GLCM has 28 features to characterize spatial patterns [163]. It extracts textures and outperforms the other extraction methods in terms of accuracy and computation time. The distance and angle of an image are determined by its gray level. Smoothness, stiffness, and

105

irregularity are the texture properties. A term is used to describe tone color variations or gray scale levels in an image.

GLCM Indicator ($l = 1$)
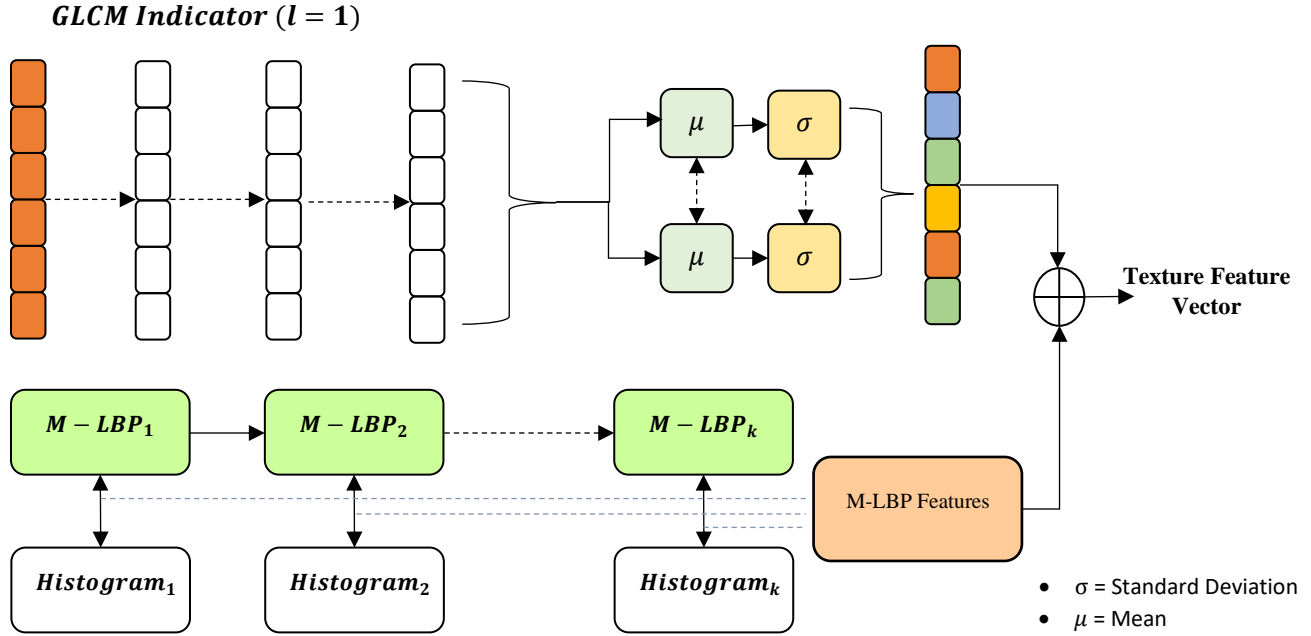
Fig. 6.4 Proposed Texture Feature Vector Model.

GLCM measures the frequency of appearance of pairs of pixels with different grey-level intensities and distances from each other. The averages of the directions 0, 45, 90, and 135 were then calculated. Meanwhile, the distance value (l) is 1. X and Y represent the distance in two directions, respectively.

$$l = (l_X, l_Y) \tag{6.9}$$

GLCM is calculated by first calculating the direction and distance, which is used to determine the image value. Estimating the formed paired pixel, and lastly producing a GLCM matrix, that is then normalized using Eq. (6.10):

$$GLCM_{-K2(X,Y)} = \frac{1}{\sum GLCM_{Matrix}} GLCM_{Matrix} \tag{6.10}$$

Where,

$$GLCM_{-K2} = GLCM_{-(dI,dJ)(X,Y)}$$

$$= \sum_{I=1}^{M} \sum_{J=1}^{N} \begin{cases} 1, & if \quad i(I,J) = X \\ & and \quad i(I+dI, J+dJ) = Y \\ 0, & Otherwise \end{cases} \tag{6.11}$$

Where, i is the input image of size $M \times N$.

The GLCM matrix is formed using four directions and distances for each of the directions and distances considered. The matrices were all normalized.

The simplest way to group them is to recursively apply modified-LBP operators and compute final encoding histograms. In the proposed model, M-LBP computing blocks are connected in a series manner (see Fig. 6.4). The texture of a single texture is described by LBP encoding, while the texture of multiple textures is described by a second batch of LBP encoding.

The basic operations that support LBP are analyzed first, and then, recursive extractors of LBP features are put together using the binarization function $L(A_{ref}, A_k)$ [164]. The binarization function is useful since it is unaffected by scaling and translation.

$$L(p_1 A_{ref} + p_2, p_1 A_k + p_2) = L(A_{ref}, A_k) \tag{6.12}$$

Where $p_1 = \frac{A_l - A_{ref}}{A_l - A_{ref}}$, and $p_2 = A_{ref} \frac{A_l - A_k}{A_l - A_{ref}}$ \tag{6.13}

The control parameters of active contour-based segmentation are tabulated in Table 6.1.

Table 6.1 Initial parameters of Active Contour Based Segmentation.

Parameter	Snake	PIG	GVF
Initial Iteration	50	45	50
Membrane energy	-	-	0.1
Thin plate energy	-	-	0.1
Learning rate	1 e^{-5}	1 e^{-5}	1 e^{-5}
Step size	0.5	0.5	0.5
m_u	-	-	0.2f
α	1	0.3	1
β	1	1	1
σ_1	-	-	0.8f
σ_2	-	-	1f
No. Neighbors	9	9	9

Algorithm: Active Contour and Texture Feature Vector Model

Input: $K_{ULT}(g \times h)$; Original ultrasound image with g=no. of rows and h= no. of column

Procedure

Preprocessing: Initialize the image $K_{ULT}(g \times h)$ for preprocessing

Apply image segmentation $y, z \in [0,1]^{a \times b}$

where $a = 0,1,....,n;$

$b = 0,1,....,n;$

Feature Descriptor: Apply Active Contour Feature Vector (ACFV) to calculate K_1;

$$K_1 = Length + C(Area) + E_{AC}$$

Calculate K_2 using Texture Feature Vector (TFV);

$$K_2 = (GLCM + M - LBP)K_1$$

$$GLCM_{-(dI,dJ)(X,Y)} = \sum_{I=1}^{M} \sum_{J=1}^{N} \begin{cases} 1, \; if \quad i(I,J) = X \, and \\ \qquad\quad i(I+dI, J+dJ) = Y \\ 0, \qquad Otherwise \end{cases}$$

Output: K; Feature Vector

$$(FV) = K = K_1 \oplus K_2$$

Utilize the obtained image sequences to train/test the proposed ACTFV model for estimation and detection

6.4. Computational Complexity

The time and space complexities of the proposed approach are mentioned in the preceding subsections.

6.4.1. Time Complexity

The initialization of ACTFV needs $O(K_{ULT}(g \times h))$ time. Where K_{ULT} is the ultrasound image. g and h are the number of rows and columns, respectively.

ACTFV is divided into two parts such as ACFV and TFV. The time taken by ACFV is

$O(AC_{SNAKE}(g \times h)) + O(AC_{PIG}(g \times h)) + O \rightleftarrows (AC_{GEO}(g \times h))$

Here, AC_{SNAKE}, AC_{PIG} and AC_{GEO} are the outputs obtained from snake active contour, Poisson inverse gradient, and geodesic active contour, respectively.

The time taken by TFV is $O((T_{GLCM}(g \times h))K_1) + O((T_{M-LBP}(g \times h))K_1)$.

Here, K_1 is the output obtained from the ACFV block. T_{GLCM} and T_{M-LBP} are the features obtained from GLCM and modified-LBP block, respectively.

Time taken by training and testing of the proposed model is $O_{TT} = O(K_{ULT}(Train)) + O(K_{ULT}(Test))$.

K_{ULT} represents ultrasound image features.

Therefore, the overall time complexity of the proposed model is $O\left(\left(AC_{SNAKE}(g \times h)\right) + \left(AC_{PIG}(g \times h)\right) + \left(AC_{GEO}(g \times h)\right) \oplus O\left(\left(T_{GLCM}(g \times h)\right)K_1 + \left(T_{M-LBP}(g \times h)\right)K_1\right)\right)$

6.4.2. Space Complexity

The feature extraction model's space complexity is considered during the initialization. The overall space complexity of the proposed approach is $O(K_{ULT}(g \times h)) + O(K_{ULT}(Train)(g \times h))$.

6.5. Performance Evaluation

In order to ensure efficacy and reliability, it is essential to assess the performance of the proposed model for breast cancer detection. The performance of the proposed model was tested on the Breast Ultrasound Images (BUSI) dataset [165].

6.5.1. Dataset Used

The images in BUSI dataset are taken from women aged 25 to 75 years old [166]. The dataset includes 780 PNG images of 600 patients with an image of 500x500 pixels. Table 6.2 depicts the characterization of the BUSI dataset.

Table 6.2 Characterization of BUSI Dataset.

Total no. of individuals	600
Total no. of images	780

No. of normal images	133
No. of benign images	487
No. of malignant images	133

6.5.2. Performance Measures

The effectiveness of the proposed approach is measured by using mean, standard deviation, and energy. The other well-known performance metrics namely accuracy, precision, recall, and Jaccard are used to evaluate the proposed model. The accuracy value assesses the proportion of patients who are correctly classified as malignant and benign. The recall value determines the proportion of malignant instances classified as malignant cases by the model. The Jaccard Index is used to compare the similarity of two sample sets. The Jaccard index has a value between 0 and 1. The resemblance is considered to be strong as the value approaches 1.

6.6.   Results and Discussion

The proposed methodology is evaluated both qualitatively and quantitatively. Here, 80% of the dataset is used for training, while the remaining 20% is used as test data. The images are first preprocessed and then fed to ACTFV. The inside and outside tumor zones of the breast must be segmented, yet their shapes will occasionally be noisy, crowded, and ambiguous. Poisson inverse gradient is used to highlight the contour. Fig. 6.5. shows the steps of tumor mapping using the active contour method.

(a)   (b)   (c)   (d)
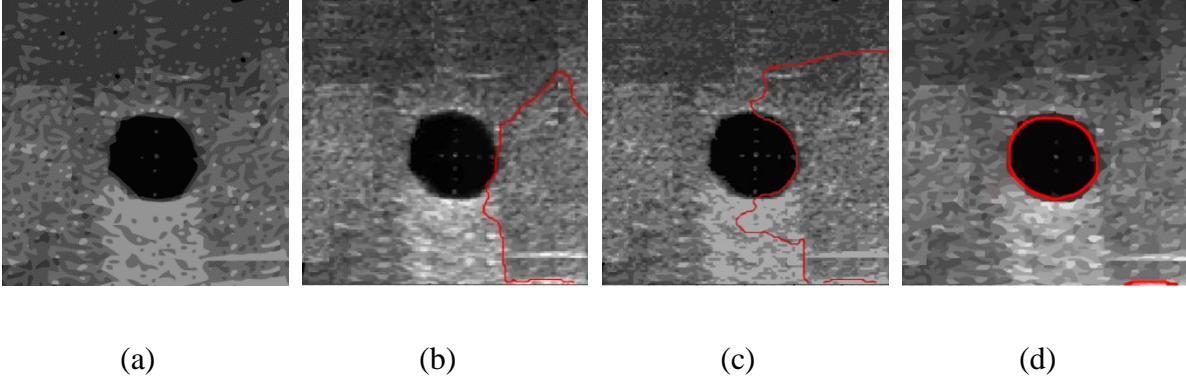
Fig. 6.5 Results obtained from Poisson inverse gradient (PIG) active contour, (a) original image, (b) 1st stage of mapping, (c) 2nd stage of mapping, and (d) the fully mapped tumor shape .

Fig. 6.6. shows the results of the geodesic active contour, with the edge map and gradient field

in the direction of x and y axis, respectively.

(a) Original   **(b) Edge**   **(c) fx**   **(d) fy**

(e) GVFx   **(f) GVFy**   **(g) f**   **(h) GVF**
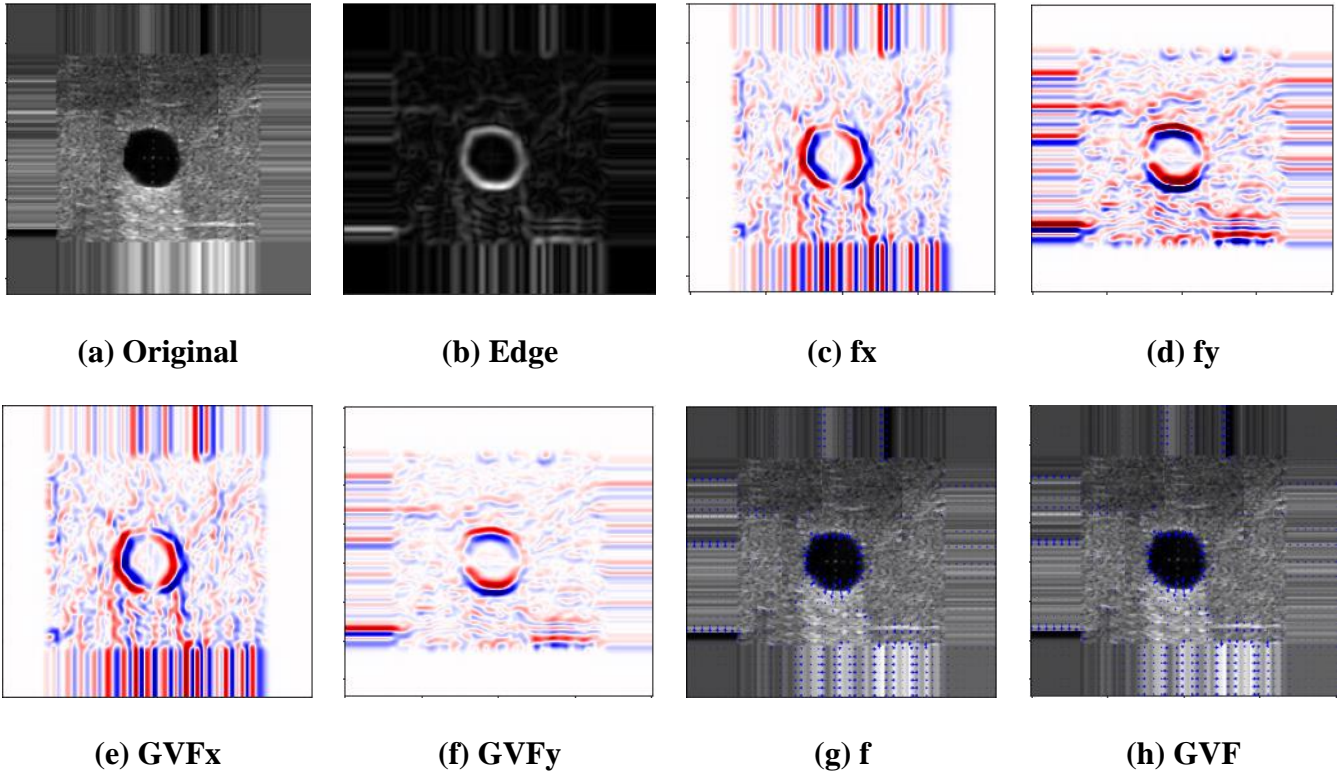
Fig. 6.6 Results of geodesic active contour, (a) gray scale original image, (b) edge map of the original image, (c) gradient field in x axes, (d) gradient field in y axes, (e) the gradient vector flow in x, (f) gradient vector flow in y directions, (g) overall gradient field and (h) total gradient vector, flow around the edge of the tumor.

Table 6.3 illustrates a comparative analysis of the proposed approach with the existing

techniques in terms of performance measures. The feature fusion method used in the proposed

112

work produces the best results for ultrasound images. The accuracy (Acc), recall (RC), precision (P), Jaccard index (JI), and F1 score obtained from the proposed approach are 99.4%, 94.8%, 94.3 %, 94.9.76 %, and 93.3%, respectively. Ultrasound characteristics such as acoustic enhancement and shadowing can occasionally be predictive of lesion characteristics in the area surrounding the lesion. This could be one of the reasons for the positive results produced with features taken from the lesion's adjacent region as input. The features extracted from lesion area are more meaningful and preserve more information than the texture features. It is observed from Table 6.3 that the proposed method outperforms the other existing methods.

Table 6.3 Quantitative results on BUSI dataset, as well as the number of parameters for all networks built using our suggested model.

Ref.	Feature Extraction		Parameters			
	ACF	TF	Acc	RC	P	F1
[167]	✓	✓	96.25	88.79	80.39	86.25
[69]	✓	✗	95.4	89.9	94.05	91.4
[168]	✗	✓	87.58	91.44	88.29	89.87
[169]	✗	✓	88.37	86.36	62.38	63.18
[170]	✗	✗	93.70	94.62	88.62	92.66
Proposed	✓	✓	**99.4**	**94.8**	**94.9**	**93.3**

This study proposes an automated model for detecting tumors using snake active contour and analyzes a wide range of features for breast ultrasound (BUS) classification. The features of the lesion include its size, shape, geodesic, and texture. While the study yielded promising results, it only focuses on unimodal systems; future computer-aided diagnosis (CAD) systems should consider incorporating multimodal systems for improved accuracy.

6.6.1. Ablation Study

To explore the effect of features extracted from the proposed model for the detection of breast cancer, an ablation study was carried out in terms of DICE score (D), Jaccard index (JI), and Hausdorff Distance (H). Model 1 uses a very basic design that employs snake and PIG active counters at the segmentation part. The results are shown in Table 6.4 Next, the base model is extended as model 2, by replacing PIG with the GVF active contours. Model 2 provides a more refined description of segmented images, with respect to Model 1. In model 3, PIG and GVF active contours are used for the segmentation part. The results are almost the same as those of model 1.

Finally, in the proposed model, the results of PIG, Snake, and GVF active contours are fused for proper segmentation. There is a significant improvement in terms of DICE score, Jaccard index (JI), and Hausdorff Distance (H). Table 6.4 shows the comparison of different variants along with the proposed one.

Table 6.4 Comparison of Segmentation Results.

Model	D	H	JI
Model 1	0.911	7.24	70.42
Model 2	0.956	5.982	78.44
Model 3	0.921	6.73	72.98
Proposed	0.981	5.5	81.76

6.7. Summary

This work discusses the potential of using active contour and texture patterns with the hope of eventually developing an efficient breast cancer recognition system that aids therapists in the diagnosis and monitoring of malignant tissue. The proposed model has been constructed by

fusing the most active contour and texture features to find complete and discriminative patterns. A simple yet effective feature extraction algorithm including geodesic and texture features, for the classification of breast lesions in ultrasound images with the aid of Resnet-18 was proposed. Accuracy obtained from the proposed scheme was 99.4%, which was 3.15% more than the existing model [167].

is also observed that torque ripples are less when IHC is employed as speed controller instead of the conventional PI controller.

CHAPTER 7
Modified Transformer based Pixel Segmentation for Breast Tumor Detection

7.1. Preamble

Transformer-based models have outperformed traditional models in a variety of tasks, meeting advanced benchmarks. Transformer-based models, in particular, excel at completing diverse tasks to meet the desired standards in Natural Language Processing (NLP) [171]. Transformers' self-attention mechanism enables dynamic highlighting of key features within word sequences. Transformers have exceptional capabilities in modelling long-term dependencies and capturing extensive contextual information, according to existing literature. As a result, they are useful as backbone encoders in computer vision tasks detecting breast lesions by combining the benefits of residual convolutional networks and transformers. For breast cancer classification, the model employs a support residual deep learning network to generate meaningful features, while the transformer component makes use of self and cross-attention mechanisms. The proposed model demonstrates the ability to identify breast cancer in both simple (3-stage) and complex (5-stage) classification scenarios. The methodology used in this study is consistent throughout the stages of data collection, preprocessing, patch creation, and breast lesion identification.

7.2. Proposed Approach

In this work, deep feature extraction is achieved using a new segmentation method along with deep learning techniques, and multi classification is achieved using a transformer-based model.

To increase the precision of breast cancer detection in mammogram images, the proposed deep learning model requires that a few requirements be met, as shown in Fig. 7.1. Firstly, the collected medical images were in PNG format. Preprocessing was then used to get rid of unwanted objects and improve the border of the segmented breast images. Then, augmentation, patching, and labelling processes were carried out. Finally, the proposed model was trained and tested using the generated patch images.
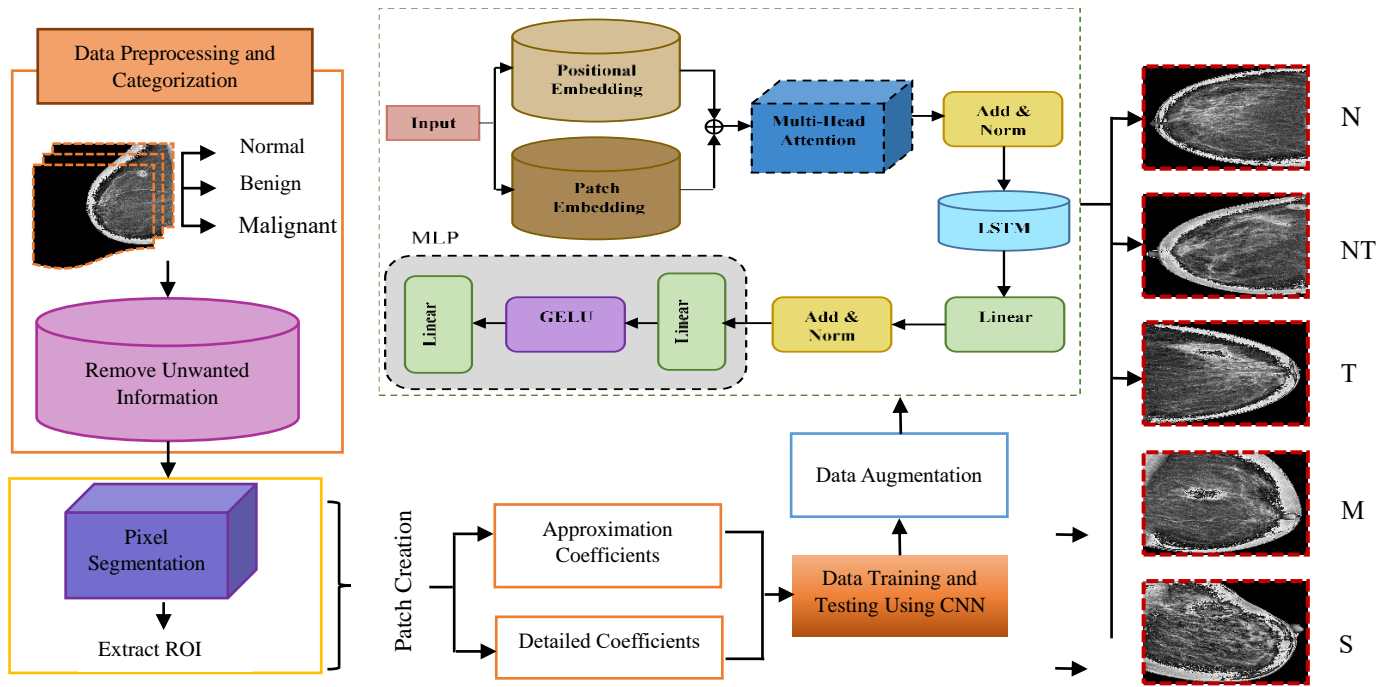
Fig. 7.1 Proposed Model for breast cancer classification in mammogram images.

(i) Data Acquisition and Image Collection

In this study, the proposed model is developed and tested using breast image data from the publicly available dataset INBreast. This database is publicly available and can be obtained from [38]. There are 410 FFDM mammograms from 115 patients in this collection. For healthy and unhealthy cases, the INbreast includes both Craniocaudal (CC) and Mediolateral Oblique (MLO) views. Every mammogram has a DICOM file with an XML document, some case-specific information as well as ground truth descriptions of any lesions found in

117

unhealthy mammograms. Similar to previous studies, the domain researchers assigned the tumor class of the original annotated breast image to its extracted patch ROIs from that image [172–174]. Therefore, the label of an image is taken from the dataset's metadata and kept for the created patches. For example, if an original image has a malignant label, the extracted patch images will have the same malignant label, and so forth. Furthermore, the dataset contains information for each patient that include breast density, left or right breast, the image view, the type and distribution of their abnormalities, their assessments, their pathology, and their subtlety [38].

(ii) Data Preprocessing

The mammogram images of the dataset are in PNG format. During the pre-processing step, unwanted artifacts features were removed first, and then the boundary of the breast image was smoothed. The image thresholding technique was used for removing unwanted artifacts from each mammogram [175]. The same threshold value is used for every pixel. A maximum value is set if the pixel value is greater than the threshold; otherwise, it is set to 0.

The first argument is the source image, which must be grayscale. The second input is the threshold value, which is used to categorize the pixel values. The third input is the maximum value allocated to pixel values greater than the threshold. The procedure produces two outputs. The threshold used is the first output, and the thresholded image is the second. This process was used to convert the grayscale image into a binary format so that different parts of mammogram could be easily distinguished. The thresholding technique has different operation types such as binary, trunc, and tozero, as shown in Fig. 7.2.

Fig 7.2 (a) shows the original image, Fig 7.2 (b) is the generated image using binary thresholding. It is of simple thresholding technique that uses a defined adaptive threshold to segment the image. Fig. 7.2 (c) shows the generated image using binary inversion operation.

Fig. 7.2 (d) shows the image using the Trunc operation. Here, values greater than the threshold are reduced to the threshold value. Every other pixel remains the same. Fig (e) and Fig (f) show the generated image using Tozero and Tozero Inversion operations, respectively. In the Tozero operation, pixels have an intensity value less than the threshold value and set to 0.

| (a) Original Image | (b) Binary | (c) Binary Inversion | (d) Trunc | (e) Tozero | (f) Tozero Inversion |
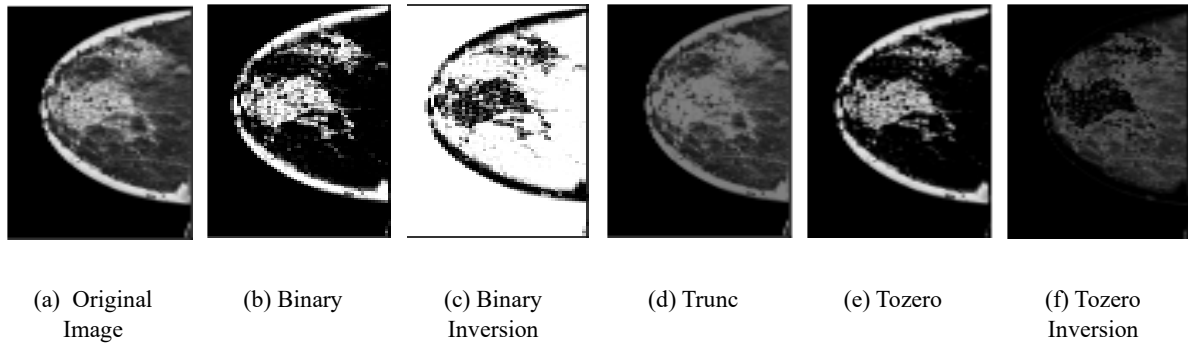
Fig. 7.2 Different operations of thresholding techniques: (a) Original Mammogram, (b) the generated image using Binary operation, (c) the generated image using Binary Inversion operation, (d) the generated image using Trunc operation, (e) the generated image using Tozero operation, and (f) the generated image using Tozero Inversion operation

(iii) Pixel-based patch creation

Pixel segmentation is used to improve learning accuracy. The features extracted from the threshold operation are used to decide whether a pixel belongs to the tumor class or non-tumor class. This objective is obtained by employing pre-processed images. When compared to previous pixel segmentation methods, the proposed pixel-based segmentation produces high-quality boundary coherence. For segmentation, it is possible to extract many characteristics from pixels, including color, texture, appearance, and location. However, in filamentary images, texture is the fundamental distinction between the background and foreground regions [176]. According to [177], the Gabor feature is suited particularly well for texture representation and discrimination. As a result, in this work, Gabor features from each input image are extracted. Gabor features analyze whether a image contains any specific frequency content in a specific direction in a localized region around the point of analysis. Each pixel in the input image has seven features. The first six features give the normalized

maximum Gabor filter response among 18 directions in the green channel of an image, whereas the 7th feature gives the normalized intensity of the green channel. 18 directions are being $10°, 20°, 30°, 40°, … … 100°, … . .180°$. Gabor filter is used to create an a by b cell array whose elements are y by z matrices. a and b the number of scales and orientations for the Gabor filter here, respectively y and z are the number of rows and columns, respectively. A Gaussian filter gives the function modulated by a complex sinusoidal plane wave.

$$G_{(m,n)} = \frac{f_u}{\pi\gamma\eta} \exp\left(-(\alpha^2 m'^2 + \beta^2 n'^2)\exp(2\pi f_u m')\right) \tag{7.1}$$

Where

$$m' = \left(m - \frac{y+1}{2}\right)Cos\theta b + \left(n - \frac{z+1}{2}\right)Sin\theta b \tag{7.2}$$

$$n' = -\left(m - \frac{y+1}{2}\right)Sin\theta b + \left(n - \frac{z+1}{2}\right)Cos\theta b \tag{7.3}$$

Here, α and β are the spread of the function in two dimensions, respectively. γ and η are the spatial aspect ratio. f_u is the frequency. The values obtained are the pixel feature that gives the region of interest. Fig. 7.3. shows the result obtained after pixel segmentation.

| (a) | (b) | (c) | (d) | (e) |
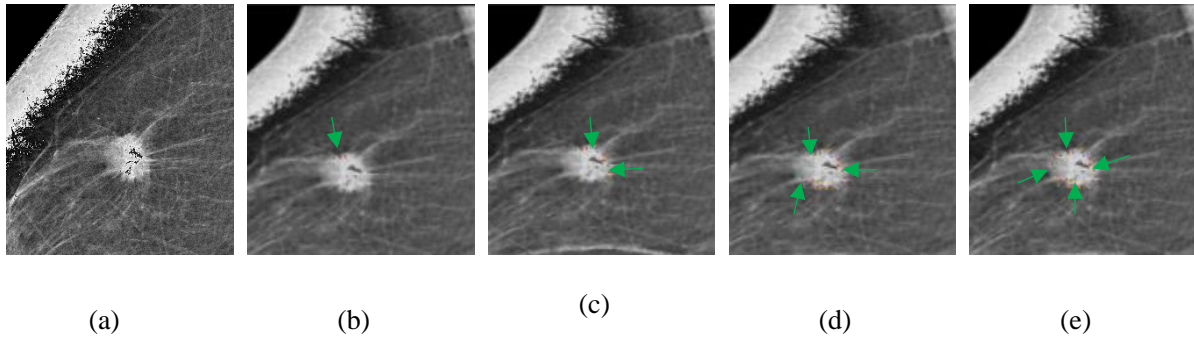
Fig. 7.3 Results obtained from pixel segmentation: (a) original image, (b) 1st stage of patch creation, (c) 2nd stage of patch creation (d) 3rd stage of patch creation, and (e) fully mapped tumor shape .

After applying the two procedures, a total of 1230 patch images were created including 185 normal patches and 1045 patches, 600 of which were malignant, and 445 were benign. All

normal patches were stored in a folder, whereas abnormal patches were stored in two different folders: one for benign and the second for malignant.

Further, DWT is also applied to calculate the approximation and detailed coefficients of the patches created using pixel segmentation.

The row f_r and column f_c frequencies are calculated as follows:

$$f_r == \sqrt{{}^{1}\!/\!{mn} \sum_{x=0}^{m-1} \sum_{y=0}^{n-1}(f(x,y) - f(x, y-1))^2} \qquad (7.4)$$

$$f_c = \sqrt{{}^{1}\!/\!{mn} \sum_{x=0}^{m-1} \sum_{y=0}^{n-1}(f(x,y) - f(x-1, y))^2} \qquad (7.5)$$

The patch f with grey scale $f(x, y)$ at location (x, y) is of size $m \times n$.

Area, intensity, and other helpful image characteristics have been determined using these.

Algorithm for patch creation

Input: $M_{ORI}(m \times n)$, original mammogram image with

$\quad$ m = no. of rows and n = no. of columns

Preprocessing: Initialize the input image for preprocessing

Apply thresholding.

$\quad$ Begin

$\quad$ Read M_{ORI}

$\quad$ Threshold value, $T_{ini} = 0$

$\quad$ Maximum value, T_{max} = 255

$\quad$ Thresh = CV2.threshold (M_{ORI})

$\quad$ Return image M_{new}

Apply pixel segmentation on $M_{new}(m \times n)$

$\quad$ Create a patch based on multi-exposure images

While (x < $PixelSegmentation_{iteration}$) do

For each patch do

Update the image patches obtained through segmentation

End for

End while

Update M_{new}

For i = 1 to n

End for

Calculate the detailed coefficient (DC) and approximation coefficients (AC) for each image

Calculate fused coefficients

For i = 1 to n

$f(M_{new}) = fusion\_rule(F(M_{DC})), F(M_{AC}))$

End for

End Procedure

(iv) Data Augmentation and Splitting

After patch creation, we proposed changes to the benign and malignant categories according to their texture and size. Table 7.1 shows the description of proposed changes for multi-classification.

Table 7.1 Proposed multi-classification description.

Name	Category	Explanation
N	Normal	No tumor
B1		Tumor < 3cm, no features
B2	Benign	Tumor >3 but <7, Does not spread beyond the milk ducts

M1	Malignant	Tumor >7, cancer cells have invaded the surrounding normal tissues
M2		Metaplastic, aggressive

Two datasets are created in this procedure, by employing generated patches based on the texture features and size of the tumor. (i) Original dataset classification (3 classes); and (ii) multiclass classification (5 classes). Both datasets were generated as reported in Table 7.2. The first dataset has three generated folders called ('N', 'B', and 'M') that hold all 410 patches. The patch dataset was augmented to create a balanced dataset. There are a total of 410 original images in total (including all three classes). Augmenting is the process of using original patches to create new ones that are identical to those in the benign, normal, and malignant folders. This step was repeated several times until the total number of files in the folder get balanced. In this paper, augmentation was applied only to the training set following data splitting to avoid overlapping.

Table 7.2 Datasets splitting training, and testing description.

Basic Classification			
Data Splitting	**Normal (N)**	**Benign (B)**	**Malignant (M)**
Training (80%)	148	356	480
Testing (20%)	37	89	120
Total Patches	185	445	600
Multiclass Classification			

Data Splitting	Normal	Benign (B1)	Benign (B2)	Malignant (M1)	Malignant (M2)
Training (80%)	148	320	36	285	195
Testing (20%)	37	80	9	71	49
Total Patches	185	400	45	356	244

(v) Proposed Transformer

A transformer is a deep learning technique that employs the self-attention process to apply different weights for determining the importance of each input data in an encoder-decoder structure. In this paper, we introduce a modified Transformer that completely forgoes recurrence in favor of two different attention methods (self and cross) to identify global interdependence between input and output. The function of queries must be understood to modulate the cross-attention in the Transformer decoder and encoder with the help of this formulation.
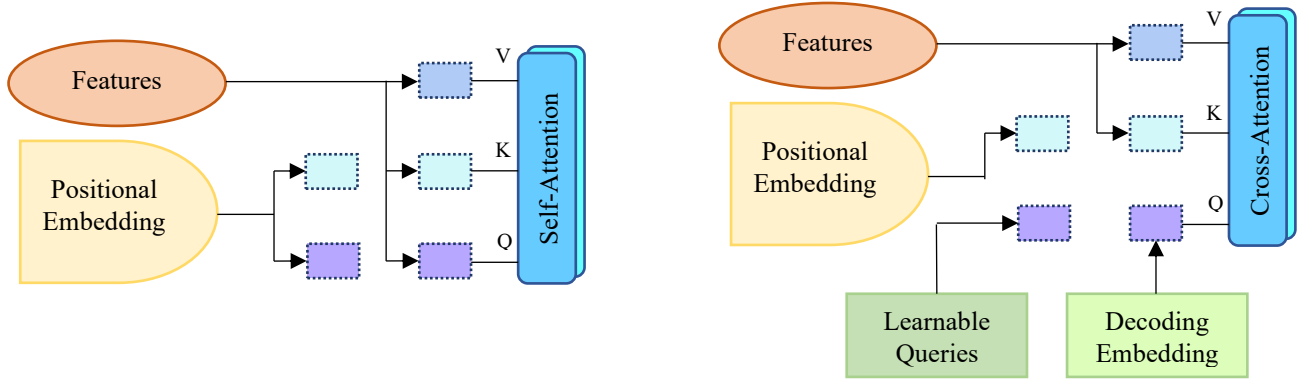
Fig. 7.4 Comparison of self-attention in encoders and cross-attention in encoders and decoders. The queries are the main difference between them because they share the same key and value components.

Self and cross attention are applied in the encoder and cross attention in the decoder to find the key difference between their inputs that come from the queries, as shown in Fig. 7.4. Each query in an encoder is composed of an image feature (content information) and a positional embedding (positional information), whereas each query in a decoder is composed of a decoder embedding (content information) and a learnable query (positional information). Self-attention uses scaled dot-product attention to determine how each patch in a single input sequence connects to the other patches, which can be computed as by:

$$SA_t(K,V,Q) = Softmax\left(\frac{Q_k^t}{\delta k}\right) c \qquad (7.6)$$

where V, K, and Q represent value, key, and query, respectively. The input consists of queries and keys of dimension δk, and values of dimension δc. We compute the dot products of the query with all keys and divide each by $\sqrt{\delta k}$, a softmax function to obtain the weights before applying. Whereas cross-attention can be computed as:

$$CA_t(K,V,Q) = Softmax\left(\frac{Q_K^t}{\sqrt{\frac{C}{H}}}\right) \qquad (7.7)$$

The embedding dimension is denoted as C and the number of heads is denoted as H. The SoftMax function converts the scaled dot product into an Attention Score. This mechanism is

an important module of the transformer for giving concurrent attention to the overall content

of the input at the same time. The model can respond to input from numerous representation

subspaces at various locations simultaneously with the support of multi-head attention. V, K,

and Q of the multi-head attention are linearly extended by s times using a variety of learned

linear projections and can be expressed as:
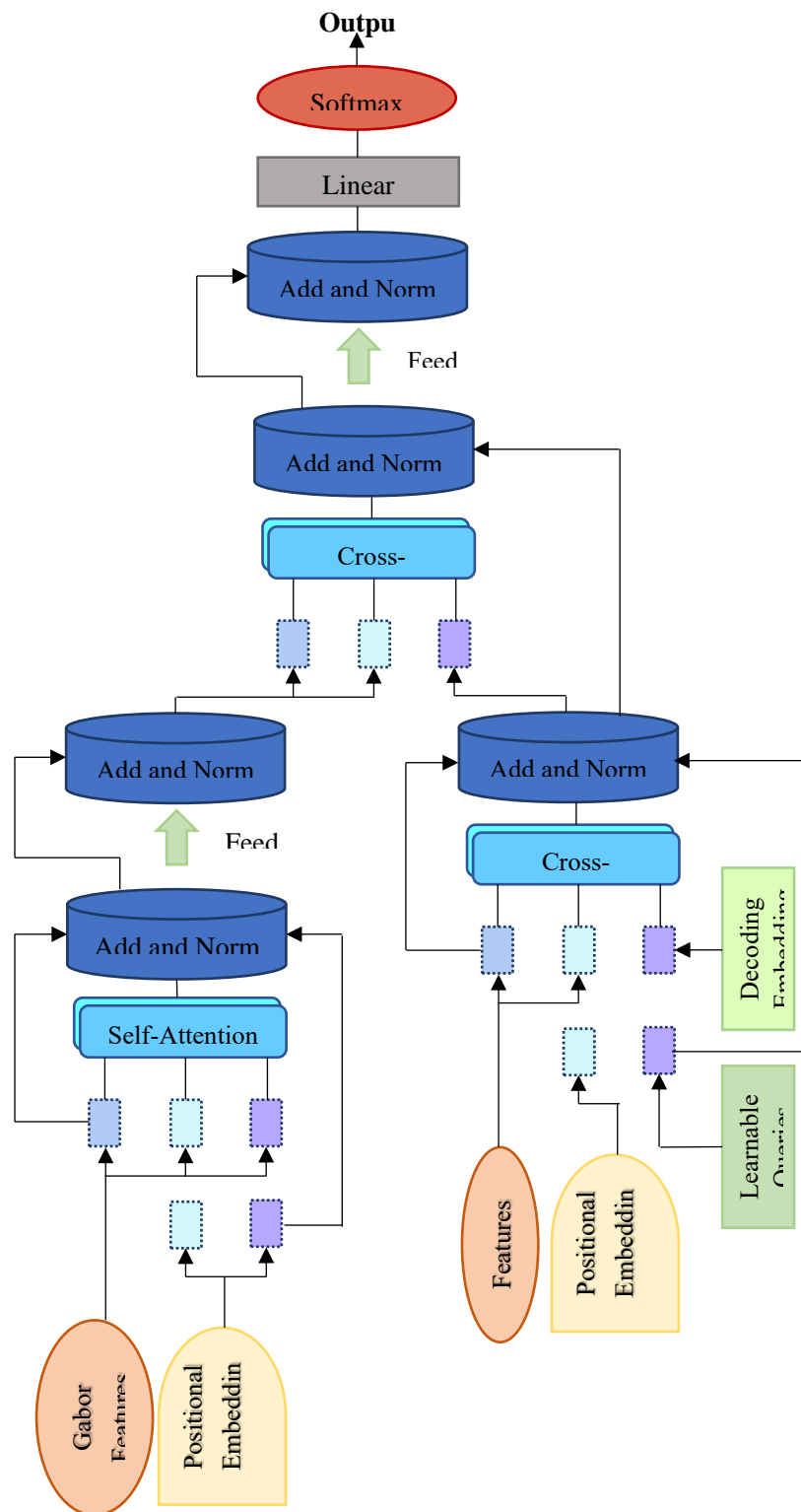
Fig. 7.5 Proposed modified Transformer model.

$$M_{Head}(K, V, Q) = Con(H_1, H_2, \ldots, H_s)W^o \tag{7.8}$$

Here,

$$H_i = A_t\left(KW_i^K, QW_i^Q, VW_i^V\right) \tag{7.9}$$

where the projections are matrices of parameters

$W_i^K \in Z^{\delta_{model} \, x \, \delta_k}$,

$W_i^Q \in Z^{\delta_{model} \, x \, \delta_k}$,

$W_i^V \in Z^{\delta_{model} \, x \, \delta_k}$, and $W^o \in Z^{s \, \delta_c \, x \, \delta_{model}}$

Multilayer Perceptron Layer (MLP), on the other hand, is made up of three separate blocks, each of which has a linear layer with Gaussian Error Linear Units (GELU), 734 neurons, Batch Normalization, and dropout layers with a 50% dropping rate across all dropout layers. The proposed modified transformer is given in Fig. 7.5.

7.3. Results and Discussion

The detection and classification stages were assessed using common evaluation metrics employed by many researchers such as accuracy, F1-score, Receiver Operating Characteristics (ROC) Curve metrics, recall/sensitivity, Cohen's kappa coefficient (C_K), Matthews correlation coefficient (M_{CC}), and precision [178]. Five cross-validation trails were used to track all evaluation metrics. The accuracy (A_{cc}) of machine learning model can be expressed as a percentage or as a value between 0 and 1. The sensitivity (S_n) of a test is a number that represents how accurately it can identify patients with breast cancer. The precision of method (P) shows how well it correctly classifies cases. Whereas F1-score consolidates sensitivity and precision into a single measurement. The following are the mathematical interpretations of each of these metrics:

$$A_{cc} = \frac{T_P + T_N}{T_P + T_N + F_P + F_N} \tag{7.10}$$

$$S_n = \frac{T_P}{T_P + F_N} \tag{7.11}$$

$$P = \frac{T_P}{T_P + F_P} \tag{7.12}$$

$$F_1 = \frac{2 \times P_R \times S_N}{P_R + S_N} \tag{7.13}$$

$$M_{CC} = \frac{T_P T_N + F_N F_P}{\sqrt{(T_P + F_P)(T_P + F_N)(T_N + F_P)(T_N + F_N)}} \tag{7.14}$$

$$C_A = \frac{q_0 - q_e}{1 - q_e} \tag{7.15}$$

Where

$$q_0 = \frac{T_P + T_N}{T_P + T_N + F_P + F_N} = A_{cc} \tag{7.16}$$

$$q_e = \frac{(T_P + F_P)(T_P + F_N)(T_N + F_P)(T_N + F_N)}{(T_P + T_N + F_P + F_N)^2} \tag{7.17}$$

The parameters of true negative (T_N), false negative (F_N), true positive (T_P), and false positive F_P are derived using classification confusion metrics. Meanwhile the ability of a classifier to differentiate between classes was assessed using the Receiver Operating Characteristics (ROC) Curve metrics, Cohen's kappa coefficient (C_K), and Matthews correlation coefficient (M_{CC}).

(A) Experimental Setup

The experiment is done using a ThinkPad laptop with the following requirements: Intel core i7 (11th generation) processor with integrated AMD Radeon Graphics, clock speeds ranging from 1.90 GHz to 4.40 GHz, and 16 GB of RAM. This study's experiments were carried out on Windows 11 using Jupyter Notebook, Python 3.8.0, and the Keras and TensorFlow backend libraries. Table 7.3 shows the parameters used for training and testing for the proposed methodology.

Table 7.3 Proposed methodology parameters.

Parameters	Value
Patch size	128 x 128 x 3
Augmentation	360° rotations (X-Y), (0.8 – 1.1) re-scaling Alpha deformation (0, 1500) Sigma deformation (30, 50)
Data-train split	80%
Data-test split	20%
Optimizer	Adam
Epochs	100

(B) Basic Classification: Normal, Benign, and Malignant

The first dataset is based on the original dataset folder. It has three folders namely, Normal (N), Benign (B), and Malignant (M) with 185, 445, and 600 patches, respectively. 80% of the dataset is used for training and 20% for testing the patches that are developed. Here, different fully connected layers are used to integrate the CNN model for classification. After extracting the features one at a time, all of the networks use Global Average Pooling 2D to flatten all of the layers into a vector by computing the mean value for each of the source channels simultaneously. The concatenate layer is then used to combine all the individual vectors into a single vector. Then, six layers are used to fine-tune the integrated features for classification, followed by SoftMax. We use four batch normalization layers in our classification model, each

of which is crucial. The batch normalization layer will rescale all of the data so that we can normalize it. The rescaled data will aid in the training phase and also reduce network initialization sensitivity. The gradient descent's loss and optimizer function are two key hyperparameters for training a model. We used Adam as an optimizer function because it combines the key features of RMSProp and AdaGrad, allowing it to handle sparse gradients on large amounts of data. A dense layer is densely connected to all the neurons in the previous and current layers. These layers process the data and produce a result. In this case, four dense layers are used, with the last dense layer performing the classification task, followed by the activation function. This layer will make a prediction based on the length of prediction class. The activation function takes the outcome probability and determines which features are most closely related to the predicted class. In the SoftMax activation function, the outcome value is between 0 and 1, causing the neuron to fire. It is defined as:

$$Soft\max(s)_i = \frac{\exp(s_i)}{\sum_{m=1}^{n} \exp(s_m)} \tag{7.18}$$

This model is evaluated using a confusion matrix, training and validation accuracy, and training and validation loss. The classification results using the confusion matrix are presented in Fig. 7.6. Normal, Benign, and Malignant are represented by Classes A, B, and C, respectively.
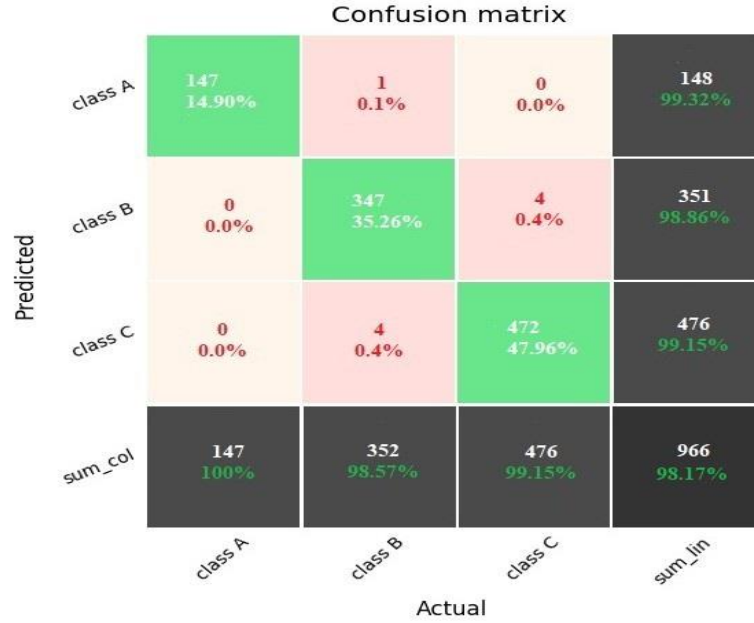
Fig. 7.6 Confusion matrix for Dataset I.

Figs. 7.7. (a) and (b) show the results of pixel segmentation with the training-testing accuracy and training-testing loss for 100 epochs. The maximum overall test/validation accuracy and the minimum test/validation loss reported on this dataset are 0.9817 and 0.004, respectively.

(a)   (b)
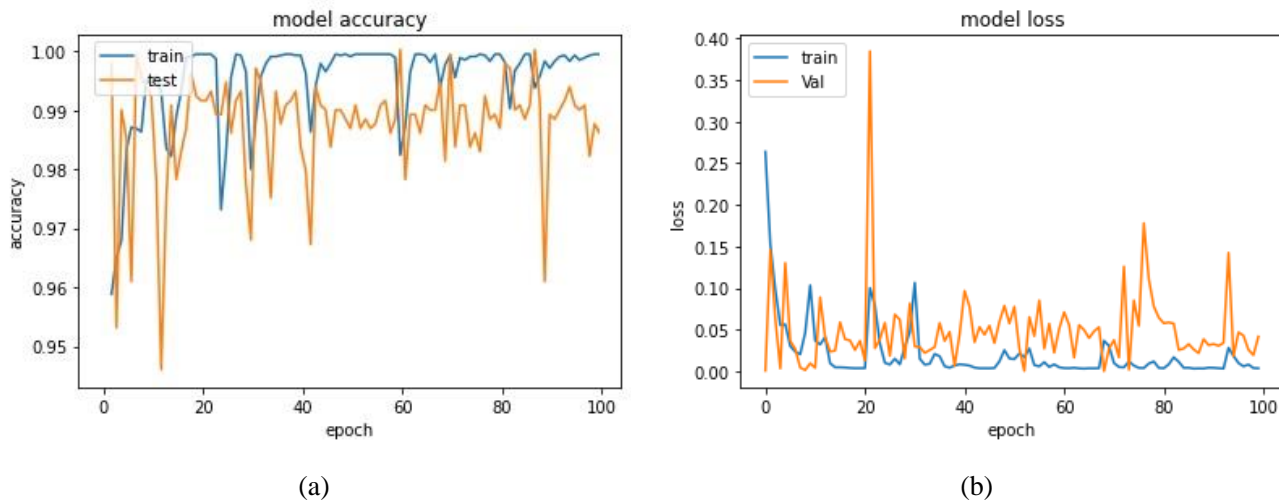
Fig. 7.7 (a) Training-Testing accuracy curve for Dataset I, (b) Training-Testing loss curve for Dataset I.

(C) Multi-class Classification

Fig. 7.8 Confusion matrix for Dataset II.

In this scenario, the experiment was to check the performance using the modified transformer to distinguish more difficult features (i.e., normal (N), benign (B1 and B2), and malignant cases (M1 and M2) based on dataset 2. In this assessment, the dataset was divided into train and test sets, where each tumor patch appeared in either train or test set. The classification results using the confusion matrix are presented in Fig. 7.8. Classes A, B, C, D, and E show Normal (N), Benign tumor (B1), Benign tumor (B2), Malignant (M1), and Malignant (M2) classes, respectively.

Figs. 7.9. (a) and (b) show the results of pixel segmentation with the training-testing accuracy and training-testing loss for 100 epochs. The maximum overall test/validation accuracy and the minimum test/validation loss reported on this dataset are 0.9674 and 0.06, respectively.

(a)

(b)
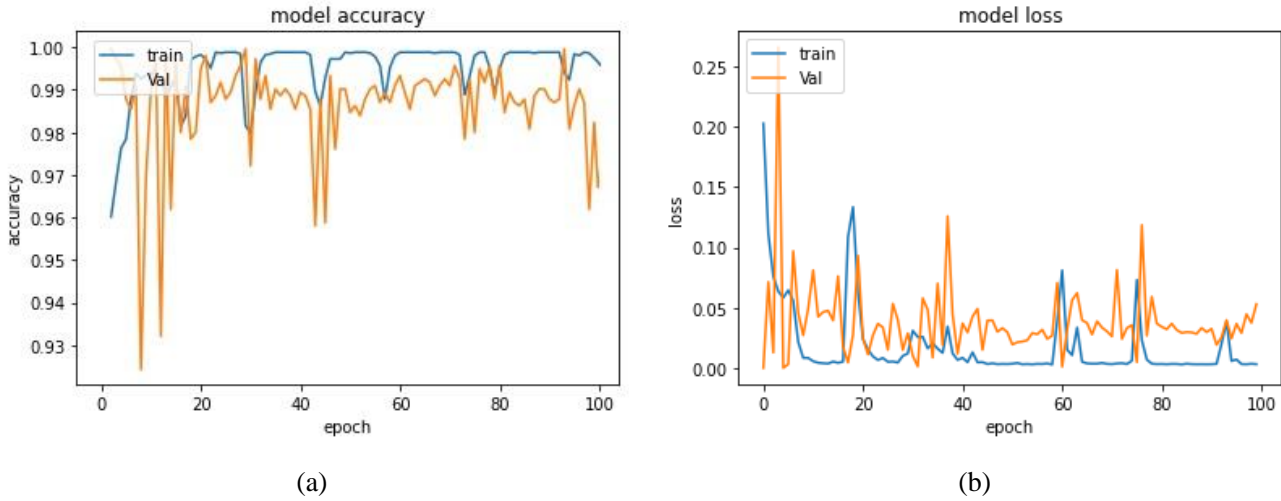
Fig. 7.9 (a) Training-Testing accuracy curve for Dataset II, (b) Training-Testing loss curve for Dataset II.

Table 7.4 Summarizes the final accuracy of both models, for all classes of dataset I and II.

Dataset	Classes	No. of Samples	Performance Measure			
			A_{cc}	S_n	P	F1
Dataset I	Normal	148	100%	100	100	100
	Benign	356	98.57%	99.60	98.80	98.60
	Malignant	480	99.15%	99.60	97.56	98.29
Dataset II	Normal	148	100%	100	100	100
	B1	320	97.16%	93.11	85.12	89.02
	B2	36	97.14%	90.11	93.55	89.96
	M1	285	98.19%	91.12	89.00	94.00
	M2	195	99.47%	94.63	99.25	98.34

The summarization of accuracy, sensitivity, precision, and F1-score for the normal class are all 100 in both datasets, as shown in Table 7.4. Dataset I achieved marginally better results than Dataset II.

Table 7.5 Comparison with related studies' results based on the DL techniques used for breast cancer detection using INbreast dataset

Ref	Predicted Classes	Technique	A_{cc}	S_n	P	F1	M_{CC}	C_K
[179]	Normal, Malignant	CNN	90.34%	75.2	97.6	85.1	79.1	90.8
[146]	Malignant, Benign	YOLOV4	95%	86.76	88.0	0.94	89.2	82.6
[180]	Malignant, Benign	YOLOV2	95.32%	95.32	93.52	95.32	89.2	84.7
[181]	Normal, Abnormal	CNN(GoogleNet, VGG and AlexNet)	98.50%	98.06	98.98	98.52	92.7	90.8
Proposed	Malignant, Benign, Normal	CNN and Modified Transformer	98.17%	98.24	97.56	98.89	94.3	94.3

Finally, Table 7.5 summarizes the results of the related studies based on the DL techniques used for breast cancer detection using mammogram datasets by comparing them with the outcomes of the proposed model. that the proposed method could produce competitive and encouraging evaluation results on real-world datasets. For this study, we summarize the related studies that used the INbreast dataset for indirect comparisons. Such indirect comparison lacks

fair comparison with other studies in the literature research domain due to different dataset distribution, different data splitting settings, different models used, or even different execution environments to perform the CNN models training and evaluation. Any deep learning model should be fine-tuned again for each modality because medical images always have shared common traits that contain contextual similarities. As a result, we believe the suggested model may be useful for other tumor types, such as liver, lung, skin, and other cancers, in addition to assisting with the diagnosis of breast cancer.

7.4.   Summary

This work discusses the potential of using proposed models to create a framework for different stages of breast cancer. To improve breast cancer prediction using digital X-ray mammograms, we design and construct the proposed model by fusing the most emerging new techniques of deep learning and Transformer. Preprocessing, segmentation, patch creation, and testing and training procedures, were the foundational steps for the proposed model. In the preprocessing stage, unwanted artifacts were eliminated, and the border of the breast image was smoothed. Following the selection of the ROI, patches are made using pixel segmentation. The evaluation was based on two types of datasets created from publicly available INbreast datasets. The generated datasets were divided into two groups for training and testing data for basic and multiclass classification. Applying a random augmentation allowed us to overcome the overfitting and small amount of data size. The proposed CNN model outperformed the existing techniques in terms of accuracy, achieving 98.17%.

CHAPTER 8

Deep Learning Techniques for Detection of Breast tumors

8.1. Preamble

Convolutional neural networks have been widely used in a variety of medical imaging tasks. Neural network designs that perform well for natural images may not be relevant to medical image processing due to these differences. First, an approach for detecting breast cancer based on thermal imaging is adopted in this work. To select the most informative areas, the model first applies a memory-efficient network to the entire image. It then uses a relatively deep CNN to collect information from certain locations from the thermal image dataset. Due to the inherent locality of convolution operation, CNNs typically perform poorly when modeling dependencies, specifically long-range, which are necessary for accurately determining or recognizing corresponding breast lesion features. This motivated me to employ the Vision Transformer block along with VGG19 for the detection of breast cancer. A powerful model that effectively combines global and local features is also introduced in this work. Lastly, the model is trained independently using Database for Mastology Research and INbreast, two distinct modalities of datasets.

8.2. An Interpretable Network to Thermal Images for Breast Cancer Detection

Diagnostic systems that use an infrared camera and deep convolutional neural networks help to enhance diagnostic accuracy and consistency [182]. The capability of a Convolutional Neural Network (CNN) may be utilized to extract attributes from medical images and help in the classification of benign and malignant lesions. While looking at the research in the

literature, it is clear that different classification and feature extraction methods are utilized for the diagnosis of breast cancer. In a 2015 study, Conci et al. [183] used the KNN (K-Nearest Neighbors) algorithm as a classifier. The diagnosis of breast cancer using thermography was accomplished by employing statical representations as features. Future research should evaluate other categorization methods, such as NN and SVM to enhance the dependability of performance. Madhavi et al. [184] used URLBP and KPCA methods to extract features from thermal breast images for the diagnosis of breast cancer. These feature vectors were used to train the SVM. Shahari et al. [185] investigated a successful image segmentation method based on color properties of pictures by utilizing the K-means clustering methodology. They also advised that the Fuzzy C-Means and Level Set methods to improve the proposed strategy and get better outcomes. Obtaining a database that can be investigated is one of the most essential aspects of the research. The majority of the investigations in the literature made use of thermal imaging obtained from local hospitals [186]. The Database for Mastology Research dataset commonly known as DMR, produced by researcher at University of Federal Fluminense, was found to provide the required parameters for this study [113] [187]. Detection of breast cancer was carried out in this study using a Gabor filter and a Convolutional Neural Network (CNN).

8.3. Methodology

The major goal of this implementation is to identify breast cancer using thermal pictures. To accomplish this, we created a deep learning model that can extract characteristics from a given dataset, while also providing on-the-fly prediction.
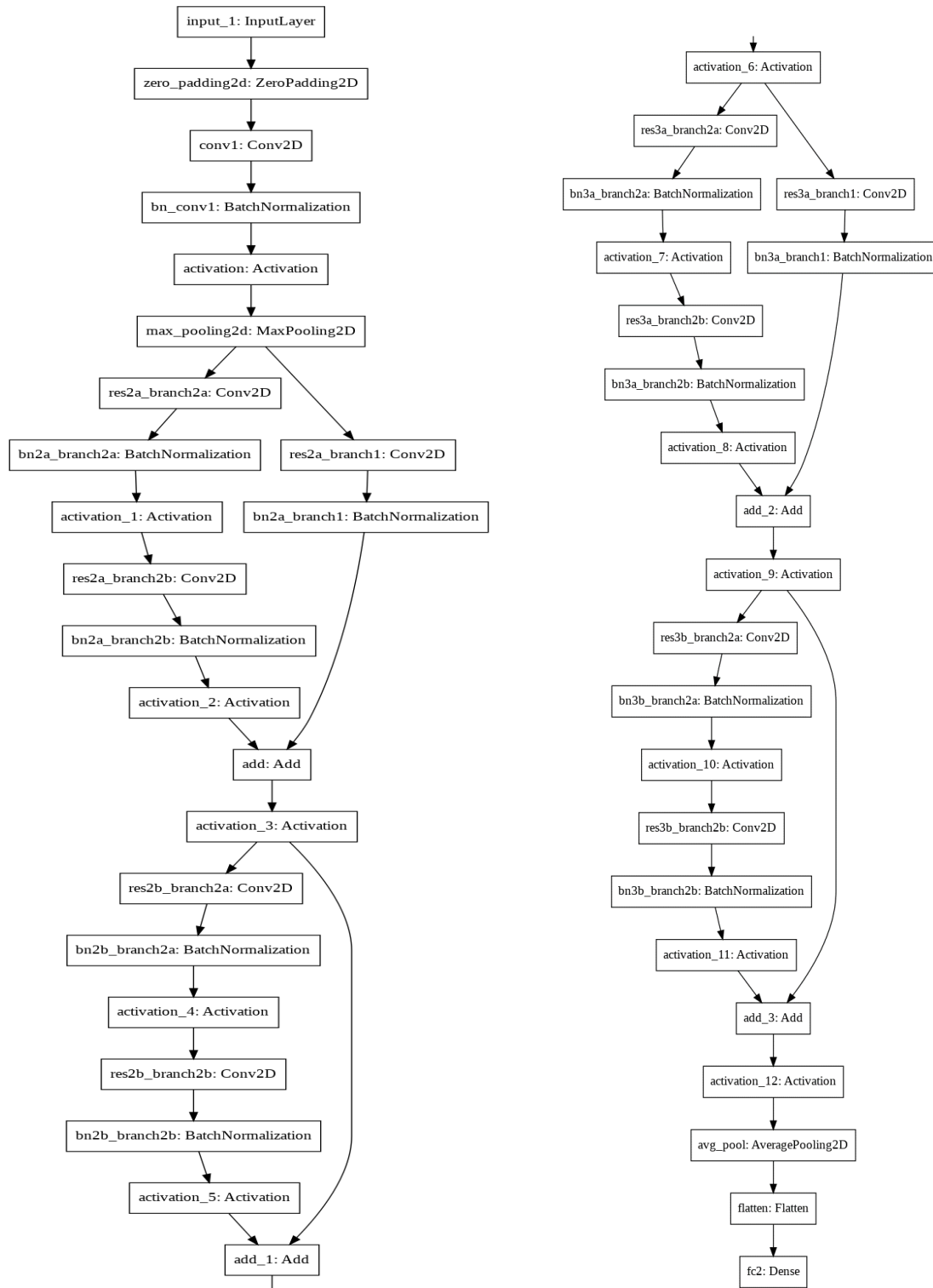
Fig. 8.1 Network architectures for ResNet18.

To achieve optimal output, images from the dataset are pre-processed. We used contrasting,

resizing, equalization, and cutting to process the raw thermal images. We rotated and reversed

the thermal images in the augmentation to enhance training data. Deep Learning was used when a large quantity of data needed to be taught with a Graphical Processing Unit. It was utilized in feature extraction because it allowed for a greater number of epochs and iterations during the training of deep CNN like ResNet 18.

Fig. 8.1 shows the network architecture for ResNet 18 created for the proposed work. In ResNet 18, a parameter layer contains 4 sub-layers. Convolutional Neural Network (CNN) is the first layer and is in charge of identifying the form and size of the impacted region. Batch normalization is the second layer (BN). BN is in charge of normalizing picture quality in order to obtain the most optimal weights. Max pool is the third tier. The Rectified Linear Unit is the final layer and serves as an activation function as well as an update function for bias and weights. The result will be sent to the parameter layer with the starting inputs after each parameter layer computation, and the cycle will continue until the last parameter layer.

8.4. Results and Discussion

Trials were performed using the DMR-IR dataset of breast thermography. In addition, the dataset was configured to 80% of training and 20% of testing. Figs. 8.2 (a) and 8.2 (b) displays the output accuracy and loss of the model with ResNet 18. It can be evident from figures that the loss at the last epoch is minimum and test accuracy using the proposed model is 92.52%. Table 8.1 compares the best results achieved from experimental investigations using various Deep Neural Networks for Breast Cancer Detection using Thermography. The proposed ResNet18 is the most effective network in fixing this issue.

(a)   (b)
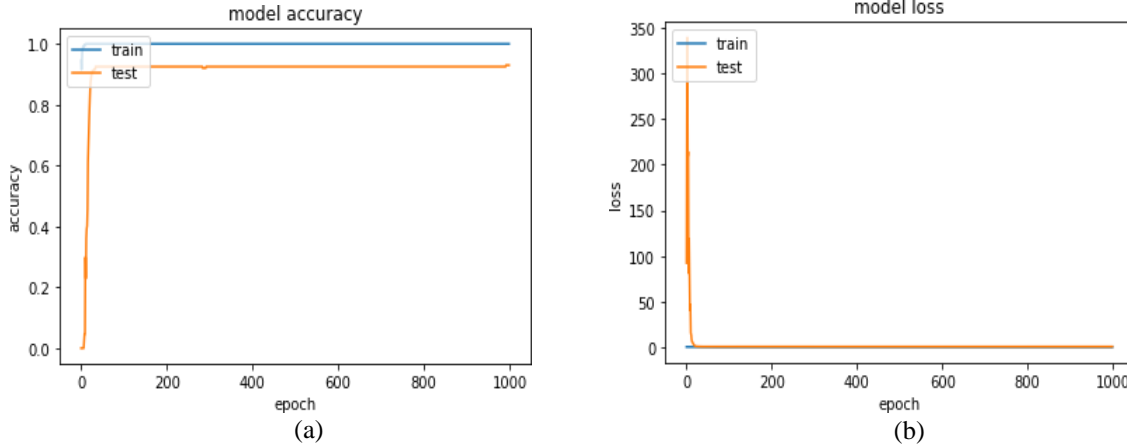
Fig. 8.2 Model accuracy and loss.

Table 8.1 Comparison of the performance assessment of latest work done on thermal imaging dataset for breast cancer detection.

Ref.	No. of Images	Feature Extraction	Test Acc
[184]	16	URLBP, KPCA	86%
[188]	22	pixel avg.	90.9%
[186]	144	CNN	88.89%
Proposed	144	CNN	92.52%

8.5. Detection and Localization of Breast Lesion with VGG19 Optimized Vision Transformer

When the authors of [189] proposed the Vision Transformer architecture for image categorization, they were inspired by the growth of self-attention centered deep neural networks. The general training procedure for those models is based on treating each embedded patch in the input image as a word in natural language processing. These models employ self-attention modules to learn the relationship between these embedded patches [190].

Hence, this work employs Transformers in medical image analysis and investigates the usage of self-attention-based architectures to categorize breast cancer images. A model based on

VGG19 optimized vision transformer is used for automatic and precise breast tumor. The proposed model uses transformer and convolution blocks to gather local and global input, respectively, and then combine them using a cross-attention fusion mechanism with both local and global feature processes.

(a) Methodology

This section would help to highlight the overall framework of our strategy as shown in Fig. 8.3. The proposed model is the parallel module based on VGG19 and vision transformer. The information is extracted from a dataset with an input size of $H \times W \times D \times 4$ and down-sample using the convolution Block. The extracted information is sent to two models, namely VGG19 and vision transformer. Both the models extract the important features to distinguish cancerous and non-cancerous data from breast cancer datasets. The information obtained from both the datasets is fused together to make the classification better.
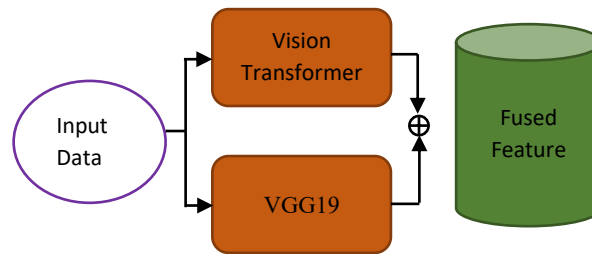
Fig. 8.3 Basic architecture of proposed model.

A parallel module is created from the vision transformer and VGG19 to extract global and local features, respectively. Additionally, cross-attention is used for fusion to combine local and global features with significant semantic variations.

(B) Local feature extraction via VGG19

VGG19 is an improved version of VGG16 that was first created in [191]. VGG19 also known as deep CNN, is made up of max pooling and convolutional layers, which are also known as

feature extractors. Following these layers is at least one FC (fully connected) layer, which works as the classifier. Fig. 8.4 shows the basic architecture of VGG19. A SoftMax takes over the output layer. This activation function defines the type of cancer, with the input layer's size set to 64x64. Without spending all that time manually inspecting them, it is simple to find the features that can differentiate different cancer type thanks to the feature extraction capability of VGG19.

Block 1
Conv 3x3

Block 2
Conv 3x3
K = 128

Block 3
Conv 3x3
K = 256

Block 4
Conv 3x3
K = 512

Block 5
Conv 3x3
K = 512

Flatten
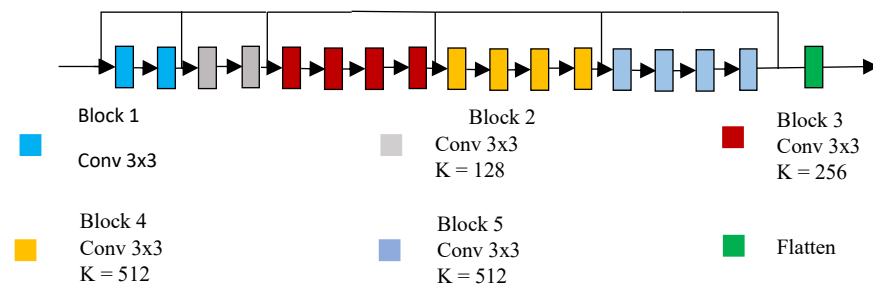
Fig. 8.4 Architecture of VGG19.

(C) Global feature extraction via Vision Transformer

Vision Transformer [189] is an innovative work for using transformers directly on images. The main factor contributing to the high computational cost of the transformer is the multi-head self-attention (MSA), as seen in Fig. 8.5. The complexity of the computation is inversely proportional to the number of tokens in this case. Unlike conventional transformers, the one being proposed uses window based MSA to reduce computation.
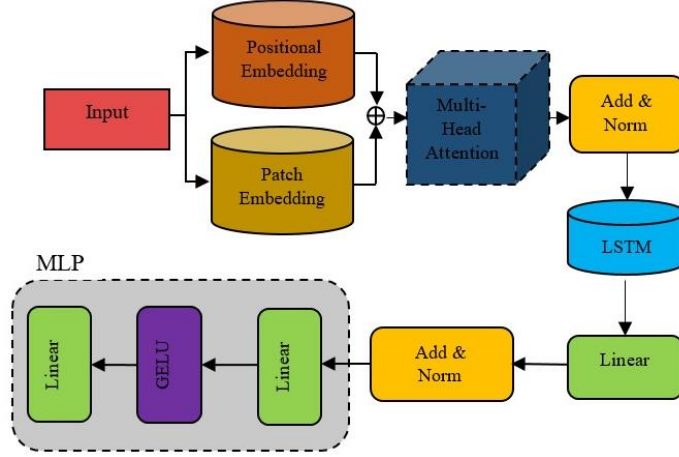
Fig. 8.5 Block diagram of Vision Transformer.

With MLP and multi head attention approach, Vision Transformer layers can be written as:

$$V_T^{'} = MHA(L_N(V_T^{n-1}) + V_T^{n-1}) \tag{8.1}$$

$$V_T = MLP(L_N(V_T^{'n-1}) + V_T^{'n-1}) \tag{8.2}$$

In the proposed vision transformer, $V_T^{'}$ and V_T represent the output global features of MHA and MLP module, respectively. Layer normalization and the multilayer perceptron module are abbreviated as MLP and LN, respectively [189,192,193]. The masked self-attention in MHA can be expressed as follows using the masked attention map (M_{mask}):

$$M_{attention} = soft\,max\left(\frac{KQ^T}{\sqrt{r}} + M_{mask}\right) \tag{8.3}$$

Where $M_{attention}$ stands for the masking attention matrix. Query, key, and value matrices are denoted as Q, K, and V. T stands for transpose and Q/K dimension is r.

(D) Fusion of local and global features

A fusion with local and global features with semantic differences is proposed, which is inspired by many literatures on multimodal feature fusion with the help of attention mechanism

[194][193][195][196]. Auxiliary (I_1) and master input (I_2) are features of the fusion, that can be expressed as follows:

$$M_{attention} = soft\,max\left(\frac{z_1(I_1)z_2(I_2)}{\sqrt{r}}\right) \tag{8.4}$$

$$F_{fuse} = M_{attention}(z_3)(I_2) \tag{8.5}$$

$$Output = z_4(F_{fuse}) + (I_2) \tag{8.6}$$

Here, z_1, z_2, z_3 and z_4 are depth-wise convolution. The attention matrix ($M_{attention}$) reflects how important the master features are in comparison to the auxiliary features, and then by using Eq. (8.5) fused features are obtained. Finally, *Output* is obtained by adding I_2 and F_{fuse}, which enables effective backpropagation during training.

8.6. Result and Discussion

The model is trained and tested on two different datasets, INbreast and DMR. The model is trained using 80% of the data from both datasets and tested using the remaining 20% using transfer learning. The network was trained using a batch size of 50 and a learning rate of 0.01 over the course of 100 epochs. Adam has been chosen as the optimization function for this network. The model parameters with the best performance were selected and applied to the testing images after 100 epochs in order to assess the network's overall performance.
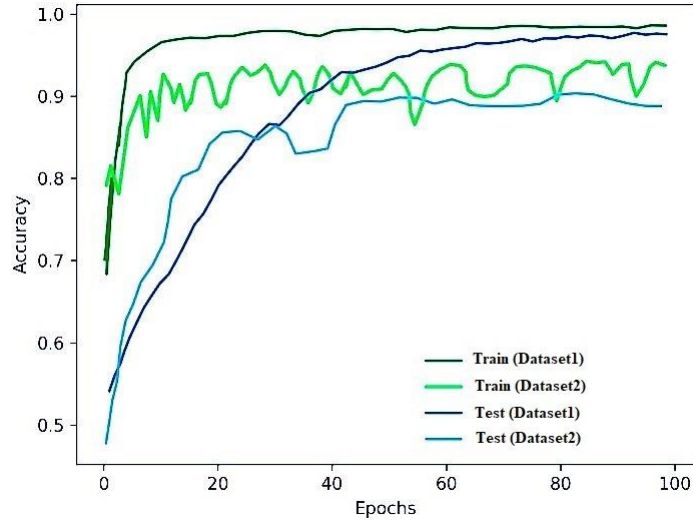
Fig. 8.6 Accuracy obtained for INbreast and DMR Dataset.

Following network training, images from the respective dataset are tested, and performance is assessed using overall accuracy. Fig. 8.6 shows the overall accuracy obtained for the proposed model for both the datasets. Dataset1 is the INbreast dataset and Dataset2 is the DMR dataset. The accuracy during training and testing of Dataset1 was 0.988 and 0.98, respectively. While the accuracy during training and testing for Dataset 2 was 0.949 and 0.899, respectively.

Table 8.2 Summary of Obtained Accuracy for both the Datasets.

	Epoch	**Acc**	
		Dataset1	**Dataset2**
Train	25	0.953	0.942
	50	0.975	0.933
	100	0.988	0.949
Test	25	0.887	0.878
	50	0.941	0.90
	100	0.98	0.899

Table 8.2 summarizes the train and test results for both the datasets. As can be seen, there is little difference between train and test results, indicating that the proposed model is not overfitting. The results revealed that the model worked best for INbreast dataset and slightly less for DMR dataset.

Table 8.3 Comparison with recent works on breast cancer detection using INbreast Dataset.

Ref	Year	Acc	Sn	P
[179]	2022	90.34	75.2	97.6
[146]	2021	95	86.76	88.0
[180]	2020	95.32	95.32	93.52
Proposed	2022	98	96.2	97.9

Table 8.3 compares the proposed work to the recent work on breast cancer detection with respect to INbreast dataset. It shows that the model works good on mammogram data.

8.7. Summary

A deep neural network was used to identify breast cancer using thermographic images in this work. The highest accuracy of 92.52% is obtained from the tests. The network discovered a cancer feature that allowed it to detect breast cancer in real-time basis. The model was created with a light-weight design, allowing the entire architecture to be saved on a mobile device. This made such a solution more accessible to the general population. In future research, it will be attempted to improve the overall system performance by increasing the number of pictures utilized in the network's training and by experimenting with alternative segmentation techniques.

A parallel model is made up of vision transformer and VGG19 is proposed here for the aim of identifying breast cancer. Additionally, an efficient model is used to fuse global and local features, which was motivated by numerous studies of multimodal feature fusion. The experimental result on Dataset1 and 2 show that the proposed model achieved good accuracy score on Dataset1 and a marginally low for Dataset2. It proves that transformer-based networks may achieve good performance for any medical image modality.

The biggest disadvantage of a medical image is a lack of datasets. In the future, experiments using some self-supervised new learning techniques, in addition to transformers, will be conducted for detection of cancer at an early stage.

CHAPTER 9
Conclusions and Future Scope

This thesis investigates efficient screening procedures for identifying and categorizing breast tumors. In this last chapter, we highlight the most important contributions made, summarize our main findings, and speculate on future directions for this area of study.

9.1. Conclusion

This research endeavor started with the aim of investigating the existing enhancement and classification techniques for medical images. Mammography, computed tomography (CT), breast ultrasound, magnetic resonance imaging (MRI), and thermography are some of the diagnostic and planning tools that are available for initial screening and diagnosis of breast cancer. The outcomes of these screening methods enable medical professionals to better assist in the process of choosing treatments or monitoring a patient's recuperation. The objective of this work is to share valuable information that aids in the identification and categorization of breast tumors. This, in turn, facilitates the early detection of the illness, leading to life-saving outcomes. In such cases, producing a proper preprocessing and enhancement method is important. Here, a multimodal medical dataset-based approach is used to create synthetic images.

An innovative model for synthetic construction is proposed for the purpose of producing synthetic mammogram images (Fulfils objectives II, III, and IV). In addition to this, a stochastic gradient descent optimizer is used in conjunction with the U-DARTS technique in order to locate and categorize the breast lesion(s). Experimentations are evaluated over both INbreast and DMR datasets to validate the efficiency and efficacy with regard to MAE, PSNR,

and SSIM. The proposed model produced an MAE value of 30.92, which is significantly lower than that of its competitors, whereas the PSNR value produced an outcome that is somewhat lower than that of its competitors. On the other hand, the proposed model generated an SSIM value of 0.88, which is the highest of any of them. In addition, an accuracy of 98% is achieved during validation and 91% during training, with losses of 0.12 and 0.23, respectively, when applied to the INbreast dataset. Regarding the DMR dataset, the validation accuracy and loss are 85% and 0.25, respectively. The lack of availability of complete data is the root cause of the low value of accuracy for the DMR dataset.

The results obtained from mammography-thermography multi-modal breast cancer detection using deep learning technique gave the idea of fusing two different modality datasets. The additional information obtained from the combined images can be used to narrow down the tumor's exact location. But the fusion of two images from different modalities continues to be difficult in the medical field because the output image may have spectral variations. To resolve this issue, a novel technique namely, AWT-SPS is developed for the fusion of two different modality breast cancer images (Fulfils objectives II, and III). It was discovered that the proposed method produced superior results visually as well as statistically when compared to the standard DWT methods. This is discovered by comparing the results produced by the proposed method with those produced by the standard methods. The approach that has been proposed will unquestionably be of assistance in the effective removal of redundant information and ambiguities, providing improvements in image clarity, and resulting in a clear, precise, and comprehensive target prediction. This will prove to be helpful for detecting breast cancer at an early stage without leaving any room for ambiguity while not putting women at risk in any way.

The active contour and texture pattern-based hybrid model was proposed for breast cancer detection from ultrasonic images (Fulfils objective II). An effective breast cancer recognition system is developed that assists therapists in the diagnosis and monitoring of malignant tissue. This allows the model to find more complete and accurate patterns. To get rid of the problem of noise and acoustic shadowing in ultrasound images, the active contour and texture features are taken into consideration as potential solutions. It is evident from the results that the features extracted from the proposed scheme are significant and preserve more information when compared to the schemes that are already in use. The proposed scheme acquires the highest and most robust parameter among the various existing systems used here, with an accuracy of 99.4%, an increase of 3.15% over the previous model.

To efficiently classify the pre-processed and enhanced medical images, a deep-learning model with a modified transformer is proposed to detect the breast lesions (Fulfils objective IV). The model is developed by combining the cutting-edge methods of deep learning and Transformer to improve the accuracy using digital X-ray mammograms. The image of the breast had its edges softened and artifacts eliminated during the preprocessing phase. After the ROI is chosen, pixel segmentation is used to create the patches. Two different datasets derived from the freely available INBreast dataset are used in the analysis. The generated datasets are divided into a training set and a test set for both simple and complex classification tasks. The proposed CNN model outperformed the state-of-the-art research, with 98.17% accuracy across all primary classification metrics (normal, benign, and malignant). The transformer had the highest multiclass accuracy, with a value of 96.74%.

The proposed model can perform detection tasks with a high degree of accuracy when compared to other models.

A real-time solution to determine breast cancer for the general population is developed using DNN with the aid of thermographic images. The model is developed with a light-weight design that gives inimitable accuracy (Fulfils objectives II, and IV). In order to achieve such eminent accuracies, another model is introduced for multimodal feature fusion using global and local parameters. A parallel model is created that utilizes the advancements of vision transformer and VGG19.

9.2. Future Scope of The Work

Recognizing any limitations related to deep learning techniques for breast cancer detection is crucial. Here are some of the potential future scopes:

i. The primary limitation of medical images is inadequate datasets. For this reason, developing a new database for breast cancer images based on a non-radioactive modality (such as thermograms) should be a priority moving forward.

ii. When a person is exposed to radioactive rays or other forms of ionizing radiation, safety becomes a major concern. Some patients may be sensitive to or should avoid screenings that employ the use of harmful waves. A system's design should prioritize the use of nonionizing radiation and the precision of its results.

iii. Most of the ultrasound images suffer from noise and acoustic shadowing, which reduces the accuracy of tumor detection. To make the breast ultrasound image more informative, a technique should be developed to improve detection accuracy.

iv. Detecting breast cancer at an early stage requires a multimodality-based approach. Breast cancer screening tools must broaden their knowledge base by incorporating a

multimodal approach to improve the accuracy of their results. This will help in eliminating radioactive modality.

v. The significance of breast cancer detection models based on deep learning in the medical field has been demonstrated. The clinical application of these models is yet to be done. Clinicians will benefit from incorporating these models into their work.

REFERENCES

[1] M.A. Mohammed, B. Al-Khateeb, A.N. Rashid, D.A. Ibrahim, M.K. Abd Ghani and S.A. Mostafa, *Neural network and multi-fractal dimension features for breast cancer classification from ultrasound images*, Comput. Electr. Eng. 70 (2018), pp. 871–882.

[2] Z. Momenimovahed and H. Salehiniya, *Epidemiological characteristics of and risk factors for breast cancer in the world*, Breast Cancer (London). 11 (2019), pp. 151.

[3] M.M.Y. Al-Hashimi and X.J. Wang, *Breast cancer in Iraq, incidence trends from 2000-2009*, Asian Pac. J. Cancer Prev. 15 (2014), pp. 281–286.

[4] N. Azamjah, Y. Soltan-Zadeh and F. Zayeri, *Global trend of breast cancer mortality rate: A 25-year study*, Asian Pacific J. Cancer Prev. 20 (2019), pp. 2015–2020.

[5] *WHO report on cancer: setting priorities, investing wisely and providing care for all.*. Available at https://www.knowledge-action-portal.com/en/content/who-report-cancer-setting-priorities-investing-wisely-and-providing-care-all.

[6] American Cancer Socienty, *Breast Cancer Occurrence 3 Breast Cancer Risk Factors 12 What Is the American Cancer Society Doing about Breast Cancer? 26 Sources of Statistics 30 References 32*, Breast Cancer Facts Fig. 2019-2020 (2019), pp. 1–44.

[7] O.I. Obaid, M.A. Mohammed, M.K. Abd Ghani, S. A. Mostafa and F.T. AL-Dhief, *Evaluating the performance of machine learning techniques in the classification of Wisconsin Breast Cancer*, (2018), .

[8] D. Chen, M. Huang and W. Li, *Knowledge-Powered Deep Breast Tumor Classification with Multiple Medical Reports*, IEEE/ACM Trans. Comput. Biol. Bioinforma. PP (2019), pp. 1–1.

[9] J. Ferlay, I. Soerjomataram, R. Dikshit, S. Eser, C. Mathers, M. Rebelo et al., *Cancer*

incidence and mortality worldwide: Sources, methods and major patterns in GLOBOCAN 2012, Int. J. Cancer 136 (2015), pp. E359–E386.

[10] S.W. Duffy, L. Tabár, H.H. Chen, M. Holmqvist, M.F. Yen, S. Abdsalah et al., *The impact of organized mammography service screening on breast carcinoma mortality in seven Swedish Counties: A collaborative evaluation*, Cancer 95 (2002), pp. 458–469.

[11] C.L. Carcinoma, *Prognostic Factors for Patients with Small*, (2002), pp. 576–583.

[12] S.W. Duffy, L. Tabár and R.A. Smith, *The mammographic screening trials: commentary on the recent work by Olsen and Gøtzsche*, CA. Cancer J. Clin. 52 (2002), pp. 68–71.

[13] US Preventive Services Task Force, *Clinical Guidelines Preventive Services Task Force*, Ann. Intern. Med. 137 (2002), pp. 917–933.

[14] N.F. Boyd, L.J. Martin, L. Sun, H. Guo, A. Chiarelli, G. Hislop et al., *Body size, mammographic density, and breast cancer risk*, Cancer Epidemiol. Biomarkers Prev. 15 (2006), pp. 2086–2092.

[15] H. Bahramiabarghouei, E. Porter, A. Santorelli, B. Gosselin, M. Popovíc and L.A. Rusch, *Flexible 16 antenna array for microwave breast cancer detection*, IEEE Trans. Biomed. Eng. 62 (2015), pp. 2516–2525.

[16] J. Xu, L. Xiang, Q. Liu, H. Gilmore, J. Wu, J. Tang et al., *Stacked sparse autoencoder (SSAE) for nuclei detection on breast cancer histopathology images*, IEEE Trans. Med. Imaging 35 (2016), pp. 119–130.

[17] J.P. Stone, R.L. Hartley and C. Temple-oberle, *Breast Cancer in Transgender Patients: A Systematic Review. Part 2: Female to Male*, Eur. J. Surg. Oncol. (2018), .

[18] L.J. Gooren, M.A.A. van Trotsenburg, E.J. Giltay and P.J. van Diest, *Breast Cancer*

Development in Transsexual Subjects Receiving Cross-Sex Hormone Treatment, J. Sex. Med. 10 (2013), pp. 3129–3134.

[19] C.J.M. De Blok, C.M. Wiepjes, N.M. Nota, K. Van Engelen, M.A. Adank, K.M.A. Dreijerink et al., *Breast cancer risk in transgender people receiving hormone treatment: Nationwide cohort study in the Netherlands*, BMJ 365 (2019), .

[20] D. V. Nikolic, M.L. Djordjevic, M. Granic, A.T. Nikolic, V. V. Stanimirovic, D. Zdravkovic et al., *Importance of revealing a rare case of breast cancer in a female to male transsexual after bilateral mastectomy*, World J. Surg. Oncol. 10 (2012), pp. 2–5.

[21] R.L. Siegel, K.D. Miller and A. Jemal, *Cancer statistics, 2019*, CA. Cancer J. Clin. 69 (2019), pp. 7–34.

[22] *Report of population based cancer registries 2012–2018 national cancer registry programme.*. Available at https://www.ncdirindia.org/Reports.aspx.

[23] S. Duffy, L. Tabár and R.A. Smith, *The mammographic screening trials: commentary on the recent work by Olsen and Gøtzsche.*, J. Surg. Oncol. 81 (2002), pp. 68–71.

[24] P.A. Carney, D.L. Miglioretti, B.C. Yankaskas, K. Kerlikowske, R. Rosenberg and C.M. Rutter, *Erratum: Individual and combined effects of age, breast density, and hormone replacement therapy use on the accuracy of screening mammography (Annals of Internal Medicine (2003) 138 (168-175))*, Ann. Intern. Med. 138 (2003), pp. 771.

[25] M.G. Marmot, D.G. Altman, D.A. Cameron, J.A. Dewar, S.G. Thompson and M. Wilcox, *The benefits and harms of breast cancer screening: An independent review*, Br. J. Cancer 108 (2013), pp. 2205–2240.

[26] X. Gu, B. Wang, H. Zhu, Y. Zhou, A.M. Horning, T.H.M. Huang et al., *Age-associated genes in human mammary gland drive human breast cancer progression*, Breast Cancer

Res. 22 (2020), pp. 1–15.

[27] N.L. Ferguson, J. Bell, R. Heidel, S. Lee, S. Vanmeter, L. Duncan et al., *Prognostic value of breast cancer subtypes, Ki-67 proliferation index, age, and pathologic tumor characteristics on breast cancer survival in caucasian women*, Breast J. 19 (2013), pp. 22–30.

[28] P. Rana, J. Ratcliffe, J. Sussman, M. Forbes, M. Levine and N. Hodgson, *Young women with breast cancer: Needs and experiences*, Cogent Med. 4 (2017), pp. 1–11.

[29] B.O. Anderson, C.H. Yip, R.A. Smith, R. Shyyan, S.F. Sener, A. Eniu et al., *Guideline implementation for breast healthcare in low-income and middle-income countries: Overview of the breast health global initiative Global Summit 2007*, Cancer 113 (2008), pp. 2221–2243.

[30] T. Hopp, N. Duric and N. V. Ruiter, *Image fusion of Ultrasound Computer Tomography volumes with X-ray mammograms using a biomechanical model based 2D/3D registration*, Comput. Med. Imaging Graph. 40 (2015), pp. 170–181.

[31] E.D. Pisano, R.E. Hendrick, M.J. Yaffe, J.K. Baum, S. Acharyya, J.B. Cormack et al., *Diagnostic accuracy of digital versus film mammography: Exploratory analysis of selected population subgroups in DMIST*, Radiology 246 (2008), pp. 376–383.

[32] C. Karakas, *Paget's disease of the breast*, J. Carcinog. 10 (2011), pp. 31.

[33] *Types of Breast Cancer*. Available at https://www.breastcancer.org/types.

[34] *In Treatment for Breast Cancer*. Available at https://www.breastcancer.org/about-you/in-treatment.

[35] G.N. Sharma, R. Dave, J. Sanadya, P. Sharma and K.K. Sharma, *Various types and management of breast cancer: an overview.*, J. Adv. Pharm. Technol. Res. 1 (2010), pp.

109–26.

[36]   *The   mini-MIAS   database   of   mammograms*.   Available   at
       http://peipa.essex.ac.uk/info/mias.html.

[37]   *DDSM: Digital Database for Screening Mammography*. .

[38]   I.C. Moreira, I. Amaral, I. Domingues, A. Cardoso, M.J. Cardoso and J.S. Cardoso,
       INbreast: Toward a Full-field Digital Mammographic Database, Acad. Radiol. 19
       (2012), pp. 236–248.

[39]   S. Prapavesis, B.D. Fornage, C.F. Weismann, A. Palko and P. Zoumpoulis, *Breast
       ultrasound and US-guided interventional techniques: a multimedia teaching file*,
       Thessaloniki, Greece (2003), .

[40]   M.H. Yap, G. Pons, J. Marti, S. Ganau, M. Sentis, R. Zwiggelaar et al., *Automated
       breast ultrasound lesions detection using convolutional neural networks*, IEEE J.
       Biomed. Heal. informatics 22 (2017), pp. 1218–1226.

[41]   W. Al-Dhabyani, M. Gomaa, H. Khaled and A. Fahmy, *Dataset of breast ultrasound
       images*, Data Br. 28 (2020), pp. 104863.

[42]   H.H. Man Ng, N. Khoo, J. Velaga, J. Yeong, J. Yeo Teo, B. K.P Goh et al., *Hepatitis B
       virus-Associated Intrahepatic Cholangiocarcinoma Has Distinct Clinical, Pathological
       and Radiological Characteristics: A Systematic Review*, Surgery, Gastroenterol. Oncol.
       24 (2019), pp. 5.

[43]   *RIDER Breast MRI*. .

[44]   *QIN Breast DCE-MRI*. .

[45]   L.F. Silva, D.C.M. Saade, G.O. Sequeiros, A.C. Silva, A.C. Paiva, R.S. Bravo et al., *A
       new database for breast research with infrared image*, J. Med. Imaging Heal.

Informatics 4 (2014), pp. 92–100.

[46] M.K. Bhowmik, U.R. Gogoi, G. Majumdar, D. Bhattacharjee, D. Datta and A.K. Ghosh, *Designing of ground-truth-annotated DBT-TU-JU breast thermogram database toward early abnormality prediction*, IEEE J. Biomed. Heal. informatics 22 (2017), pp. 1238–1249.

[47] M. Mahrooghy, A.B. Ashraf, D. Daye, E.S. McDonald, M. Rosen, C. Mies et al., *Pharmacokinetic tumor heterogeneity as a prognostic biomarker for classifying breast cancer recurrence risk*, IEEE Trans. Biomed. Eng. 62 (2015), pp. 1585–1594.

[48] V.P. Singh, S. Srivastava and R. Srivastava, *Effective mammogram classification based on center symmetric-LBP features in wavelet domain using random forests*, Technol. Heal. Care 25 (2017), pp. 709–727.

[49] D. Ribli, A. Horváth, Z. Unger, P. Pollner and I. Csabai, *Detecting and classifying lesions in mammograms with Deep Learning*, Sci. Rep. 8 (2018), pp. 16–20.

[50] S. Ekici and H. Jawzal, *Breast cancer diagnosis using thermography and convolutional neural networks*, Med. Hypotheses 137 (2020), pp. 109542.

[51] R. Roslidar, K. Saddami, F. Arnia, M. Syukri and K. Munadi, A study of fine-tuning CNN models based on thermal imaging for breast cancer classification, in 2019 IEEE International Conference on Cybernetics and Computational Intelligence (CyberneticsCom), 2019, pp. 77–81.

[52] Z. Wang, L. Zhang, X. Shu, Q. Lv and Z. Yi, *An end-to-end mammogram diagnosis: a new multi-instance and multi-scale method based on single-image feature*, IEEE Trans. Cogn. Dev. Syst. PP (2020), pp. 1.

[53] Y. Wang, N. Wang, M. Xu, J. Yu, C. Qin, X. Luo et al., *Deeply-Supervised Networks*

with Threshold Loss for Cancer Detection in Automated Breast Ultrasound, IEEE Trans. Med. Imaging 39 (2020), pp. 866–876.

[54] X. Shu, L. Zhang, Z. Wang, Q. Lv and Z. Yi, *Deep Neural Networks with Region-Based Pooling Structures for Mammographic Image Classification*, IEEE Trans. Med. Imaging 39 (2020), pp. 2246–2255.

[55] S.J. Schnitt, *Classification and prognosis of invasive breast cancer: From morphology to molecular taxonomy*, Mod. Pathol. 23 (2010), pp. 60–64.

[56] M.C. Edman, R.R. Marchelletta and S.F. Hamm-Alvarez, *Lacrimal gland overview*, Encycl. Eye (2010), pp. 522–527.

[57] A. Gupta, K. Shridhar and P.K. Dhillon, *A review of breast cancer awareness among women in India: Cancer literate or awareness deficit?*, Eur. J. Cancer 51 (2015), pp. 2058–2066.

[58] A.D. Brooks, A.B. Nover, S. Jagtap, W. Anjum, H. Yegingil, W.Y. Shih et al., *Modern breast cancer detection: A technological review*, Int. J. Biomed. Imaging 2009 (2009), .

[59] K.J. Nam, B.K. Han, E.S. Ko, J.S. Choi, E.Y. Ko, D.W. Jeong et al., *Comparison of full-field digital mammography and digital breast tomosynthesis in ultrasonography-detected breast cancers*, Breast 24 (2015), pp. 649–655.

[60] D. Abdelhafiz, C. Yang, R. Ammar and S. Nabavi, *Deep convolutional neural networks for mammography: Advances, challenges and applications*, BMC Bioinformatics 20 (2019), .

[61] M. Heidari, S. Mirniaharikandehei, W. Liu, A.B. Hollingsworth, H. Liu and B. Zheng, *Development and Assessment of a New Global Mammographic Image Feature Analysis*

Scheme to Predict Likelihood of Malignant Cases, IEEE Trans. Med. Imaging 39 (2020), pp. 1235–1244.

[62] S. Shen, Y. Zhou, Y. Xu, B. Zhang, X. Duan, R. Huang et al., *A multi-centre randomised trial comparing ultrasound vs mammography for screening breast cancer in high-risk Chinese women*, Br. J. Cancer 112 (2015), pp. 998–1004.

[63] R.F. Brem, M.J. Lenihan, J. Lieberman and J. Torrente, *Screening breast ultrasound: Past, present, and future*, Am. J. Roentgenol. 204 (2015), pp. 234–240.

[64] T.M. Kolb, J. Lichy and J.H. Newhouse, *Comparison of the performance of screening mammography, physical examination, and breast US and evaluation of factors that influence them: An analysis of 27,825 patient evaluations*, Radiology 225 (2002), pp. 165–175.

[65] C. Munoz-Meza and W. Gomez, *A feature selection methodology for breast ultrasound classification*, 2013 10th Int. Conf. Electr. Eng. Comput. Sci. Autom. Control. CCE 2013 (2013), pp. 245–249.

[66] H. Qin, L. Zhang and Q. Guo, *Computer-Aided Diagnosis System for Breast Ultrasound Reports Generation and Classification Method Based on Deep Learning*, Appl. Sci. 13 (2023), pp. 6577.

[67] H. Tanaka, S.-W. Chiu, T. Watanabe, S. Kaoku and T. Yamaguchi, *Computer-aided diagnosis system for breast ultrasound images using deep learning*, Phys. Med. Biol. 64 (2019), pp. 235013.

[68] N. Schwartz, I. Oguz, J. Wang, A. Pouch, N. Yushkevich, S. Parameshwaran et al., *Fully Automated Placental Volume Quantification From <scp>3D</scp> Ultrasound for Prediction of Small-for-Gestational-Age Infants*, J. Ultrasound Med. 41 (2022), pp.*

1509–1524.

[69] M. Lotfollahi, M. Gity, • Jing, Y. Ye and • A Mahlooji Far, *Segmentation of breast ultrasound images based on active contours using neutrosophic theory*, J. Med. Ultrason. 45 .

[70] Y. Liang, R. He, Y. Li and Z. Wang, Simultaneous segmentation and classification of breast lesions from ultrasound images using Mask R-CNN, in 2019 IEEE International Ultrasonics Symposium (IUS), 2019, pp. 1470–1472.

[71] N. Nyayapathi, R. Lim, H. Zhang, W. Zheng, Y. Wang, M. Tiao et al., *Dual Scan Mammoscope (DSM) - A New Portable Photoacoustic Breast Imaging System with Scanning in Craniocaudal Plane*, IEEE Trans. Biomed. Eng. 67 (2020), pp. 1321–1327.

[72] R.M. Mann, N. Cho and L. Moy, *Reviews and Commentary • State of the Art*, Radiology 292 (2019), pp. 520–536.

[73] P. Sun, D. Wang, V.C. Mok and L. Shi, *Comparison of Feature Selection Methods and Machine Learning Classifiers for Radiomics Analysis in Glioma Grading*, IEEE Access 7 (2019), pp. 102010–102020.

[74] Q. Li, X. Xiao, L. Wang, H. Song, H. Kono, P. Liu et al., *Direct Extraction of Tumor Response Based on Ensemble Empirical Mode Decomposition for Image Reconstruction of Early Breast Cancer Detection by UWB*, IEEE Trans. Biomed. Circuits Syst. 9 (2015), pp. 710–724.

[75] M. Mahrooghy, A.B. Ashraf, D. Daye, E.S. McDonald, M. Rosen, C. Mies et al., *Pharmacokinetic tumor heterogeneity as a prognostic biomarker for classifying breast cancer recurrence risk*, IEEE Trans. Biomed. Eng. 62 (2015), pp. 1585–1594.

[76] V.P. Singh, S. Srivastava and R. Srivastava, *Effective mammogram classification based*

on center symmetric-LBP features in wavelet domain using random forests, Technol. Heal. Care 25 (2017), pp. 709–727.

[77] N. Wu, J. Phang, J. Park, Y. Shen, Z. Huang, M. Zorin et al., *Deep Neural Networks Improve Radiologists' Performance in Breast Cancer Screening*, IEEE Trans. Med. Imaging 39 (2020), pp. 1184–1194.

[78] M.C. Kale, B.D. Clymer, R.M. Koch, J.T. Heverhagen, S. Sammet, R. Stevens et al., *Multispectral co-occurrence with three random variables in dynamic contrast enhanced magnetic resonance imaging of breast cancer*, IEEE Trans. Med. Imaging 27 (2008), pp. 1425–1431.

[79] S. Srivastava, N. Sharma, S.K. Singh and R. Srivastava, *Quantitative analysis of a general framework of a CAD tool for breast cancer detection from mammograms*, J. Med. Imaging Heal. Informatics 4 (2014), pp. 654–674.

[80] G. Murtaza, L. Shuib, A.W. Abdul Wahab, G. Mujtaba, G. Mujtaba, H.F. Nweke et al., *Deep learning-based breast cancer classification through medical imaging modalities: state of the art and research challenges*, Artif. Intell. Rev. 53 (2020), pp. 1655–1720.

[81] Z. Haeri, M. Shokoufi, M. Jenab, R. Janzen and F. Golnaraghi, *Electrical impedance spectroscopy for breast cancer diagnosis: Clinical study*, Integr. Cancer Sci. Ther. 3 (2016), pp. 1–6.

[82] L.F.E. Huerta-Nuñez, G. Gutierrez-Iglesias, A. Martinez-Cuazitl, M.M. Mata-Miranda, V.D. Alvarez-Jiménez, V. Sánchez-Monroy et al., *A biosensor capable of identifying low quantities of breast cancer cells by electrical impedance spectroscopy*, Sci. Rep. 9 (2019), pp. 1–12.

[83] D. Lederman, B. Zheng, X. Wang, X.H. Wang and D. Gur, *Improving breast cancer*

risk stratification using resonance-frequency electrical impedance spectroscopy through fusion of multiple classifiers, Ann. Biomed. Eng. 39 (2011), pp. 931–945.

[84]   L.C. Ward, E. Dylke, S. Czerniec, E. Isenring and S.L. Kilbreath, *Confirmation of the reference impedance ratios used for assessment of breast cancer-related lymphedema by bioelectrical impedance spectroscopy*, Lymphat. Res. Biol. 9 (2011), pp. 47–51.

[85]   M. Etehadtavakol, V. Chandran, E.Y.K. Ng and R. Kafieh, *Breast cancer detection from thermal images using bispectral invariant features*, Int. J. Therm. Sci. 69 (2013), pp. 21–36.

[86]   J.L. Gonzalez-Hernandez, A.N. Recinella, S.G. Kandlikar, D. Dabydeen, L. Medeiros and P. Phatak, *An inverse heat transfer approach for patient-specific breast cancer detection and tumor localization using surface thermal images in the prone position*, Infrared Phys. Technol. 105 (2020), pp. 103202.

[87]   R. Roslidar, K. Saddami, F. Arnia, M. Syukri and K. Munadi, *A study of fine-tuning CNN models based on thermal imaging for breast cancer classification*, Proc. Cybern. 2019 - 2019 IEEE Int. Conf. Cybern. Comput. Intell. Towar. a Smart Human-Centered Cyber World (2019), pp. 77–81.

[88]   S.J. Mambou, P. Maresova, O. Krejcar, A. Selamat and K. Kuca, *Breast cancer detection using infrared thermal imaging and a deep learning model*, Sensors (Switzerland) 18 (2018), .

[89]   F. Casalegno, T. Newton, R. Daher, M. Abdelaziz, A. Lodi-Rizzini, F. Schürmann et al., *Caries Detection with Near-Infrared Transillumination Using Deep Learning*, J. Dent. Res. 98 (2019), pp. 1227–1233.

[90]   M. Klemm, J.A. Leendertz, D. Gibbins, I.J. Craddock, A. Preece and R. Benjamin,

Microwave radar-based breast cancer detection: Imaging in inhomogeneous breast phantoms, IEEE Antennas Wirel. Propag. Lett. 8 (2009), pp. 1349–1352.

[91]   Q. Li, X. Xiao, L. Wang, H. Song, H. Kono, P. Liu et al., *Direct extraction of tumor response based on ensemble empirical mode decomposition for image reconstruction of early breast cancer detection by UWB*, IEEE Trans. Biomed. Circuits Syst. 9 (2015), pp. 710–724.

[92]   T.M. Grzegorczyk, P.M. Meaney, P.A. Kaufman, R.M. Diflorio-Alexander and K.D. Paulsen, *Fast 3-D tomographic microwave imaging for breast cancer detection*, IEEE Trans. Med. Imaging 31 (2012), pp. 1584–1592.

[93]   A.H. Tunçay and I. Akduman, *Realistic microwave breast models through T1-weighted 3-D MRI data*, IEEE Trans. Biomed. Eng. 62 (2015), pp. 688–698.

[94]   T. Yin, F.H. Ali and C.C. Reyes-Aldasoro, *A robust and artifact resistant algorithm of ultrawideband imaging system for breast cancer detection*, IEEE Trans. Biomed. Eng. 62 (2015), pp. 1514–1525.

[95]   T.J. Kao, G. Boverman, B.S. Kim, D. Isaacson, G.J. Saulnier, J.C. Newell et al., *Regional admittivity spectra with tomosynthesis images for breast cancer detection: Preliminary patient study*, IEEE Trans. Med. Imaging 27 (2008), pp. 1762–1768.

[96]   P. Baran, S. Mayo, M. McCormack, S. Pacile, G. Tromba, C. Dullin et al., *High-resolution X-ray phase-contrast 3-d imaging of breast tissue specimens as a possible adjunct to histopathology*, IEEE Trans. Med. Imaging 37 (2018), pp. 2642–2650.

[97]   T. Botterill, T. Lotz, A. Kashif and J.G. Chase, *Reconstructing 3-D skin surface motion for the DIET breast cancer screening system*, IEEE Trans. Med. Imaging 33 (2014), pp. 1109–1118.

[98]   A.L. McKnight, J.L. Kugel, P.J. Rossman, A. Manduca, L.C. Hartmann and R.L. Ehman, *MR elastography of breast cancer: Preliminary results*, Am. J. Roentgenol. 178 (2002), pp. 1411–1417.

[99]   A. Goddi, M. Bonardi and S. Alessi, *Breast elastography: A literature review*, J. Ultrasound 15 (2012), pp. 192–198.

[100]   V. Kumar and N. Dogra, *A Comprehensive Review on Deep Synergistic Drug Prediction Techniques for Cancer*, Arch. Comput. Methods Eng. 29 (2022), pp. 1443–1461.

[101]   A. Helwan and R. Abiyev, *Shape and texture features for the identification of breast cancer*, Lect. Notes Eng. Comput. Sci. 2226 (2016), pp. 542–547.

[102]   V. R.Pandit and R. J. Bhiwani, *Image Fusion in Remote Sensing Applications: A Review*, Int. J. Comput. Appl. 120 (2015), pp. 22–32.

[103]   A. El Hami and P. Pougnet, *Embedded Mechatronic System 2: Analyses of Failures, Modeling, Simulation and Optimization*, (2019), pp. 300.

[104]   Y. Yang, W. Wan, S. Huang, F. Yuan, S. Yang and Y. Que, *Remote sensing image fusion based on adaptive IHS and multiscale guided filter*, IEEE Access 4 (2016), pp. 4573–4582.

[105]   V.P.S. Naidu and J.R. Raol, *Pixel-level image fusion using wavelets and principal component analysis*, Def. Sci. J. 58 (2008), pp. 338–352.

[106]   G. Murtaza, L. Shuib, A.W. Abdul Wahab, G. Mujtaba, G. Mujtaba, H.F. Nweke et al., *Deep learning-based breast cancer classification through medical imaging modalities: state of the art and research challenges*, Artif. Intell. Rev. 53 (2020), pp. 1655–1720.

[107]   S. Agarwal, *Data Mining: Data Mining Concepts and Techniques*, 2014.

[108]   N.I.R. Yassin, S. Omran, E.M.F. El Houby and H. Allam, *Machine learning techniques*

for breast cancer computer aided diagnosis using different image modalities: A systematic review, Comput. Methods Programs Biomed. 156 (2018), pp. 25–45.

[109] N.P. Gupta, P.K. Malik and B.S. Ram, *A review on methods and systems for early breast cancer detection*, Proc. Int. Conf. Comput. Autom. Knowl. Manag. ICCAKM 2020 (2020), pp. 42–46.

[110] Y. Lu, J.Y. Li, Y.T. Su and A.A. Liu, *A Review of Breast Cancer Detection in Medical Images*, VCIP 2018 - IEEE Int. Conf. Vis. Commun. Image Process. (2018), pp. 11–14.

[111] A.I. Huppe, A.K. Mehta and R.F. Brem, *Molecular Breast Imaging: A Comprehensive Review*, Semin. Ultrasound, CT MRI 39 (2018), pp. 60–69.

[112] O.N. Oyelade and A.E.S. Ezugwu, *A State-of-the-Art Survey on Deep Learning Methods for Detection of Architectural Distortion from Digital Mammography*, IEEE Access 8 (2020), pp. 148644–148676.

[113] M.A.S. Al Husaini, M.H. Habaebi, S.A. Hameed, M.R. Islam and T.S. Gunawan, *A Systematic Review of Breast Cancer Detection Using Thermography and Neural Networks*, IEEE Access 8 (2020), pp. 208922–208937.

[114] R.L. Hartley, J.P. Stone and C. Temple-oberle, *Breast Cancer in Transgender Patients: A Systematic Review. Part 1: Male to Female*, Eur. J. Surg. Oncol. (2018), .

[115] D.-R. Beddiar, · Mourad Oussalah and T. Seppänen, *Automatic captioning for medical imaging (MIC): a rapid review of literature*, Artif. Intell. Rev. (123AD), .

[116] M.J. Page, J.E. McKenzie, P.M. Bossuyt, I. Boutron, T.C. Hoffmann, C.D. Mulrow et al., *The PRISMA 2020 statement: an updated guideline for reporting systematic reviews*, BMJ (2021), pp. n71.

[117] T. Agarwal and V. Kumar, *A Systematic Review on Bat Algorithm: Theoretical*

Foundation, Variants, and Applications, Arch. Comput. Methods Eng. 29 (2022), pp. 2707–2736.

[118] T. Yin, F.H. Ali and C.C. Reyes-Aldasoro, *A robust and artifact resistant algorithm of ultrawideband imaging system for breast cancer detection*, IEEE Trans. Biomed. Eng. 62 (2015), pp. 1514–1525.

[119] G. Alexandrou, N. Moser, K.T. Mantikas, J. Rodriguez-Manzano, S. Ali, R.C. Coombes et al., *Detection of Multiple Breast Cancer ESR1 Mutations on an ISFET Based Lab-on-Chip Platform*, IEEE Trans. Biomed. Circuits Syst. 15 (2021), pp. 380–389.

[120] E. Landhuis, *Deep learning takes on tumours*, Nature 580 (2020), pp. 551–553.

[121] Y. Bengio, *Learning deep architectures for AI*, Found. Trends Mach. Learn. 2 (2009), pp. 1–27.

[122] J. Eismann, Y.J. Heng, K. Fleischmann-Rose, A.M. Tobias, J. Phillips, G.M. Wulf et al., *Interdisciplinary Management of Transgender Individuals at Risk for Breast Cancer: Case Reports and Review of the Literature*, Clin. Breast Cancer 19 (2019), pp. e12–e19.

[123] B. Fu, P. Liu, J. Lin, L. Deng, K. Hu and H. Zheng, *Predicting Invasive Disease-Free Survival for Early Stage Breast Cancer Patients Using Follow-Up Clinical Data*, IEEE Trans. Biomed. Eng. 66 (2019), pp. 2053–2064.

[124] J. Dheeba and S.T. Selvi, *A CAD system for breast cancer diagnosis using modified genetic algorithm optimized artificial neural network*, Lect. Notes Comput. Sci. (including Subser. Lect. Notes Artif. Intell. Lect. Notes Bioinformatics) 7076 LNCS (2011), pp. 349–357.

[125] X. Wang, X. Chen and C. Cao, *Hierarchically engineering quality-related perceptual*

features for understanding breast cancer, J. Vis. Commun. Image Represent. 64 (2019), pp. 102644.

[126] A. Gubern-Mérida, M. Kallenberg, R.M. Mann, R. Martí and N. Karssemeijer, *Breast segmentation and density estimation in breast MRI: A fully automatic framework*, IEEE J. Biomed. Heal. Informatics 19 (2015), pp. 349–357.

[127] P. Bándi, O. Geessink, Q. Manson, M. Van Dijk, M. Balkenhol, M. Hermsen et al., *From Detection of Individual Metastases to Classification of Lymph Node Status at the Patient Level: The CAMELYON17 Challenge*, IEEE Trans. Med. Imaging 38 (2019), pp. 550–560.

[128] H. Le, R. Gupta, L. Hou, S. Abousamra, D. Fassler, L. Torre-Healy et al., *Utilizing Automated Breast Cancer Detection to Identify Spatial Distributions of Tumor-Infiltrating Lymphocytes in Invasive Breast Cancer*, Am. J. Pathol. 190 (2020), pp. 1491–1504.

[129] L. Shen, L.R. Margolies, J.H. Rothstein, E. Fluder, R. McBride and W. Sieh, *Deep Learning to Improve Breast Cancer Detection on Screening Mammography*, Sci. Rep. 9 (2019), .

[130] M. Graziani, V. Andrearczyk and H. Müller, *Regression concept vectors for bidirectional explanations in histopathology*, Lect. Notes Comput. Sci. (including Subser. Lect. Notes Artif. Intell. Lect. Notes Bioinformatics) 11038 LNCS (2018), pp. 124–132.

[131] P. Jonnalagedda, D. Schmolze and B. Bhanu, *MVPNets: Multi-viewing path deep learning neural networks for magnification invariant diagnosis in breast cancer*, Proc. - 2018 IEEE 18th Int. Conf. Bioinforma. Bioeng. BIBE 2018 (2018), pp. 189–194.

[132] N. Arya and S. Saha, *Multi-modal classification for human breast cancer prognosis prediction : Proposal of deep-learning based stacked ensemble model*, 5963 (2020), pp. 2–11.

[133] R. Sanyal, D. Kar, R. Sarkar and S. Member, *Carcinoma type classification from high-resolution breast microscopy images using a hybrid ensemble of deep convolutional features and gradient boosting trees classifiers*, 5963 (2021), pp. 1–14.

[134] D. Wang, A. Khosla, R. Gargeya, H. Irshad and A.H. Beck, *Deep Learning for Identifying Metastatic Breast Cancer*, (2016), pp. 1–6.

[135] S. Reis, P. Gazinska, J.H. Hipwell, T. Mertzanidou, K. Naidoo, N. Williams et al., *Automated Classification of Breast Cancer Stroma Maturity from Histological Images*, IEEE Trans. Biomed. Eng. 64 (2017), pp. 2344–2352.

[136] X. Feng, L. Song, S. Wang, H. Song, H. Chen, Y. Liu et al., *Accurate prediction of neoadjuvant chemotherapy pathological complete remission (PCR) for the four sub-types of breast cancer*, IEEE Access 7 (2019), pp. 134697–134706.

[137] S. Pizer, J. Zimmerman and E. Staab, *Adaptive grey level assignment in CT scan display.*, J. Comput. Assist. Tomogr. (1984), .

[138] H. Yang, J. Sun, A. Carass, C. Zhao, J. Lee, J.L. Prince et al., *Unsupervised MR-to-CT Synthesis Using Structure-Constrained CycleGAN*, IEEE Trans. Med. Imaging 39 (2020), pp. 4249–4261.

[139] H. Liu, K. Simonyan and Y. Yang, *DARTS: Differentiable Architecture Search*, (2018), .

[140] J.M. Wolterink, A.M. Dinkla, M.H.F. Savenije, P.R. Seevinck, C.A.T. van den Berg and I. Išgum, *Deep MR to CT synthesis using unpaired data*, Lect. Notes Comput. Sci.

(including Subser. Lect. Notes Artif. Intell. Lect. Notes Bioinformatics) 10557 LNCS (2017), pp. 14–23.

[141] Z. Zhang, L. Yang and Y. Zheng, *Translating and Segmenting Multimodal Medical Volumes with Cycle- and Shape-Consistency Generative Adversarial Network*, Proc. IEEE Comput. Soc. Conf. Comput. Vis. Pattern Recognit. (2018), pp. 9242–9251.

[142] H. Yang, J. Sun, A. Carass, C. Zhao, J. Lee, Z. Xu et al., *Unpaired brain mr-to-ct synthesis using a structure-constrained cyclegan*, Lect. Notes Comput. Sci. (including Subser. Lect. Notes Artif. Intell. Lect. Notes Bioinformatics) 11045 LNCS (2018), pp. 174–182.

[143] Y. Ge, Z. Xue, T. Cao and S. Liao, *Unpaired whole-body MR to CT synthesis with correlation coefficient constrained adversarial learning*, (2019), pp. 4.

[144] M.A. Al-antari, M.A. Al-masni, M.-T. Choi, S.-M. Han and T.-S. Kim, *A fully integrated computer-aided diagnosis system for digital X-ray mammograms via deep learning detection, segmentation, and classification*, Int. J. Med. Inform. 117 (2018), pp. 44–54.

[145] G.H. Aly, M. Marey, S.A. El-Sayed and M.F. Tolba, *YOLO Based Breast Masses Detection and Classification in Full-Field Digital Mammograms*, Comput. Methods Programs Biomed. 200 (2021), pp. 105823.

[146] G. Hamed, M. Marey, S. Amin and M.F. Tolba, *Automated Breast Cancer Detection and Classification in Full Field Digital Mammograms using Two Full and Cropped Detection Paths Approach*, IEEE Access (2021), .

[147] D.A. Zebari, D.A. Ibrahim, D.Q. Zeebaree, M.A. Mohammed, H. Haron, N.A. Zebari et al., *Breast Cancer Detection Using Mammogram Images with Improved Multi-*

Fractal Dimension Approach and Feature Fusion, Appl. Sci. 11 (2021), pp. 12122.

[148] R. Achanta, A. Shaji, K. Smith and A. Lucchi, *SLIC Superpixels Compared to State-of-the-Art Superpixel Methods*, 34 (2012), pp. 2274–2281.

[149] S. Wang and Y. Zhao, *A Novel Patch-Based Multi-Exposure Image Fusion Using Super-Pixel Segmentation*, IEEE Access 8 (2020), pp. 39034–39045.

[150] H. Wang, J. Wang and X. Zhang, *Architecture and implementation of Shape Adaptive Discrete Wavelet Transform for remote sensing image onboard compression*, 2017 3rd IEEE Int. Conf. Comput. Commun. ICCC 2017 2018-Janua (2018), pp. 1803–1808.

[151] J. Jinju, N. Santhi, K. Ramar and B. Sathya Bama, *Spatial frequency discrete wavelet transform image fusion technique for remote sensing applications*, Eng. Sci. Technol. an Int. J. 22 (2019), pp. 715–726.

[152] L.F. Silva, D.C.M. Saade, G.O. Sequeiros, A.C. Silva, A.C. Paiva, R.S. Bravo et al., *A new database for breast research with infrared image*, J. Med. Imaging Heal. Informatics 4 (2014), pp. 92–100.

[153] J.A. Richards, *Remote sensing digital image analysis: An introduction*, Remote Sens. Digit. Image Anal. An Introd. 9783642300622 (2013), pp. 1–494.

[154] J. Cheng, F. Yin, D.W.K. Wong, D. Tao and J. Liu, *Sparse dissimilarity-constrained coding for glaucoma screening*, IEEE Trans. Biomed. Eng. 62 (2015), pp. 1395–1403.

[155] J. Li, L. Cheng, T. Xia, H. Ni and J. Li, *Multi-Scale Fusion U-Net for the Segmentation of Breast Lesions*, IEEE Access 9 (2021), pp. 137125–137139.

[156] R. Irfan, A.A. Almazroi, H.T. Rauf, R. Damaševičius, E.A. Nasr and A.E. Abdelgawad, *Dilated semantic segmentation for breast ultrasonic lesion detection using parallel feature fusion*, Diagnostics 11 (2021), pp. 1–20.

[157] T. Liu, J. Huang, T. Liao, R. Pu, S. Liu and Y. Peng, *A Hybrid Deep Learning Model for Predicting Molecular Subtypes of Human Breast Cancer Using Multimodal Data*, IRBM 43 (2022), pp. 62–74.

[158] M. Kass, A. Witkin and D. Terzopoulos, *Snakes: Active contour models*, Int. J. Comput. Vis. 1 (1988), pp. 321–331.

[159] W. Zhou and Y. Xie, *Interactive medical image segmentation using snake and multiscale curve editing*, Comput. Math. Methods Med. 2013 (2013), .

[160] R.J. Hemalatha, T.R. Thamizhvani, A.J.A. Dhivya, J.E. Joseph, B. Babu, R. Chandrasekaran et al., *Active Contour Based Segmentation Techniques for Medical Image Analysis*, Med. Biol. Image Anal. (2018), .

[161] S. Li, Y. Guo, Z. Pang, W. Song, A. Hao, B. Xia et al., *Automatic Dental Plaque Segmentation Based on Local-to-Global Features Fused Self-Attention Network*, IEEE J. Biomed. Heal. Informatics 26 (2022), pp. 2240–2251.

[162] T. Yang, H. Zhu, X. Gao, Y. Zhang, Y. Hui and F. Wang, *Grading of metacarpophalangeal rheumatoid arthritis on ultrasound images using machine learning algorithms*, IEEE Access 8 (2020), pp. 67137–67146.

[163] X. Chen, X. Luo, Y. Zhao, S. Zhang, G. Wang and Y. Zheng, *Learning Euler's Elastica Model for Medical Image Segmentation*, 2 (2020), pp. 1–9.

[164] K. Fernandes and J.S. Cardoso, *Deep Local Binary Patterns*, .

[165] W. Al-Dhabyani, M. Gomaa, H. Khaled and A. Fahmy, *Dataset of breast ultrasound images*, Data Br. 28 (2020), .

[166] W. Al-Dhabyani, M. Gomaa, H. Khaled and A. Fahmy, *Dataset of breast ultrasound images*, Data Br. 28 (2020), pp. 104863.

[167] X. Shen, H. Ma, R. Liu, H. Li, J. He and X. Wu, *Lesion segmentation in breast ultrasound images using the optimized marked watershed method*, Biomed. Eng. Online 20 (2021), pp. 1–23.

[168] Q. Huang, Y. Huang, Y. Luo, F. Yuan and X. Li, *Segmentation of breast ultrasound image with semantic classification of superpixels*, Med. Image Anal. 61 (2020), .

[169] H. Gong, M. Qian, G. Pan and B. Hu, *Ultrasound Image Texture Feature Learning-Based Breast Cancer Benign and Malignant Classification*, Comput. Math. Methods Med. 2021 (2021), .

[170] A. Sahu, P.K. Das and S. Meher, *High accuracy hybrid CNN classifiers for breast cancer detection using mammogram and ultrasound datasets*, Biomed. Signal Process. Control 80 (2023), pp. 104292.

[171] A. Vaswani, G. Brain, N. Shazeer, N. Parmar, J. Uszkoreit, L. Jones et al., *Attention is All you Need*, Adv. Neural Inf. Process. Syst. 30 (2017), .

[172] M.A. Al-antari, M.A. Al-masni, S.U. Park, J.H. Park, M.K. Metwally, Y.M. Kadah et al., *An Automatic Computer-Aided Diagnosis System for Breast Cancer in Digital Mammograms via Deep Belief Network*, J. Med. Biol. Eng. 38 (2018), pp. 443–456.

[173] M.A. Al-antari, S.M. Han and T.S. Kim, *Evaluation of deep learning detection and classification towards computer-aided diagnosis of breast lesions in digital X-ray mammograms*, Comput. Methods Programs Biomed. 196 (2020), pp. 105584.

[174] K. Rautela, D. Kumar and V. Kumar, *Dual-modality synthetic mammogram construction for breast lesion detection using U-DARTS*, Biocybern. Biomed. Eng. 42 (2022), pp. 1041–1050.

[175] *OpenCV: Image Thresholding*. Available at

https://docs.opencv.org/4.x/d7/d4d/tutorial_py_thresholding.html.

[176] W. Shao, S.J. Huang, M. Liu and D. Zhang, *Querying Representative and Informative Super-Pixels for Filament Segmentation in Bioimages*, IEEE/ACM Trans. Comput. Biol. Bioinforma. 17 (2020), pp. 1394–1405.

[177] J.V.B. Soares, J.J.G. Leandro, R.M. Cesar, H.F. Jelinek and M.J. Cree, *Retinal vessel segmentation using the 2-D Gabor wavelet and supervised classification*, IEEE Trans. Med. Imaging 25 (2006), pp. 1214–1222.

[178] R. M. Al-Tam and S. M. Narangale, *Breast Cancer Detection and Diagnosis Using Machine Learning: A Survey*, J. Sci. Res. 65 (2021), pp. 265–285.

[179] A. Roy, B.K. Singh, S.K. Banchhor and K. Verma, *Segmentation of malignant tumours in mammogram images: A hybrid approach using convolutional neural networks and connected component analysis*, Expert Syst. 39 (2022), pp. e12826.

[180] M.A. Al-antari, S.M. Han and T.S. Kim, *Evaluation of deep learning detection and classification towards computer-aided diagnosis of breast lesions in digital X-ray mammograms*, Comput. Methods Programs Biomed. 196 (2020), pp. 105584.

[181] N.A. Samee, G. Atteia, S. Meshoul, M.A. Al-antari and Y.M. Kadah, *Deep Learning Cascaded Feature Selection Framework for Breast Cancer Classification: Hybrid CNN with Univariate-Based Approach*, Math. 2022, Vol. 10, Page 3631 10 (2022), pp. 3631.

[182] M. Alkhaleefah and C.-C. Wu, A Hybrid CNN and RBF-Based SVM Approach for Breast Cancer Classification in Mammograms, in 2018 IEEE International Conference on Systems, Man, and Cybernetics (SMC), 2018, pp. 894–899.

[183] T.M. Mejia, M.G. Perez, V.H. Andaluz and A. Conci, Automatic Segmentation and Analysis of Thermograms Using Texture Descriptors for Breast Cancer Detection, in

2015 Asia-Pacific Conference on Computer Aided System Engineering, 2015, pp. 24–29.

[184] C.B. Vijaya Madhavi, *Assessment of Dynamic Infrared Images for Breast Cancer Screening using BEMD and URLBP*, Int. J. Pure Appl. Math. 114 (2017), pp. 261–269.

[185] S. Shahari and A. Wakankar, Color analysis of thermograms for breast cancer detection, in 2015 International Conference on Industrial Instrumentation and Control (ICIC), 2015, pp. 1577–1581.

[186] S. Kiymet, M.Y. Aslankaya, M. Taskiran and B. Bolat, Breast Cancer Detection From Thermography Based on Deep Neural Networks, in 2019 Innovations in Intelligent Systems and Applications Conference (ASYU), 2019, pp. 1–5.

[187] L.F. Silva, D.C.M. Saade, G.O. Sequeiros, A.C. Silva, A.C. Paiva, R.S. Bravo et al., *A New Database for Breast Research with Infrared Image*, J. Med. Imaging Heal. Informatics 4 (2014), pp. 92–100.

[188] L.F. Silva, G.O. Sequeiros, M.L.O. Santos, C.A.P. Fontes, D.C. Muchaluat-Saade and A. Conci, *Thermal Signal Analysis for Breast Cancer Risk Verification.*, Stud. Health Technol. Inform. 216 (2015), pp. 746–50.

[189] A. Dosovitskiy, L. Beyer, A. Kolesnikov, D. Weissenborn, X. Zhai, T. Unterthiner et al., *An Image is Worth 16x16 Words: Transformers for Image Recognition at Scale*, (2020), .

[190] A.H. Nvidia, Y. Tang, V. Nath, D. Yang, A. Myronenko, B. Landman et al., *UNETR: Transformers for 3D Medical Image Segmentation*, .

[191] K. Simonyan and A. Zisserman, *Very Deep Convolutional Networks for Large-Scale Image Recognition*, (2014), .

[192] Z. Liu, Y. Lin, Y. Cao, H. Hu, Y. Wei, Z. Zhang et al., *Swin Transformer: Hierarchical Vision Transformer using Shifted Windows*, (2021), .

[193] Z. Liu, J. Ning, Y. Cao, Y. Wei, Z. Zhang, S. Lin et al., *Video Swin Transformer*, (2021), .

[194] G. Peng, Z. Jiang, H. You, P. Lu, S. Hoi, X. Wang et al., *Dynamic Fusion with Intra- and Inter- Modality Attention Flow for Visual Question Answering*, (2018), .

[195] X. Song, H. Guo, X. Xu, H. Chao, S. Xu, B. Turkbey et al., *Cross-modal Attention for MRI and Ultrasound Volume Registration*, (2021), .

[196] X. Xu, T. Wang, Y. Yang, L. Zuo, F. Shen and H.T. Shen, *Cross-Modal Attention With Semantic Consistence for Image–Text Matching*, IEEE Trans. Neural Networks Learn. Syst. 31 (2020), pp. 5412–5425.